Doctoral Dissertation

Study on Triblock Copolymers: From Relaxation Dynamics of Solution to Toughening Mechanism of Physical Double Network Hydrogels

（トリブロック共重合体に関する研究：溶液緩和のダイナミクスからダブルネットワーク物理ゲルの高靭性化原理まで）

By

YANAN YE

Supervisor: Jian Ping Gong

Lab of Soft & Wet Matter

Transdisciplinary Life Science Course

Graduate School of Life Science

Hokkaido University

September　2018

Contents

Abstract

Hydrogels composed of three-dimensional polymer network and abundant of water are a class of typical soft and wet matters, which are used for numerous applications including force-sensitive adhesives, scaffolds of tissue engineering, gas filtration membranes, drug-controlled release and ionic conductive media. However, traditional hydrogels are mechanically weak, which limits their application severely. Recently, several tough and self-recoverable hydrogels were developed by introducing physical association as sacrificial bonds to dissipate energy, which widely extend the scope of applications even as structural biomaterials, like artificial cartilage and ligament. Despite great success in creation of tough and self-recoverable hydrogels, the developments generally relied on an empirical and trial-and-error approach as the understanding of structure and toughening mechanism of those gels is still unclear.

This thesis focuses on revealing the structure and underlying toughening mechanism of tough and self-recoverable hydrogels. Recently developed hydrogels based on self-assembly of ABA type triblock copolymer were chosen as a model system, which have been demonstrated to possess excellent mechanical property and self-recoverable capability. These gels are prepared in sequential steps: (i) firstly the triblock copolymer poly(butyl methacrylate)-*b*-poly(methacrylic acid)-*b*-poly(butyl methacrylate), PBMA-PMAA-PBMA, was dissolved in dimethylformamide (DMF) to form precursor solution; (ii) then the precursor solution undergoes a solvent exchange process along

with self-assembly of endblock PBMA into micelles acting as cross-linking to form B gels; (iii) finally the second polymer, polyacrylamide (PAAm) was introduced to form sacrificial hydrogen bonds between the carboxy group of PMAA and amino group of PAAm, and to generate the tough and self-recoverable hydrogels, named as B-DN gel. In this work, we systematically studied the preparation process and the structure-property relationship of those gels, including relaxation dynamic of precursor solution, contribution of physical crosslinks and trapped entanglements in B-gels, the effect of molecular parameters on self-assembly structure of B-gels, and the structure-property relationship of B-DN gels. Benefiting from the thoroughly understanding of chain structure and self-assembly structure in gelation process and final gels, we successfully developed thin but ultra-tough and 100% recoverable hydrogel membranes with high pH sensitivity, excellent mechanical properties and biocompatibility, which is urgently needed in many fields but rarely realized in hydrogels before.

Chapter 1. General Introduction

1.1 Block copolymer

A block copolymer always consists of at least two chemically distinct polymer block chains which joined together to form a single macromolecule. Consequently, the block chain has a general tendency to separate. However, this tendency is tempered by the restriction imposed by the covalent bonds that connect them, preventing macroscopic phase separation and promoting structural organization at microscale[1]. The microscopic morphologies depend on chemical composition, chain architecture, relative molecular weights of immiscible blocks and external stimulus such as temperature, pH or force.

1.2 Phase behavior and structure formation in block copolymer melts

In block copolymer melts, by tuning the composition of block copolymers with immiscible blocks, the block copolymers can separate into a variety of morphologies[2], including spheres (S), cylinders (C), bicontinuous gyroids (G), lamellae (L), etc., as shown in **Figure 1**[3]. The self-assembly process is driven by a dominant mixing enthalpy companied by a secondary mixing entropy. A prerequisite for the miscibility of two blocks during mixing described by Gibbs free energy ΔG as follows:

$$\Delta G = \Delta H - T\Delta S < 0 \quad (1)$$

Where ΔH is the enthalpy, T is the Kelvin temperature and ΔS is the entropy respectively. According equation (1), the entropy always favors mixing, while the energetic interaction originated from enthalpic factor determined the self-assembly process. According to Flory–Huggins solution theory[4,5], the enthalpy of mixing, ΔH, can be expressed as:

$$\Delta H = RT\chi_{AB}\phi_A\phi_B \quad (2)$$

Where R is the universal gas constant, ϕ_A and ϕ_B is the volume fraction of each blocks. The χ_{AB} is Flory-Higgins parameter which can be estimated from the Hildebrand solubility parameters δ_A and δ_B:

$$\chi_{AB} = V_{seg}(\delta_A - \delta_B)^2/RT \quad (3)$$

where V_{seg} is the actual volume of a polymer segment, the δ_A and δ_B is the Hildebrand solubility parameters. From equation (3), the χ_{AB} can be tuned by temperature or relative solubility of each block. The phase map for symmetric ABA triblock copolymers is similar to that of AB diblocks since they share the same driving force for phase separation[6].

1.3 Block copolymer in solution

The introduction of solvent leads to an increased level of complexity for block copolymer self-assembly process compared with that performed in melts. In block copolymer solution systems, the interactions between solvent and each of the monomers also contribute to the ΔG and, therefore, act as the driven force for self-assembly process. The insolubility degree is determined by the segregation product,

$\chi_{AS}N_A$, where N_A is the polymerization degree of insoluble blocks, and χ_{AS} is the Flory-Higgins interaction parameter between insoluble block and solvent. With increasing $\chi_{AS}N_A$ or decreasing temperature, the incompatibility increases, resulting in microphase separation structure. When the block copolymer has a symmetric ABA type structure in B-selective solvents, it is able to form physically associated network with B-bridged A-micelles.

1.4 Preparation of triblock gels by self-assembly process

1.4.1 Thermal-induced gelation.

The enthalpy of mixing, ΔH originated from equation (3) shows that changing temperature is an effective way to tuning the solvent quality. The thermal- induced triblock gels originates from the temperature dependence of the interaction parameter $\chi_{AS}N_A$. The mechanism of thermal induced gel formation is shown schematically in **Figure 2**[6]. There are two important transition temperatures: the first one is the critical micelle temperature where the endblock aggregates to form the micelles. As the temperature decreases, illustrated by equation (3), the solubility of endblocks decreases and solvent is expelled from the micelles[7].

1.4.2 Solvent exchange process.

Solvent exchange provides an additional method for preparing triblock gels, as illustrated in **Figure 3**[8]. During the solvent exchange, a block copolymer is initially dissolved in a good solvent for both blocks that is also miscible with nonsolvent for

endblocks. When the solution encounters the nonsolvent, the good solvent is replaced by nonsolvent, and the endblocks self-organize to form a

micelles.

1.5 Interest of this work.

The triblock gels are desirable in many fields due to their reversibility and favorable selective properties[9]. Such gels have been used for numerous applications including force-sensitive adhesives[10], scaffolds of tissue engineering[11], actuators[12], gas filtration membranes[13], drug controlled release[14] and ionic conductive media[15]. However, the mechanical performance is usually low, typically about a few hundred kPa, seriously limited its application.

An effective way to enhance toughness of hydrogels is to incorporate energy dissipation structures (sacrificial bonds). Several recent works have prepared tough hydrogels with reversible sacrificial bonds such as hydrogen bond, ionic bond or hydrophobic association to allow the fractured bond to be re-formed[16,17]. In our previous work, we prepared triblock gels by solvent exchange method (named as B gel) based on poly(butyl methacrylate)-poly(methacrylic acid)-poly(butyl methacrylate), PBMA-PMAA-PBMA (**Table 1**). To overcome the weak mechanical drawback, the second network, polyacrylamide (PAAm) was introduced to form hydrogen bond with the carboxy group of PMAA using its amino group (named as B-DN gel)[18]. This hydrogel shows high mechanical performance and self-recoverable properties. While the gel structure and toughening mechanism are still unclear.

1.6 Overview of this thesis.

In this dissertation, we firstly dissolved the triblock copolymer PBMA-PMAA-PBMA in dimethylformamide, DMF and obtained homogenous precursor solution. The relaxation dynamics of precursor solution was studied based on rheological and NMR measurements. Then the B gels were fabricated by solvent exchange process along with self-assembly of PBMA into micelles to act as cross-linking points of 1st network. The effect of polymer concentration and midblock chain length on mechanical response and micelle morphology of triblock gels were systematically studied. Subsequently the 2nd linear polymer with amino derivative groups is imported to introduce the sacrificial hydrogen bond formed between 1st and 2nd network. Based on the structure evolution of the B-DN gel by *in-situ* small X-ray scattering, the toughening mechanism were clarified.

In **Chapter 2**, the sol-gel transition behaviors of PBMA-PMAA-PBMA triblock copolymer precursor solution was observed. The relaxation dynamics of sol-gel transition behaviors was probed by combing rheology and NMR. Time-temperature superposition (TTSP) and time-concentration superposition (TCSP) are applied to derive association energy (the associative strength or energy needed to break a junction point) and longest relaxation time (τ_L) and plateau modulus (G_N) over a wide temperature range of -20 ºC - 35 ºC. For the TTSP, the shift factors against inverse of temperature show two distinct regions at critical temperature (T^*). Below T^*, the activation energy is expected to the energy needed to pull out a PBMA chain from the

aggregated micelles. Above T^*, the activation energy is related to the energy required to increase the mobility of polymer chain. The association point was further confirmed by temperature-elevated NMR. Concentration dependencies of the τ_L and G_N are stronger than the theoretically prediction of entangled polymer melt, means the macroscopic transient network grows with polymer concentration by increasing the fraction of effective bridge chain.

In **Chapter 3, t**he contributions of physical crosslinks and trapped entanglements in B gels was successfully separated. In the gel (named as B gel), with increasing concentration, the elastic modulus originated from number of elastically active chains firstly increase followed by a plateau. In addition, structure evolution was also observed in small angle X scattering (SAXS). Based on micro SAXS and macro mechanical property, we concluded that the dangling chain which has no contribution, is dominant at low concentration; while at high concentration, the bridged micelles is dominant.

In **Chapter 4**, Theoretical efforts have been made to evaluate bridge fraction in ABA triblock copolymer networks. However, there are a few experimental reports determining bridge fraction due to technologic complexity to distinguish the defect from bridge. In our work, the signals of defect and bridge were firstly observed by small angle X-ray scattering measurements. In addition, the defect-to-bridge transition was visibly observed by changing triblock copolymer concentration, which is further confirmed by same trend of normalized Young's modulus vs concentration.

In **Chapter 5**, The toughening mechanism of tough B-DN gels from a combination of *in-situ* small-angle X-ray scattering and customized tensile device, the structure evolution during deformation was revealed, which suggests that the high toughness of self-recoverable B-DN gels is a synergistic effect of multiscale energy dissipation. In initial small strain region, the breaking and reforming of hydrogen bonding in chain scale dissipates energy, resulting in 100% self-recovery; In the middle strain region, the chain pullout of endblock from the micelles and debris reorganization of 1st network for forming cluster dissipate energy; In the large strain region, microvoids form, which also dissipate energy.

For further applications, in **Chapter 6**, we propose a strategy for facile fabrication of thin, yet tough and self-recovery hydrogel membranes based on double network principle. The thin physical DN gel membranes, named as B-DN gel membranes, of controllable thickness and self-standing strength, are fabricated by two-step sequential gelation process in which the spin-coating method was used to form triblock copolymers thin gel membranes. The thin DN gel membranes, 7~110 μm thick and 75 wt% water contents, exhibit excellent mechanical properties, including high modulus (Young's modulus ~100 MPa), stretching ability (fracture strain: ~1000%), high strength (fracture stress: ~8 MPa), high toughness (work of extension: ~10^6 J/m^3), 100% self-recovery and ultrafast pH response. Additionally, the membranes exhibit excellent mechanical properties superior to those of various biological membranes, biocompatibility, and postoperative anti-adhesive property, foreshadowing their

potential use as substitutes for biological membranes or postoperative anti-adhesive membrane.

1.7 Reference

[1] Y. Mai, A. Eisenberg, *Chem. Soc. Rev.* **2012**, *41*, 5969.

[2] M. Karayianni, S. Pispas, In *Fluorescence Studies of Polymer Containing Systems*; Springer, 2016; pp. 27–63.

[3] K. Koo, H. Ahn, S.-W. Kim, D. Y. Ryu, T. P. Russell, *Soft Matter* **2013**, *9*, 9059.

[4] M. L. Huggins, *J. Chem. Phys.* **1941**, *9*, 440.

[5] P. J. Flory, *J. Chem. Phys.* **1942**, *10*, 51.

[6] M. W. Matsen, R. B. Thompson, *J. Chem. Phys.* **1999**, *111*, 7139.

[7] M. E. Seitz, W. R. Burghardt, K. T. Faber, K. R. Shull, *Macromolecules* **2007**, *40*, 1218.

[8] K. J. Henderson, K. R. Shull, *Macromolecules* **2012**, *45*, 1631.

[9] A. J. Peters, T. P. Lodge, *Macromolecules* **2016**, *49*, 7340.

[10] P. L. Drzal, K. R. Shull, *J. Adhes.* **2005**, *81*, 397.

[11] S. K. Agrawal, N. Sanabria-DeLong, G. N. Tew, S. R. Bhatia, *J. Mater. Res.* **2006**, *21*, 2118.

[12] S. Imaizumi, H. Kokubo, M. Watanabe, *Macromolecules* **2011**, *45*, 401.

[13] Y. Gu, E. L. Cussler, T. P. Lodge, *J. Memb. Sci.* **2012**, *423*, 20.

[14] C. He, S. W. Kim, D. S. Lee, *J. Control. release* **2008**, *127*, 189.

[15] S. Zhang, K. H. Lee, J. Sun, C. D. Frisbie, T. P. Lodge, *Macromolecules* **2011**, *44*, 8981.

[16] Y. Gong, M. Gao, D. Wang, H. Möhwald, *Chem. Mater.* **2005**, *17*, 2648.

[17] T. L. Sun, T. Kurokawa, S. Kuroda, A. Bin Ihsan, T. Akasaki, K. Sato, T. Nakajima, J. P. Gong, M. A. Haque, T. Nakajima, J. P. Gong, *Nat. Mater.* **2013**, *12*, 932.

[18] H. J. Zhang, T. L. Sun, A. K. Zhang, Y. Ikura, T. Nakajima, T. Nonoyama, T. Kurokawa, O. Ito, H. Ishitobi, J. P. Gong, *Adv. Mater.* **2016**, *28*, 4884.

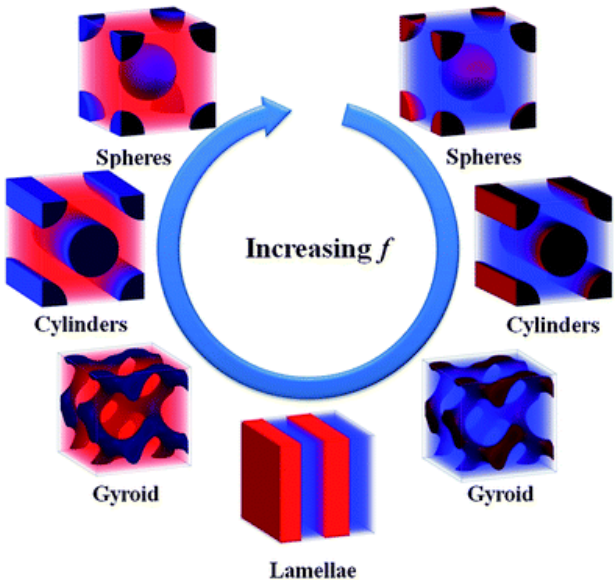

Figure 1. Various morphologies formed by the self-assembly of block copolymers. The *f* indicates volume fraction of one component[3].

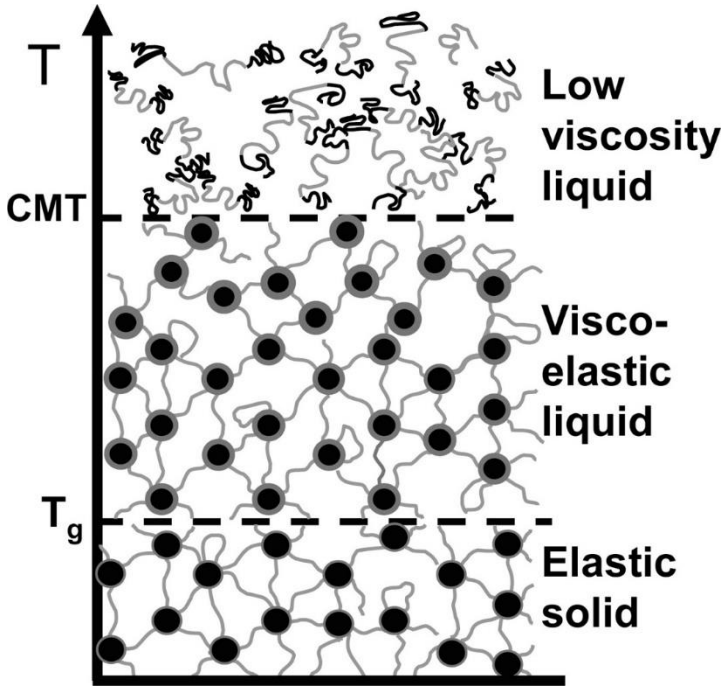

Figure 2. Schematic illustrating the temperature-dependent structure of acrylic triblock copolymer gels in 2-ethylhexanol[6].

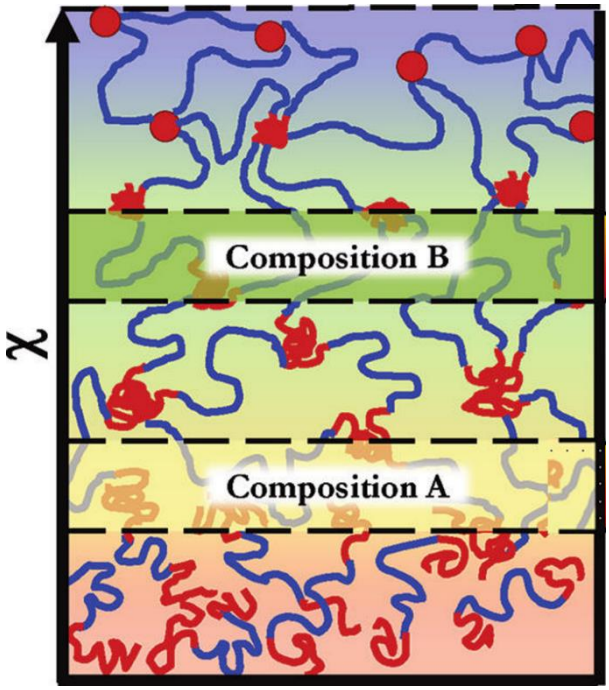

Figure 3. An illustration of the effect of solvent quality on the phase behavior of physically associated triblock copolymer gel networks[8]. Here, composition A and composition B represent good and poor solvent, respectively.

Table 1. Description of the triblock copolymers

[a)]Polymer $A_mB_nA_p$	[b)]Mn [kg/mol]	[b)]M_w/M_n	[c)]f_B	[d)]L_A		[d)]L_B	
				L_{gauss}	L_{max}	L_{gauss}	L_{max}
$A_{75}B_{81}A_{75}$	28.6	1.38	0.35	1.89	18.75	3.84	13.07
$A_{73}B_{142}A_{54}$	30.3	1.43	0.53	1.74	16	5.09	22.92
$A_{93}B_{302}A_{93}$	52.5	1.31	0.62	2.1	23.25	7.42	48.75
$A_{86}B_{444}A_{86}$	62.8	1.38	0.72	2.02	21.5	9.00	71.67

[a)] The subscripts of m, n and p represent the degree of polymerization of the endblock, midblock and endblock respectively. A and B represent poly(butyl methacrylate) (PBMA) and poly(methacrylic acid) (PMAA), respectively. [b)] Weight-average molecular weight and molecular weight distribution of the triblock copolymer, respectively. [c)] Molar fraction of midblock PMAA. [d)] The length of endblock chain L_A and midblock chain L_B at Gaussian state (L_{gauss}) and full stretching state (L_{max}).

Chapter 2: Relaxation Dynamics of Thermal-induced Sol-gel Transition in B-selective Organic Solvent

2.1 Introduction

The self-assembly of block copolymers have been subjected to extensive research in academic and applied polymer science including smart surfaces[1,2] , drug release[3–5], catalysis[6–8], gene therapy[9,10], optical switching[11] and bioimaging[12–14]. In such assemblies, the self-assembly process is determined not only by block nature but also by the selective solvent[15]. In organic solvents a strong temperature dependence of the endblock-solvent interaction parameter, χ, permits triblock copolymer self-assembly to various morphologies when cooled below sol-gel transition temperature[16]. When the polymer has an ABA type architecture, this behavior results in a sol-gel transition, as a physical associated transient network of midblock-bridged micelles forms a percolated network.

The relaxation dynamics of the transient network play a key role for the underlying macroscopic properties[17,18]. Therefore, it is valuable and highly expected to investigate the pathways for spontaneous micelles formation of amphiphilic triblock copolymers in selective solvents. Theoretically, Transient network theory are an effective tool to illuminate both relaxation dynamics and viscoelastic properties[19–21]. Recently, more work delved into a range of theoretical aspects of ABA triblock copolymer and their viscoelastic properties using molecular dynamics simulation[22,23] or dissipative particle

dynamics[24,25]. Experimentally, however, for many systems, the relaxation time is imperceptibly long and the systems are kinetically frozen because the endblock chains are usually fixed in the associated core even though the core is not in glassy state[26–30]. In this sense, the relaxation dynamics is hardly expected. In order for understanding the relaxation dynamics of transient network by ABA triblock copolymers, systems with an A blocks that are very short[31,32], or not very solvophobic[33–35], is suitable because the strength of endblock micelles is not strong enough and the micelles is swollen by solvent.

Superposition is a powerful method in rheology to probe the dynamical processes in wide variety of soft materials, thereby extending our understanding of their dynamics[36,37]. For TTSP, the association energy ΔH, one of the most important parameters of associative polymers, can be determined from horizontal shift factor according to Arrhenius plot. For example, Castelletto[38] and Lodge[39] studied the concentration dependence of longest relaxation time and plateau modulus, while no extensive explanation about the relaxation dynamics of the micelles. Tanaka and Edwards theoretically presented that the ΔH for micelle relaxation is determined by the energy barrier for endblock chain to pullout from the micelles[21,40]. The energy barrier is determined by the interaction between the solvent and the endblock segment[41]. Base on this concept, Shull tuned the E_a from 150 to 300 kJ/mol by changing second solvent composition (water content: 4 wt% - 8 wt%), as the composition-driven changes in the χ parameter characterizes the solvent-endblock interaction[16]. Inomata[42] observed that

the ΔH decrease as increasing the concentration, while shull[43] and Chassenieux[15] et al. found that ΔH is independent on the concentration. Nevertheless, the relaxation dynamics is not fully understood. In addition, for the thermosensitive systems, the TTSP is invalid for obtaining plateau moduli due to the structure dependence on temperature.

Herein, we report the discovery of a new class of thermoresponsive ABA triblock copolymers based on copolymers of PBMA and PMAA as endblock and midblock, respectively. The TTSP is performed at low and high temperature region, the shift factor (a_T) against inverse of temperature (1/T) shows two distinct regions at critical temperature (T^*). From the shift factors at each region, the association activation energy ΔH (low temperature region) is much higher than that of apparent activation energy (high temperature region). Furthermore, the TCSP is performed and from the shift factor as a function of polymer concentration, the longest relaxation time and plateau moduli is evaluated. Finally, the relaxation time of micelles is calculated based on the model of equivalent diblock polymer.

2.2 Experimental Section

2.2.1 Materials

The amphiphilic triblock copolymers, poly(butyl methacrylate)-b-poly(methacrylic acid)-b-poly(butyl methacrylate) (PBMA-b-PMAA-b-PBMA), and corresponding homo-PBMA and homo-PMAA were synthesized by the Otsuka Chemical Co., Ltd.,

Japan (**Table 1**). The solvent dimethylformamide (DMF) were purchased from Wako Pure Chemical Industries, Ltd. (Japan).

2.2.2 Rheology

An ARES-2 rheometer (TA Instruments) was used with a concentric cylinder geometry of 27.66 mm bob diameter, 30 mm cup diameter and 41.5 mm bob length. Steady shear tests were performed in the shear rate range from 10^{-3} to 10^{3} s^{-1} with 5 min as the maximum point time to ensure equilibrium is attained at every test point. All the steady shear tests were performed at at 25 ^{o}C for triblock concentration ranges from 7.92 mmol L^{-1} to 0.792 mol L^{-1}. Dynamic measurements were performed in the linear viscoelastic regime. The temperature sweep was performed from -20 ^{o}C to 40 ^{o}C at a heating rate of 1 ^{o}C min-1, a strain of 0.5%, and a frequency of 10 rad s^{-1}. The dynamic frequency sweep experiment was performed from 0.01 to 100 rad s^{-1} with a strain of 0.5% over a temperature range of -20 ^{o}C to 35 ^{o}C with a temperature interval of 5 ^{o}C. The data was processed using the manual shifting mode to perform superpositions (TTSP and TCSP) and spectrum calculations.

2.2.3 Nuclear magnetic resonance (NMR)

All the NMR measurements were performed on a Bruker Avance III HD spectrometer operating at 800 MHz for ^{1}H, using DMF-d^{7} as solvent. The triblock concentrations of 0.79, 1.03, 1.27 and 1.50 mol/L were selected for variable-temperature tests. The temperature control was achieved by a Bruker BCU II unit and a build in temperature

control unit. At first, the solutions were maintained at -30 ºC in the NMR apparatus, and subsequently NMR spectra were measured with increasing temperature from -30 ºC to 50 ºC with a temperature interval of 5 ºC. the solvent peak area (~3.1 ppm) was used as a reference for chemical shift. After arriving the prescribed temperatures, the sample was allowed to equilibrate for ~5 min for stability.

2.3 Results and discussion

2.3.1 Thermal-induced sol-gel transition

The sol-gel phase transition was firstly investigated by rheological techniques under oscillatory shear conditions. **Figure 1** shows the temperature evolution of changes in storage modulus (G') and loss moduli (G") of triblock copolymer solution with a concentration of 1.98 mol/L. At T < 0 ºC, G' > G", which is characteristic of the gel state; At T > 0 ºC, G' < G", which is a feature of the solution state. The phase transition temperature is defined as the intersection of the storage and loss moduli at a specified frequency. However, it should be noted that the crossover point method does not specify the exact gelation point position but gives an approximation where gelation is occurring[44]. An alternative approach to determine the gelation point was shown latter.

2.3.2 Time-temperature superposition (TTSP)

The representative frequency sweeps, measured isothermally at a sequence of temperatures, were superposed to a master curve by shifting horizontally with a temperature dependent shift factor α_T with a reference temperature of -20 ºC. As shown

in **Figure 2d**, the curves of G′, G″ and tanδ obtained at different temperature overlap very well, respectively. At high frequency, the G′ approaches a plateau demonstrating the response of an elastic solid, and at low frequency region, the dynamic moduli are scaled as $G' \sim \omega^2$ and $G'' \sim \omega^2$, means the terminal relaxation behavior. It should be pointed out that although a well-superposed master curve was obtained by shifting the modulus curves at each temperature along the parallel direction, the curve of lnα_T verse 1/T was divided into two distinct linear regions with different slopes at critical temperature (T^*). In our system, the T^* is defined as sol-gel transition temperature (**Figure 3**). This result demonstrates that the relaxation mechanisms for high and low temperature region (HT R-I, LT R-II) are quite different. The energetics ΔH, originated from different relaxation processes, can be extracted from the temperature dependence of α_T[16,45] in HT R-I and LT R-II, respectively. Thus, we proceed the fits in two regions following the Arrhenius equation:

$$\alpha_T = Ae^{\Delta H_a/RT} \quad (1)$$

ΔH values computed for the two regions are 52 kJ/mol and 249 kJ/mol for HT R-I and LT R-II, respectively. For the LT R-II, the ΔH_2 is smaller than reported ΔH for poly(methyl methacrylate)-block-poly(butyl acrylate)-block-poly(methyl methacrylate) (PMAA-PBMA-PMAA) in 1-butanol (~500 kJ/mol)[42] or 2-ethylhexanol (~500 kJ/mol)[46]. The value of ΔH_2 have been related to the activation energy for pullout of the endblock chain from the core of the aggregates[25,41,42,47]. The energy barrier should be influenced by interaction parameter between endblock PBMA with solvent DMF. For

the HT R-I, the ΔH_1 is expected to the energy required to overcome the chain internal friction that resists its flow.

A similar TTSP was performed on PBMA-PMAA-PBMA/DMF solution with different concentrations (**Figure 4**). Similarly, each of these modulus curves can be shift horizontally to generate a well-superposed master curve. In additionally, all the curve of $\ln\alpha_T$ verse 1/T was broken into two regions, depicting the universal relaxation behavior for all the concentrations studied (**Figure 5a**). The ΔH for all the concentrations was computed for the two regions based on equation 1 (**Figure 5b**). For the LT R-II, all ΔH_2 is independent of the concentration (~250 kJ/mol), which is consistent with the results reported for PMAA-PBMA-PMAA) in 2-ethylhexanol[46] and Br-P(nBMA50%-stat-tBMA50%)-PtBMA-P(nBMA50%-stat-tBMA50%)101-Br in dichloromethane[15]. If the ΔH_2 is energy barrier of endblock chain pullout from the micelle, the value of ΔH_2 should be determined by $\chi N_{micelle}$, where χ is the endblock-solvent interaction parameter, and $N_{micelle}$ is the degree polymerization of endblock chain. Consequently, the concentration should have negligible effect on the ΔH_2. For the HT R-II, the ΔH_1 continuously increases as increasing concentration. At high temperature, associating groups dissociate due to high thermal mobility[18]. The enhancement in ΔH_1 possibly attributes to the larger entangled chain friction at higher concentration.

To confirm that entanglement exists in the concentration regions we studied, the specific viscosity η_{sp}-concentration C_P relationship was investigated. the η_{sp} is

calculated using the formula

$$\eta_{sp} = \frac{\eta_a - \eta_0}{\eta_0} \quad (2)$$

where η_a and η_0 are the apparent viscosities of triblock copolymer/DMF solutions and pure solvent (here DMF) respectively. The η_a and η_0 can be obtained from the following relationships:

$$\eta_a = \lim_{\dot{\gamma}\to 0} \eta \text{ or } \eta_a = \lim_{\omega\to 0} \eta^* \quad (3)$$

Steady shear sweep and oscillation frequency sweep are performed for the concentration regions of $C_P < 0.79$ mol/L (**Figure 6a**) and $C_P > 0.79$ mol/L(**Figure 6b**), respectively due to rheometer sensitivity[48]. To ensure the data accuracy, the curves comparison between two methods was shown in **Figure 7**. The well-overlapped curves demonstrated that data deduced from these two methods can be combined into one curve. The dependence of the η_{sp} versus C_P gives $C^e \approx 0.9$ mol/L (**Figure 6c)**, confirming the existence of entanglement in all concentration sequence.

2.3.3 Relaxation behaviors

There exist two kinds of relaxation with different time scales. One is the relaxation of entire polymer chain, and the corresponding characteristic relaxation time is named as longest relaxation time (τ_L)[49]. Another one origins from the relaxation of micelles formed by self-assembly of endblock, and the relaxation process is always considered as that the pullout of terminal chain from the micelles ($\tau_{pullout}$)[15,16,41,42]. What's the relationship between $\tau_{pullout}$ and τ_L? As shown in **Figure 4**, all the master curves show a plateau at high frequency followed by terminal relaxation at low frequency. The plateau

modulus G_N originated from the network structure formed by bridged micelles. When the endblock chain does not pull out on the observed scale, the systems cannot relax. Therefore, the τ_L indicates that the endblock chains must have pulled out. Consequently, the endblock chain pullout time $\tau_{pullout}$ must be either corresponded to or smaller than the τ_L. As the ΔH presents the activation energy for endblock chain pullout, the $\tau_{pullout}$ was calculated via

$$\tau_{pullout} = \tau_0 \times e^{\frac{\Delta H}{RT}} \quad (4)$$

$$\tau_0 = \frac{b^2 \zeta}{6\pi^2 kT} \quad (5)$$

Where τ_0 is the relaxation time of monomer segment. N_{end} is the polymerization degree of endblock chain, b is the statistical segment length, ζ is the monomeric friction factor, T is the Kelvin temperature, k and R are the Boltzmann constant and gas constant, respectively. b, and ζ are needed to calculate $\tau_{pullout}$. The statistical segment length b = 0.67 nm was taken from the literature; The value for ζ was estimated based on published rheological data for poly(butyl methacrylate). Based on above equations, it is reasonable that the relaxation of micelles is caused by endblock chain pullout because the relaxation of chain pullout is determined by $\chi N_{micelle}$, not affected by concentration theoretically.

The longest relaxation time (τ_L) and plateau modulus (G_N) can be picked up from the master curve. In **Figure 4**a systematic shift of G′, G″ and tanδ builds a sequence of master curves at different C_P. τ_L was defined as the inverse of the frequency where G′ and G″ cross. The τ_L is plotted against in **Figure 5c** and simple scaling laws were found:

$\tau_L \sim C_P^{7.6}$. The scaling exponent is also much larger than the predicted ones for the ideal entangled Gaussian chains: ($\tau_L \sim C_P^{1.5}$) [19,50,51]. The enhanced τ_L dependence on C_P is likely controlled by the effect of hydrophobic associations. In this respect, it should be noted that, the disengagement of one hydrophobic block from a micelle does not permit the relaxation of the entire chain, since the chain is still ″anchored″ by the many other hydrophobic blocks even in the absence of entanglements[52]. Additionally, the disengaged hydrophobic block tends to anchor on neighboring micelle again due to the solvent selectivity. Therefore, the entire chain cannot relax very fast compared to systems without association. While for G_N, since G′ in the plateau region cannot be strictly horizontal, here the G_N was determined as following equation based on crossover modulus-based method tailoring for polymers with low M_w and large molecular weight distribution[53]:

$$\log\frac{G_N}{G_x} = 0.38 + \frac{2.63log\frac{M_w}{M_n}}{1+2.45log\frac{M_w}{M_n}} \quad (6)$$

where the G_x is the crossover modulus. The transient network theory predicts that the plateau modulus is given by $G_N = \nu_0 kT$, where the ν_0 is the number density of elastically effective chain[21,54]. As shown in **Figure 5c**, the scaling exponent, $G_N \sim C_P^{3.2}$, is much larger than expected one. This difference in scaling possibly can be rationalized in terms of effective chain fraction effect. Specifically, not all the polymer chain acts as the effective chain. Here, we evaluate the fraction of effective chain defined as $f = G_N/\nu kT$ where ν is the entire chain number density of PBMA-PMAA-PBMA in the solution. As shown in **Figure 5d**, at low concentration, 0.79 mol/L for example, f is

only 6%, implying that up to 94% polymer chain has no contribution to the G_N. While at high concentration, 2.22 mol/L for example, *f* reaches up to 63%. The small change of C_P leads to drastic variation of effective chain fraction, resulting in the strong dependence of G_N on C_P.

2.3.4 Concentration dependence of gel transition temperature

In additionally, sol-gel transition temperature (T*) also shows a strong concentration dependence. As shown in **Figure 5d**, the T* changes from -0.5 to 8.8 ^oC on increasing concentration from 0.79 to 2.22 mol/L. It is known that intermolecular association between endblock chains is favored at higher concentration. Therefore, a network structure could be easily formed in the solutions with higher C_P resulting in higher sol-gel transition temperature. To further confirm the association from microscale, variable-temperature ^1H NMR was carried out. The peak assignments were performed and shown in **Figure 8**. From the series of ^{1}NMR spectra obtained between -30 and 50 ^oC of triblock copolymer solution with a concentration of 1.03 mol/L (**Figure 9a**), we can see that the characteristic signal of methylene groups of BMA, around 4.2 ppm, becomes sharper with increasing temperature and its area first remains almost unchanged with negligible value, then shows a dramatic decrease and finally arrives a plateau (**Figure 9b**). Therefore, the sol-gel transition temperature (T*) is actually a temperature range, rather than a specific temperature. Here the T* is defined as the midpoint of the temperature range, bounded by the tangents to the two flat regions of the curve. The dependence of T* resulting from NMR was shown in **Figure 9c**.

Compared with the T* obtained from rheology, the values resulting from NMR are slightly larger due to its high sensitivity.

2.3.5 Time-concentration superposition (TCSP)

If the concentration variation is regarded as an inverse of temperature variation, changing the concentration is analogous to changing the temperature. Similar with TTSP, the time-concentration superposition (TCSP) was performed over a range of concentration and deformation frequencies, allowing us to probe structural relaxation at each temperature. The G′, G″ and tanδ of triblock copolymer solution with different concentration measured at -20 ºC are shown in **Figure 10a-c**. As is apparent from **Figure 10**, each of these curves at given concentration can be shift horizontally and vertically to create a concentration master curve based on the shift factors shown in **Figure 10d**. The shift factors, a_c and b_c, follow power law correction with concentration given as: $a_c \sim C_P^{6.5}$ and $b_c \sim C_P^{-3.2}$. As shown in **Figure 10f**, the scaling obtained from TCPS ($\tau_L \sim C_P^{7.4}$, $G_N \sim C_P^{3.6}$) is perfectly similar with that of the dependence of τ_L and G_N calculated from TTSP ($\tau_L \sim C_P^{7.6}$, $G_N \sim C_P^{3.2}$) indicating reducing the temperature is equivalent to increasing concentration[16,36,55]. Furthermore, the TCPS were performed to probe the relaxation dynamics at various temperature. As shown in **Figure 11a-c**, the representative master curves at different temperatures show a similar shape, and the exponents of horizontal shift factor a_c obtained from master curves obtained at various temperatures was shown in **Figure 11d**. It is apparent that the exponent of shift horizontal factor a_c, a clue representing the energy needed for the

endblock chain pullout from micelle, is a strong function of the temperature. It is because the micelles formation is a result of relative change in interaction between the solvent and the endblocks, quantitated by Flory-Huggins Parameter χ as follows:

$$\chi = V_{seg}(\delta_a - \delta_b)^2/RT \quad (7)$$

where V_{seg} is the actual volume of a polymer segment, the δ_{a} and δ_{a} is the Hildebrand solubility parameters. From equation (7), the temperature plays a key role on endblock solvency, hence the micelle formation.

2.3.6 Possible mechanism for the thermal-induced sol-gel transition

Based on above explanation, another question should be asked: whether the χ between the midblock and solvent is temperature sensitive or not? Although the temperature dependence of χ between midblocks and solvent has not been determined experimentally, some visual observation presented in **Figure 12** gives us some indirect evidence. **Figure 12** displays representative images of homopolymer samples, PBMA and PMAA, and triblock copolymer PBMA -PMAA-PBMA, in DMF solvent with same monomer concentration (1.08 mol/L). At 25 ^{o}C, all samples show transparent and good flowability, indicating the complete solubility of all the polymers. As the temperature decreases to -20 ^{o}C, the triblock copolymer solution transfers to gel, demonstrating phase separation. While PBMA solution precipitated without the protection of PMAA. This behavior shows that a strong temperature dependence of phase behaviors of the χ of PBMA. In contrast, the PMAA sample remained transparent with similar viscosity at both low and high temperatures, illustrating the good solubility

of PMAA over the experimental temperature range. This is also supported by the rheological behaviors of homo PMAA presented in **Figure 13**. The typical dynamic moduli G′ and G″ of PMAA solutions with a concentration of 1.80 mol/L measured at various temperatures (**Figure 13 a-b**) can be shifted horizontally to a reference temperature (-20 ºC) to generate a master curve (**Figure 13c**). Unlike the triblock copolymer system, the lna_T-1/T curve of homo PMAA solution shows linear relation over the whole temperature range. Based on the equation (1), the activation energy was calculated as ~20 kJ/mol. This value is much smaller than that obtained at low temperature R-I and comparable to the value obtained at high temperature R-II, demonstrating that the activation energy should origin from chain friction. This behavior confirms that there is no supramolecular structure formed in the homo PMAA solution over a wide range of temperatures. In additionally, similar experimental phenomena are observed in PMAA solution with different concentration (**Figure 14**). Consequently, the mechanism of this thermal-induced sol-gel transition for PBMA-PMAA-PBMA solution is proposed as follows. At the sol-region, the endblock shows good solubility in DMF solution, with a free state. When shifting towards to the high C_P- low T, the samples become gel, demonstrating the endblock chains collapsed into micelles due to the poor solubility. This is also supported by the ^{1}NMR in **Figure 5** in which the lower chain mobility at lower temperature due to freeze micelle state.

2.4 Conclusion

It is investigated that the relaxation dynamics of thermal-induced sol-gel transition in

the triblock copolymer consisting of PBMA-PMAA-PBMA in midblock selective solvent, DMF. The activation energy of micelle relaxation was explored using TTSP on small-amplitude frequency sweep measurements by fitting the temperature dependence of the shift factors with an Arrhenius equation. A break in slope of $\ln a_T$-1/T curve separates the activation energy of micelle relaxation from chain friction of entanglements. The activation energy of micelle relaxation, originating from endblock chain pullout from micelle, is independent of the triblock copolymer concentration. It is because the energy barrier for chain pullout is determined by $\chi N_{micelle}$, where χ is the endblock-solvent interaction parameter, and $N_{micelle}$ is the degree polymerization of endblock chain. The corresponding relaxation time of micelle also calculated and compared with longest relaxation time (τ_L). The endblock chain pullout time $\tau_{pullout}$ is much smaller than the τ_L. Despites of the concentration independence of relaxation micelles, the higher concentration induces higher sol-gel transition temperature (T*) because that intermolecular association between endblock chains is favored at higher concentration.

2.5 Reference

(1) Muthiah, P.; Hoppe, S. M.; Boyle, T. J.; Sigmund, W. Thermally Tunable Surface Wettability of Electrospun Fiber Mats: Polystyrene/Poly (N-isopropylacrylamide) Blended versus Crosslinked Poly [(N-isopropylacrylamide)-co-(methacrylic Acid)]. *Macromol. Rapid Commun.* **2011**, *32* (21), 1716–1721.

(2) Nath, N.; Chilkoti, A. Creating “smart” Surfaces Using Stimuli Responsive Polymers. *Adv. Mater.* **2002**, *14* (17), 1243–1247.

(3) Xu, X.; Flores, J. D.; McCormick, C. L. Reversible Imine Shell Cross-Linked Micelles from Aqueous RAFT-Synthesized Thermoresponsive Triblock Copolymers as Potential Nanocarriers for “pH-Triggered” Drug Release. *Macromolecules* **2011**, *44* (6), 1327–1334.

(4) Zhang, Z.; Wang, J.; Nie, X.; Wen, T.; Ji, Y.; Wu, X.; Zhao, Y.; Chen, C. Near Infrared Laser-Induced Targeted Cancer Therapy Using Thermoresponsive Polymer Encapsulated Gold Nanorods. *J. Am. Chem. Soc.* **2014**, *136* (20), 7317–7326.

(5) Gupta, M. K.; Martin, J. R.; Werfel, T. A.; Shen, T.; Page, J. M.; Duvall, C. L. Cell Protective, ABC Triblock Polymer-Based Thermoresponsive Hydrogels with ROS-Triggered Degradation and Drug Release. *J. Am. Chem. Soc.* **2014**, *136* (42), 14896–14902.

(6) Wang, B.; Liu, H.-J.; Jiang, T.-T.; Li, Q.-H.; Chen, Y. Thermo-, and pH Dual-Responsive Poly (N-Vinylimidazole): Preparation, Characterization and Its Switchable Catalytic Activity. *Polymer (Guildf).* **2014**, *55* (23), 6036–6043.

(7) Bergbreiter, D. E.; Case, B. L.; Liu, Y.-S.; Caraway, J. W. Poly (N-Isopropylacrylamide) Soluble Polymer Supports in Catalysis and Synthesis. *Macromolecules* **1998**, *31* (18), 6053–6062.

(8) Lu, Y.; Yuan, J.; Polzer, F.; Drechsler, M.; Preussner, J. In Situ Growth of

Catalytic Active Au− Pt Bimetallic Nanorods in Thermoresponsive Core− Shell Microgels. *ACS Nano* **2010**, *4* (12), 7078–7086.

(9) Twaites, B. R.; de las Heras Alarcón, C.; Lavigne, M.; Saulnier, A.; Pennadam, S. S.; Cunliffe, D.; Górecki, D. C.; Alexander, C. Thermoresponsive Polymers as Gene Delivery Vectors: Cell Viability, DNA Transport and Transfection Studies. *J. Control. release* **2005**, *108* (2–3), 472–483.

(10) Dinçer, S.; Tuncel, A.; Pişkin, E. A Potential Gene Delivery Vector: N-isopropylacrylamide-ethyleneimine Block Copolymers. *Macromol. Chem. Phys.* **2002**, *203* (10-11), 1460–1465.

(11) Reese, C. E.; Mikhonin, A. V; Kamenjicki, M.; Tikhonov, A.; Asher, S. A. Nanogel Nanosecond Photonic Crystal Optical Switching. *J. Am. Chem. Soc.* **2004**, *126* (5), 1493–1496.

(12) Zhu, H.; Li, Y.; Qiu, R.; Shi, L.; Wu, W.; Zhou, S. Responsive Fluorescent Bi2O3@ PVA Hybrid Nanogels for Temperature-Sensing, Dual-Modal Imaging, and Drug Delivery. *Biomaterials* **2012**, *33* (10), 3058–3069.

(13) Wu, W.; Zhou, T.; Berliner, A.; Banerjee, P.; Zhou, S. Smart Core− Shell Hybrid Nanogels with Ag Nanoparticle Core for Cancer Cell Imaging and Gel Shell for pH-Regulated Drug Delivery. *Chem. Mater.* **2010**, *22* (6), 1966–1976.

(14) Liu, S.; Qiao, W.; Cao, G.; Chen, Y.; Ma, Y.; Huang, Y.; Liu, X.; Xu, W.; Zhao, Q.; Huang, W. Smart Poly (N-isopropylacrylamide) Containing Iridium (III) Complexes as Water-Soluble Phosphorescent Probe for Sensing and Bioimaging

of Homocysteine and Cysteine. *Macromol. Rapid Commun.* **2013**, *34* (1), 81–86.

(15) Charbonneau, C.; Chassenieux, C.; Colombani, O.; Nicolai, T. Controlling the Dynamics of Self-Assembled Triblock Copolymer Networks via the pH. *Macromolecules* **2011**, *44* (11), 4487–4495.

(16) Henderson, K. J.; Shull, K. R. Effects of Solvent Composition on the Assembly and Relaxation of Triblock Copolymer-Based Polyelectrolyte Gels. *Macromolecules* **2012**, *45* (3), 1631–1635.

(17) Meng, F.; Pritchard, R. H.; Terentjev, E. M. Stress Relaxation, Dynamics, and Plasticity of Transient Polymer Networks. *Macromolecules* **2016**, *49* (7), 2843–2852.

(18) Leibler, L.; Rubinstein, M.; Colby, R. H. Dynamics of Reversible Networks. *Macromolecules* **1991**, *24* (16), 4701–4707.

(19) Rubinstein, M.; Semenov, A. N. Dynamics of Entangled Solutions of Associating Polymers. *Macromolecules* **2001**, *34* (4), 1058–1068.

(20) Rubinstein, M.; Semenov, A. N. Thermoreversible Gelation in Solutions of Associating Polymers. 2. Linear Dynamics. *Macromolecules* **1998**, *31* (4), 1386–1397.

(21) Tanaka, F.; Edwards, S. F. Viscoelastic Properties of Physically Crosslinked Networks. 1. Transient Network Theory. *Macromolecules* **1992**, *25* (5), 1516–1523.

(22) Anderson, J. A.; Lorenz, C. D.; Travesset, A. Micellar Crystals in Solution from

Molecular Dynamics Simulations. *J. Chem. Phys.* **2008**, *128* (18), 184906.

(23) Beltran-Villegas, D. J.; Lyubimov, I.; Jayaraman, A. Molecular Dynamics Simulations and PRISM Theory Study of Solutions of Nanoparticles and Triblock Copolymers with Solvophobic End Blocks. *Mol. Syst. Des. Eng.* **2018**.

(24) Chantawansri, T. L.; Sirk, T. W.; Mrozek, R.; Lenhart, J. L.; Kröger, M.; Sliozberg, Y. R. The Effect of Polymer Chain Length on the Mechanical Properties of Triblock Copolymer Gels. *Chem. Phys. Lett.* **2014**, *612*, 157–161.

(25) Wakimoto, K.; Sasaki, H.; Arai, N. Dissipative Particle Dynamics Simulation of the Relaxation Behaviour of a Triblock Copolymer Supramolecular Network. *Mol. Simul.* **2018**, *44* (7), 534–539.

(26) Meli, L.; Lodge, T. P. Equilibrium vs Metastability: High-Temperature Annealing of Spherical Block Copolymer Micelles in an Ionic Liquid. *Macromolecules* **2009**, *42* (3), 580–583.

(27) Watanabe, H.; Sato, T.; Osaki, K. Concentration Dependence of Loop Fraction in Styrene− Isoprene− Styrene Triblock Copolymer Solutions and Corresponding Changes in Equilibrium Elasticity. *Macromolecules* **2000**, *33* (7), 2545–2550.

(28) Sato, T.; Watanabe, H.; Osaki, K. Thermoreversible Physical Gelation of Block Copolymers in a Selective Solvent. *Macromolecules* **2000**, *33* (5), 1686–1691.

(29) Tsitsilianis, C.; Iliopoulos, I.; Ducouret, G. An Associative Polyelectrolyte End-Capped with Short Polystyrene Chains. Synthesis and Rheological

Behavior. *Macromolecules* **2000**, *33* (8), 2936–2943.

(30) Stavrouli, N.; Aubry, T.; Tsitsilianis, C. Rheological Properties of ABA Telechelic Polyelectrolyte and ABA Polyampholyte Reversible Hydrogels: A Comparative Study. *Polymer (Guildf).* **2008**, *49* (5), 1249–1256.

(31) Pham, Q. T.; Russel, W. B.; Thibeault, J. C.; Lau, W. Micellar Solutions of Associative Triblock Copolymers: The Relationship between Structure and Rheology. *Macromolecules* **1999**, *32* (15), 5139–5146.

(32) Berret, J.-F.; Calvet, D.; Collet, A.; Viguier, M. Fluorocarbon Associative Polymers. *Curr. Opin. Colloid Interface Sci.* **2003**, *8* (3), 296–306.

(33) Zana, R.; Marques, C.; Johner, A. Dynamics of Micelles of the Triblock Copolymers Poly (Ethylene Oxide)–poly (Propylene Oxide)–poly (Ethylene Oxide) in Aqueous Solution. *Adv. Colloid Interface Sci.* **2006**, *123*, 345–351.

(34) Popescu, M.-T.; Athanasoulias, I.; Tsitsilianis, C.; Hadjiantoniou, N. A.; Patrickios, C. S. Reversible Hydrogels from Amphiphilic Polyelectrolyte Model Multiblock Copolymers: The Importance of Macromolecular Topology. *Soft Matter* **2010**, *6* (21), 5417–5424.

(35) Nicolai, T.; Colombani, O.; Chassenieux, C. Dynamic Polymeric Micelles versus Frozen Nanoparticles Formed by Block Copolymers. *Soft Matter* **2010**, *6* (14), 3111–3118.

(36) Daga, V. K.; Wagner, N. J. Linear Viscoelastic Master Curves of Neat and Laponite-Filled Poly (Ethylene Oxide)–water Solutions. *Rheol. acta* **2006**, *45*

(6), 813–824.

(37) Spruijt, E.; Sprakel, J.; Lemmers, M.; Stuart, M. A. C.; van der Gucht, J. Relaxation Dynamics at Different Time Scales in Electrostatic Complexes: Time-Salt Superposition. *Phys. Rev. Lett.* **2010**, *105* (20), 208301.

(38) Castelletto, V.; Hamley, I. W.; Xue, W.; Sommer, C.; Pedersen, J. S.; Olmsted, P. D. Rheological and Structural Characterization of Hydrophobically Modified Polyacrylamide Solutions in the Semidilute Regime. *Macromolecules* **2004**, *37* (4), 1492–1501.

(39) Zhang, S.; Lee, K. H.; Sun, J.; Frisbie, C. D.; Lodge, T. P. Viscoelastic Properties, Ionic Conductivity, and Materials Design Considerations for Poly (Styrene-B-Ethylene Oxide-B-Styrene)-Based Ion Gel Electrolytes. *Macromolecules* **2011**, *44* (22), 8981–8989.

(40) Tanaka, F. Theoretical Study of Molecular Association and Thermoreversible Gelation in Polymers. *Polym. J.* **2002**, *34* (7), 479.

(41) Peters, A. J.; Lodge, T. P. Comparison of Gel Relaxation Times and End-Block Pullout Times in ABA Triblock Copolymer Networks. *Macromolecules* **2016**, *49* (19), 7340–7349.

(42) Inomata, K.; Nakanishi, D.; Banno, A.; Nakanishi, E.; Abe, Y.; Kurihara, R.; Fujimoto, K.; Nose, T. Association and Physical Gelation of ABA Triblock Copolymer in Selective Solvent. *Polymer (Guildf).* **2003**, *44* (18), 5303–5310.

(43) Kjøniksen, A.-L.; Laukkanen, A.; Galant, C.; Knudsen, K. D.; Tenhu, H.;

Nyström, B. Association in Aqueous Solutions of a Thermoresponsive PVCL-G-C11EO42 Copolymer. *Macromolecules* **2005**, *38* (3), 948–960.

(44) Owczarz, P.; Ziółkowski, P.; Dziubiński, M. The Application of Small-Angle Light Scattering for Rheo-Optical Characterization of Chitosan Colloidal Solutions. *Polymers (Basel).* **2018**, *10* (4), 431.

(45) Zhang, Z.; Huang, C.; Weiss, R. A.; Chen, Q. Association Energy in Strongly Associative Polymers. *J. Rheol. (N. Y. N. Y).* **2017**, *61* (6), 1199–1207.

(46) Seitz, M. E.; Burghardt, W. R.; Faber, K. T.; Shull, K. R. Self-Assembly and Stress Relaxation in Acrylic Triblock Copolymer Gels. *Macromolecules* **2007**, *40* (4), 1218–1226.

(47) Tanaka, F.; Edwards, S. F. Viscoelastic Properties of Physically Crosslinked Networks: Part 2. Dynamic Mechanical Moduli. *J. Nonnewton. Fluid Mech.* **1992**, *43* (2–3), 273–288.

(48) Heo, Y.; Larson, R. G. The Scaling of Zero-Shear Viscosities of Semidilute Polymer Solutions with Concentration. *J. Rheol. (N. Y. N. Y).* **2005**, *49* (5), 1117–1128.

(49) Rubinstein, M.; Colby, R. H. *Polymer Physics*; Oxford university press New York, 2003; Vol. 23.

(50) Khatory, A.; Lequeux, F.; Kern, F.; Candau, S. J. Linear and Nonlinear Viscoelasticity of Semidilute Solutions of Wormlike Micelles at High Salt Content. *Langmuir* **1993**, *9* (6), 1456–1464.

(51) Cates, M. E. Reptation of Living Polymers: Dynamics of Entangled Polymers in the Presence of Reversible Chain-Scission Reactions. *Macromolecules* **1987**, *20* (9), 2289–2296.

(52) Regalado, E. J.; Selb, J.; Candau, F. Viscoelastic Behavior of Semidilute Solutions of Multisticker Polymer Chains. *Macromolecules* **1999**, *32* (25), 8580–8588.

(53) Liu, C.; He, J.; Van Ruymbeke, E.; Keunings, R.; Bailly, C. Evaluation of Different Methods for the Determination of the Plateau Modulus and the Entanglement Molecular Weight. *Polymer (Guildf).* **2006**, *47* (13), 4461–4479.

(54) Jacq, K.; David, F.; Sandra, P. Analysis of Residual Solvents in Pharmaceuticals Using Static Headspace-GC-FID/MS, Agilent Technologies Publication 5989-9726EN. 2008.

(55) Liu, J.; Cao, D.; Zhang, L.; Wang, W. Time− Temperature and Time− Concentration Superposition of Nanofilled Elastomers: A Molecular Dynamics Study. *Macromolecules* **2009**, *42* (7), 2831–2842.

Table 1. Discription of triblock copolymer and homopolymer

Code[a)]	[b)]**Polymer**	[c)]**Mn [kg/mol]**	[d)]$\mathbf{M_w/M_n}$	[e)]$\mathbf{f_B}$
ABA- C_P	$A_{75}B_{81}A_{75}$	28.6	1.38	0.35
A-C_P	$PBMA_{223}$	37.1	1.22	0
B-C_P	$PMAA_{498}$	42.9	1.37	1

[a)] A, B represent poly(butyl methacrylate) and poly(methacrylic acid), respectively. C_P represents the monomer concentration (mol/L); [b)] the superscripts represent the degree of polymerization; [c,d)] number-averaged molecular weight and molecular weight distribution; [e)]molar ratio of midblock chain in a chain.

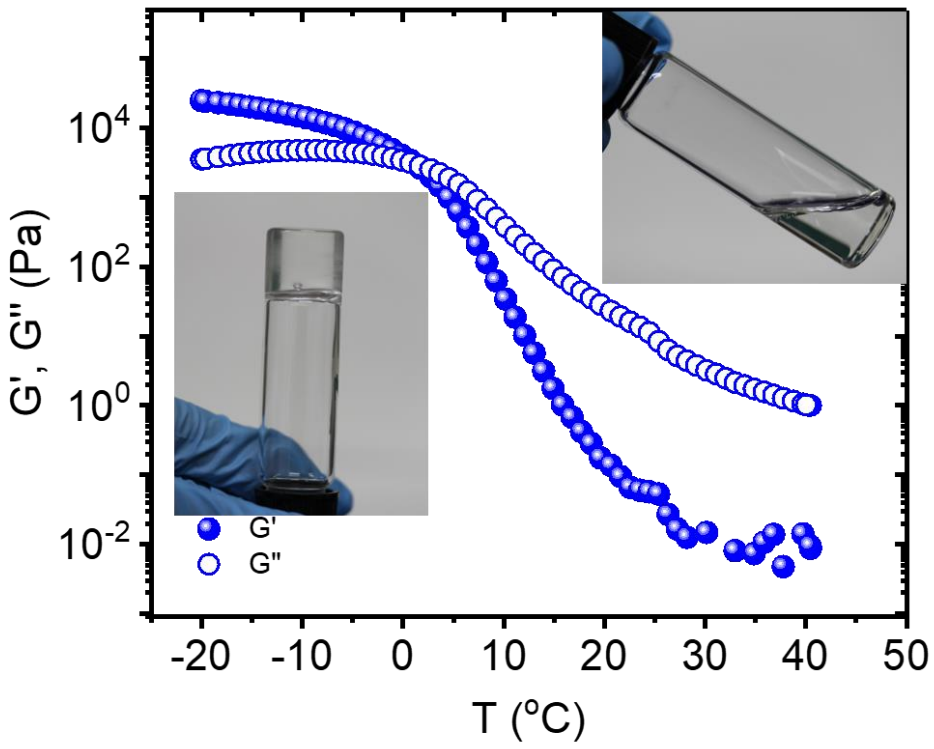

Figure 1. Temperature dependence of storage modulus, G′ (filled) and loss modulus, G″ (unfilled) at ω= 10 rad/s for 1.98 mol/L triblock copolymer in DMF solvent.

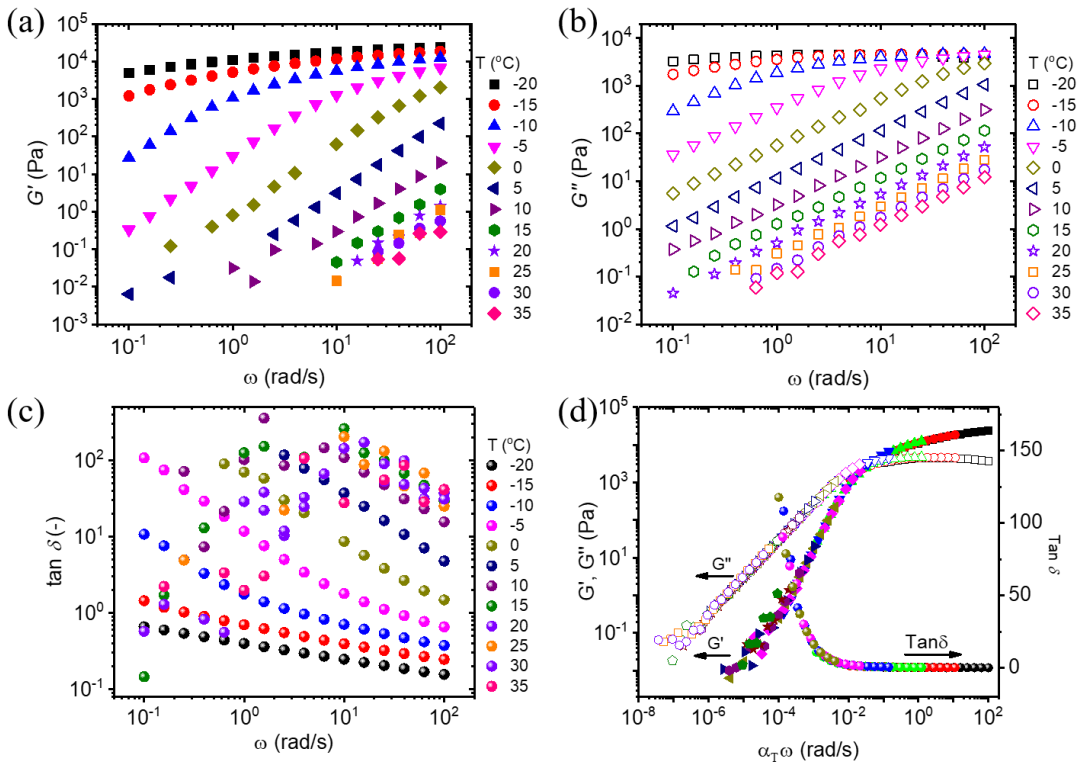

Figure 2. Frequency dependence of the storage moduli G' (a), the loss moduli G'' (b) and the loss factor tanδ for 1.98 mol/L triblock copolymer solution at different temperatures and a strain of 0.5%. (d) Time-temperature superposition master curve deduced from the data reported in (a-c) using one rescaling coefficient: α_T for the angular frequency. Reference temperature: -20 °C.

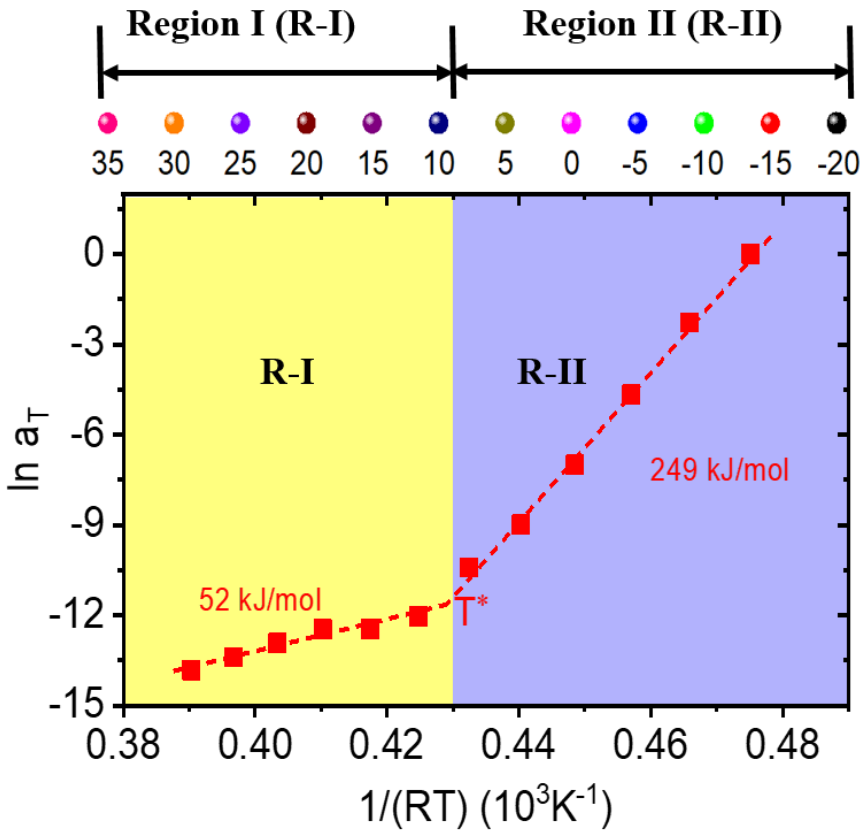

Figure 3. Arrhenius plot depicting the temperature dependence of the shift factors used to generate master curve. The apparent activation energy values were calculated from the slope of the curve. The two regions (R-I, R-II) are related to two different activation energies: the apparent activation energy at higher temperature and the association activation energy at lower temperature. The critical temperature is simply called as T^*.

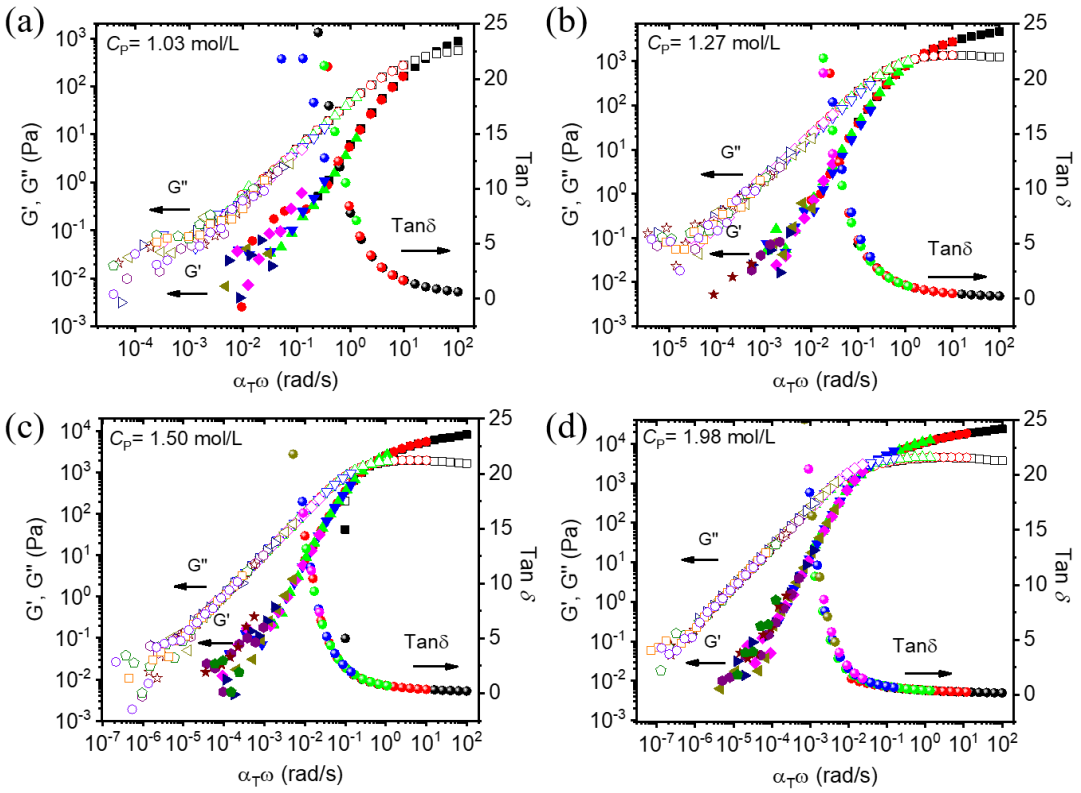

Figure 4. Representative Time-temperature superposition master curves illustraing storage modulus G', loss modulus G'' and loss factor tanδ for triblock copolymer solution with concentration of (a) C_p = 1.03 mol/L, (b) C_p = 1.27 mol/L, (c) C_p = 1.50 mol/L and (d) C_p = 1.98 mol/L; Reference temperature: -20 °C. (e) Arrhenius plot depicting the temperature dependence of the shift factors used for generating master curves in triblock copolymer solutions with different concentrations.

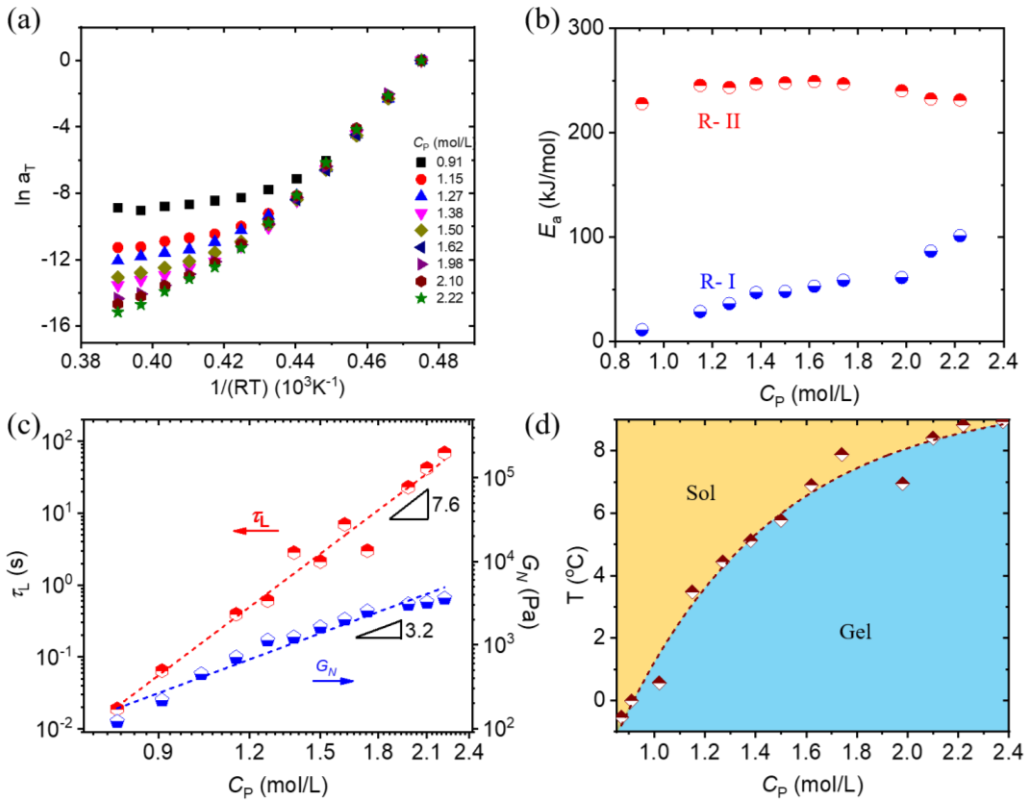

Figure 5. (a) Representative Arrhenius plot depicting the temperature dependence of the shift factors used to generate master curve. (b) The dependence of activation energies on the concentration in R-I and R-II; (c) The dependence of longest relaxation time τ_L and plateau modulus G_N on the concentration at -20 °C. (d) Phase diagram obtained from critical temperature T* from R-I to R-II.

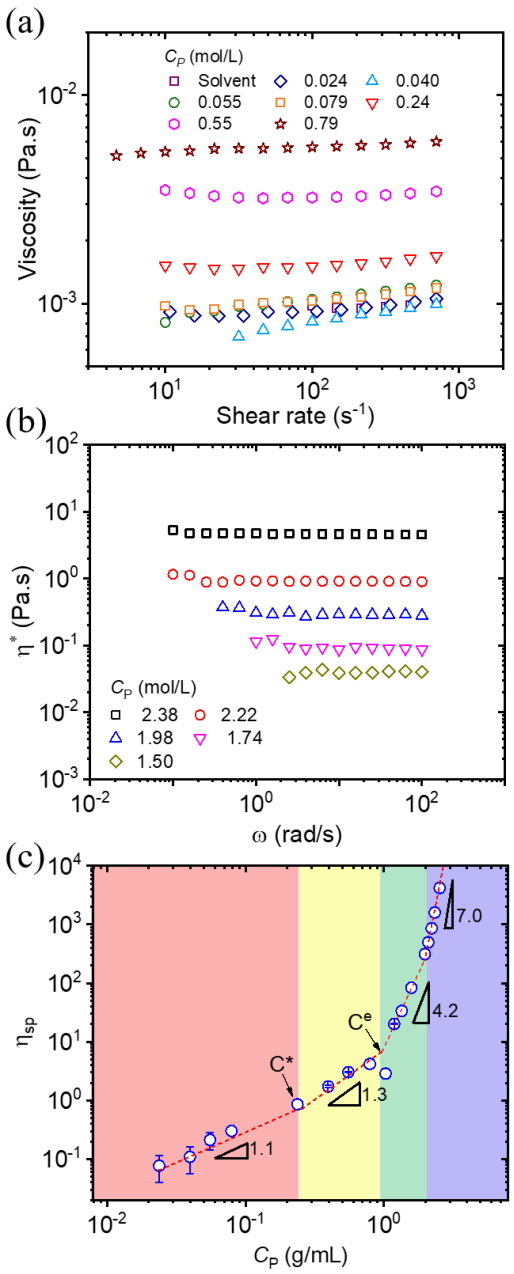

Figure 6. (a) Shear viscosity vs shear rate for triblock copolymer solutions at concentrations ranges from 0.001 to 0.1 g/mL. (b) Complex viscosity vs frequency for triblock copolymer solutions at concentrations ranges from 0.1 to 0.3 g/mL. (c) Concentration dependence of the specific viscosity η_{sp}. The four domains are related to four different concentration regimes: dilute, semidilute non-entangled, semidilute entangled and concentrated entangled regions, respectively. Temperature: 25 °C.

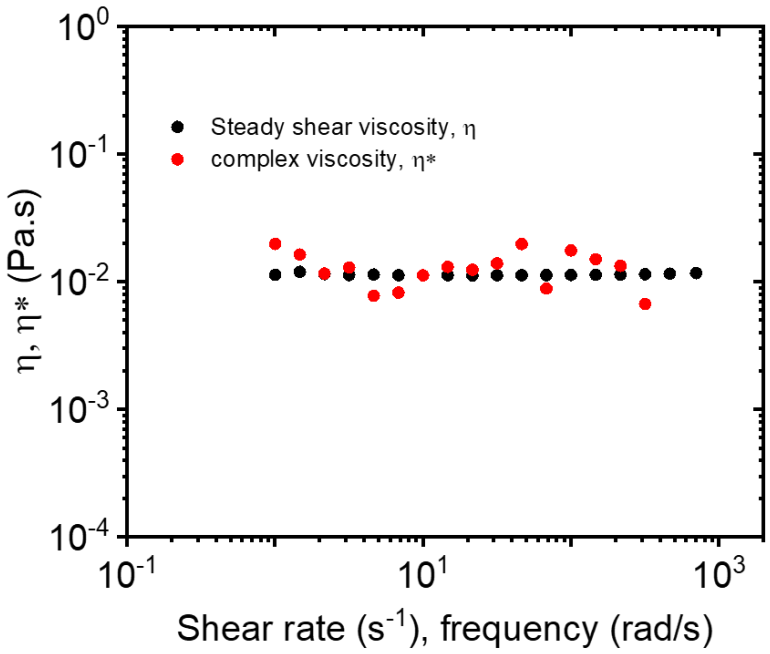

Figure 7. Steady shear viscosity and dynamic viscosity for triblock copolymer solution with a concentration of 1.62 mol/L.

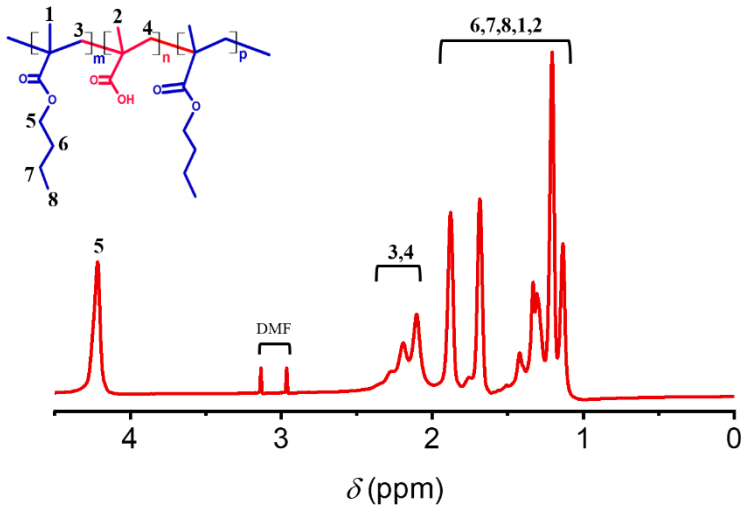

Figure 8. 1H NMR spectrum of triblock copolymer solution, recorded in DMF-D7, with peak assignments.

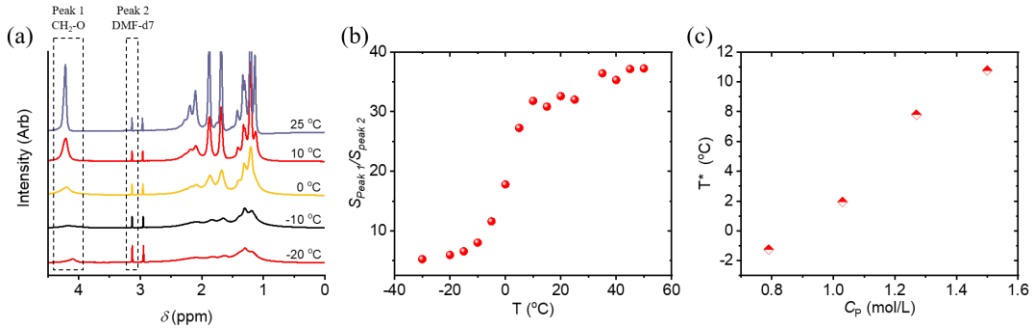

Figure 9. (a) Temperature variation of 1H NMR spectrum of triblock copolymer with a concentration of 1.80 mol/L and (b) The temperature dependence of normalized area of CH_2-O signal at various concentrations. (c) Concentration dependence of sol-gel transition points.

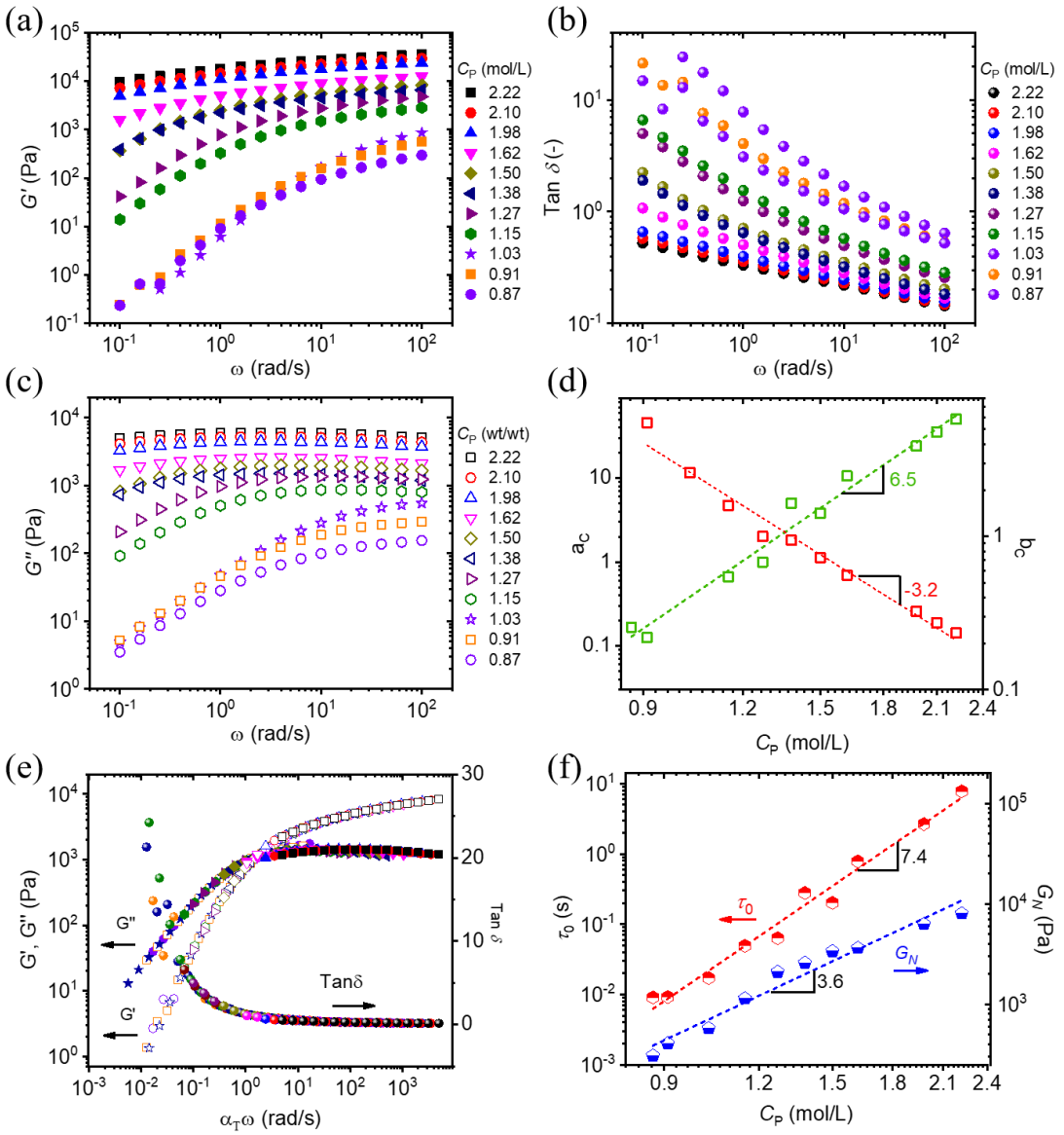

Figure 10. (a) Frequency dependence of the storage modulus G′ (a), the loss modulus G″ (b) and loss factor tanδ (c) for triblock copolymer solutions at different concentrations at -20 ºC; Reference concentration: 1.98 mol/L. (d) the concentration dependence of horizontal shift factor α_c and vertical shift factor b_c used for generating the Time-concentration superposition master curves; (e) Master curve deduced from the data in (a-c) using two rescaling coefficients: b_c for the modulus and α_c for the angular frequency. (f) Concentration dependence of the longest relaxation time τ_0 and G_N. Reference concentration: 1.98 mol/L.

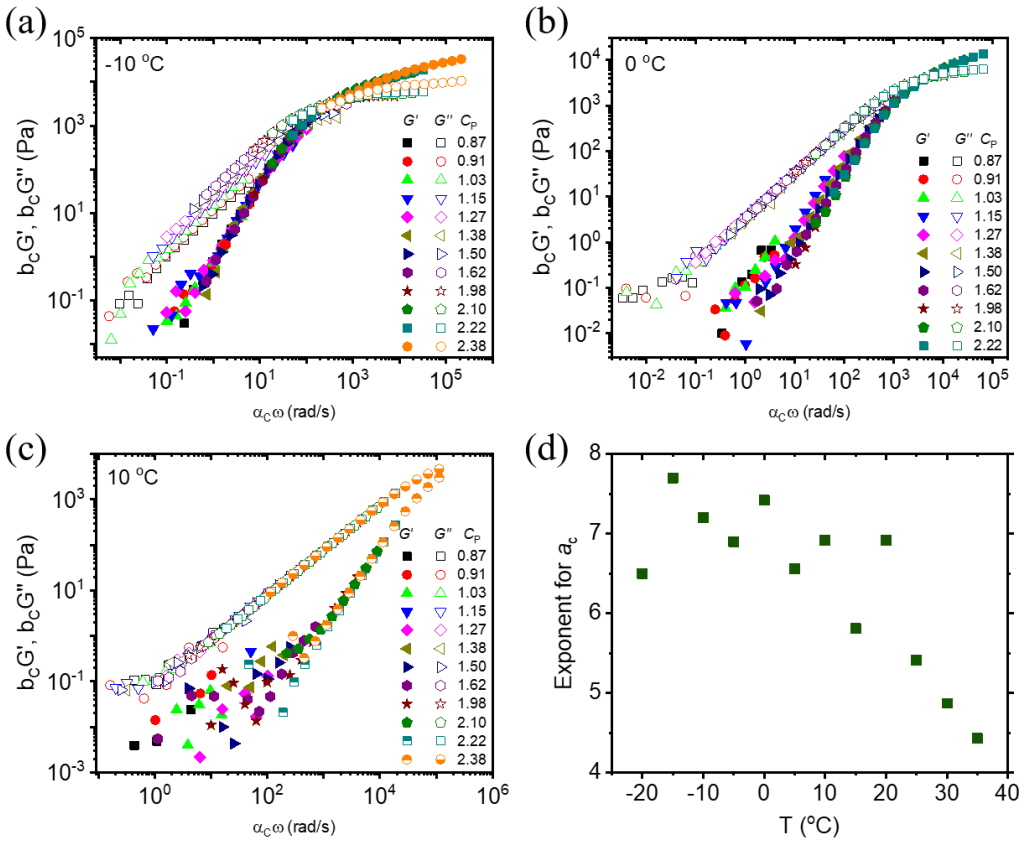

Figure 11. Representative Time-concentration superposition master curves illustraing storage modulus G', loss modulus G'' and loss factor tanδ for triblock copolymer solution at temperature of (a) T = -10 ºC, (b) T = 0 ºC and (c) T = 10 ºC; Reference concentration: 1.98 mol/L. (d) Temperature dependences of exponent of horizontal shift factors α_c used for generating master curves in triblock copolymer solutions at different temperature.

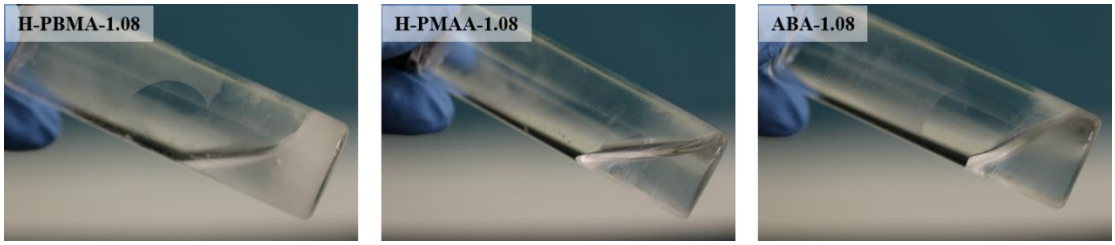

Figure 12. Optical figures of triblock copolymer and corresponding homo-polymers of PBMA and PMAA at -20 ºC. Concentration: 1.08 mol/L.

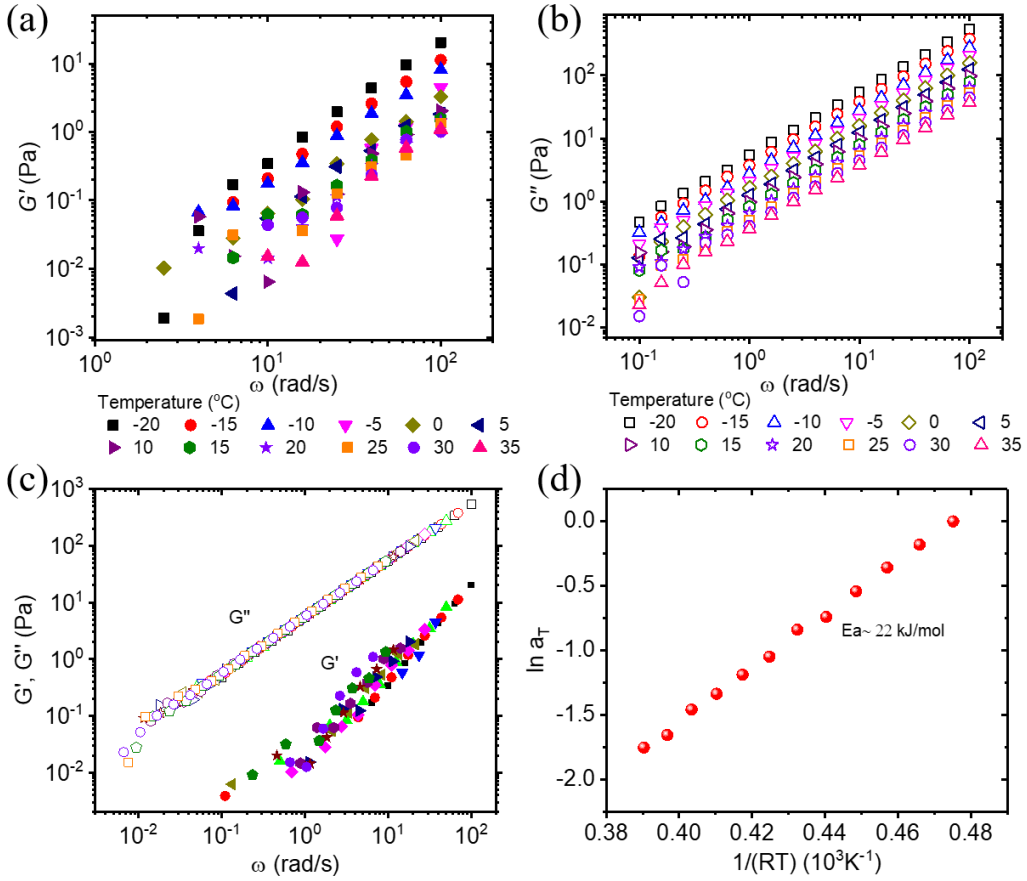

Figure 13. Frequency dependence of the storage moduli G' (a), the loss moduli G'' (b) for 1.80 mol/L homo PMAA solution at different temperatures and a strain of 0.5%. (c) Time-temperature superposition master curve deduced from the data reported in (a-b) using one rescaling coefficient: α_T for the angular frequency. Reference temperature: -20 °C; (d) the Arrehnius plot derived from (c) for homo PMAA with concentration of 1.80 mol/L.

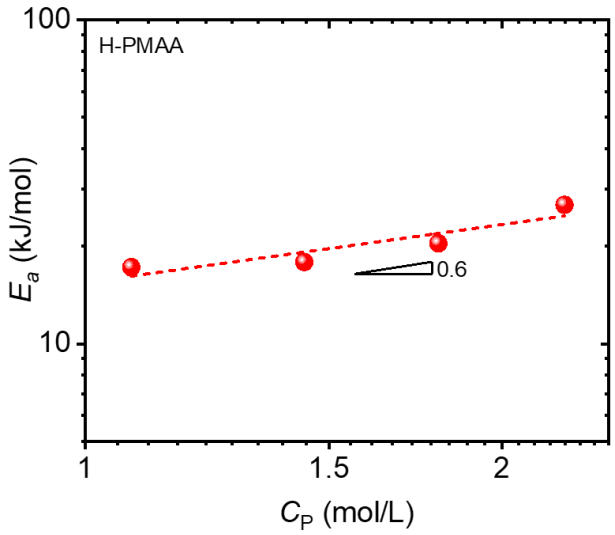

Figure 14. The dependence of activation energies on the concentration.

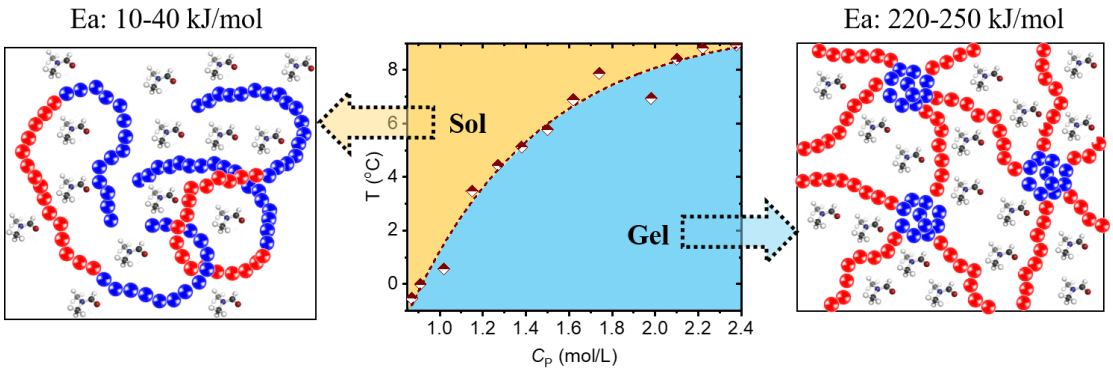

Figure 15. Scheme of the structure of triblock copolymer solutions in different phases. The midblock chain PMAA and endblock chain PBMA are represented in red and blue, respectively. The solvent DMF is represented in ball-and-stick model. The blue intermolecular associations due to organophobic interaction are represented in blue micelles.

Chapter 3: Contribution of Physical Crosslinks and Trapped Entanglements in Transient Network of Triblock Copolymer in Aqueous Condition

3.1 Introduction

Long linear polymers even without crosslinks exhibit many properties indicating the existence of a temporary network formed by entanglements[1]. For example, the specific viscosity dependence of polymer concentration above certain molecular weight shows a sharp transition in exponent from 1 to 3.9 at critical concentration[2]; Oscillatory dynamic measurements show a pseudo-equilibrium rubber plateau which can completely recover for short time deformations[3]. After the introduction of chemical crosslinks, the contribution of entanglements and newly introduced crosslinks to the elastic network is very essential for their macroscopic behavior. Most of entanglements are permanently trapped in the network due to the presence of cross-links, providing topological constraints yielding additional elastic modulus[4]. The entire network can be regarded as superposition of two networks originated from entanglements and crosslinks, which can be interpreted quantitatively by Edwards tube model[5]. The modulus of the entangled polymer network can be approximated as a simple sum[6]:

$$G \cong G_c + G_e \approx \rho RT \left(\frac{1}{M_c} + \frac{1}{M_e}\right) \quad (1)$$

Where the G, G_c and G_e is the total modulus, crosslink modulus and entangled modulus,

respectively. ρ is the network density (mass per unit volume), R is the gas constant, T is the Kelvin temperature, M_c and M_e is the number-averaged molar mass of a network strand from crosslinks and entanglements, respectively. In modern molecular theories field, modeling entanglement effects to rubber elasticity has been a focus. Several molecular models employing different treatments of entanglements have been proposed, including diffused-constraint model[7], slip-link model[8] and tube models of several version[9–12]. Some of models have been compared with experiments results. Ferry used the two-network model to describe uniaxial extension experiments for extracting the contribution of trapped entanglements from crosslinks to elastic modulus on 1,2-polytbutadiene crosslinked near T_g by γ-irradiation[5]. Klüppel calculates the contribution ratio of crosslinks and entanglements to the reduced stress from experimental stress-strain data[13]. Kohijya et al. successfully used the slip-link model to describe the biaxial stress-train curves of the end-linked poly(dimethyl siloxane) with different entanglement densities[4].

Besides the theoretical fields, since 2003, Gong et al. uses the concept of trapped entanglements in chemical crosslinked networks, for the first time to prepare high-strength tough double network gels (DN hydrogel)[14,15]. In their work, the high toughness of BN gels originates from a double network structure inside the gels: reinforcing a tightly cross-linked rigid gel (first network) with mutually entangled flexible long polymers (second network) penetrating in the first network. The applications of this concept enabling enormous tough materials being prepared. And

one might argue this is a key step in the industrialization of synthetic biology leading to a new era of biotechnology. The only disadvantage of the common DN gel is that they have permanent internal damage after applying large deformation because internal covalent-bond fractures in the brittle first network are irreversible. Recent work has replaced the covalent bonds of the tough DN gels with physical (non-covalent) alternatives, including hydrogen bond, ionic bond or hydrophobic associations that allow the sacrificial bonds to be re-formed[16–21]. Studies along these lines have successfully produced tough hydrogels with partial or full self-recovery after internal rupture[18]. Sun et al[17]. demonstrated that the key role of entanglement in their tough, self-recoverable polyampholytes gel. Clearly, these are interesting systems due to coexistence of physical crosslinks and entanglements, while from the theoretical viewpoint, nevertheless, contributions from each part to the macroscopic mechanical performance is still unclear.

In the present study, we extract the entanglements from physical crosslinks in endblock triblock copolymer networks with different entanglement densities. Using solvent exchange process, the triblock copolymer gels are prepared from the solutions with different precursor solutions followed by introduction of physical crosslink through self-assembly of endblocks. Firstly, the triblock copolymer was dissolved in its good solvent, dimethylformamide DMF. At the uncrosslinked state, the time-temperature superposition was performed to capture the plateau modulus originating from the entanglement. By solvent exchange process, the physical crosslinks were locally

formed by self-assembly of endblock into micelles. The stress relaxation and uniaxial tensile measurements were used to probe the elastic modulus in final gels. Finally, the entanglement contribution to the final gel modulus was successfully extracted from physical crosslinked network.

3.2 Experiments

3.2.1 Materials

The amphiphilic triblock copolymers, poly(butyl methacrylate)-b-poly(methacrylic acid)-b-poly(butyl methacrylate) (PBMA-b-PMAA-b-PBMA), and corresponding homo-PBMA and homo-PMAA were synthesized by the Otsuka Chemical Co., Ltd., Japan (**Table 1**). The solvent dimethylformamide (DMF) were purchased from Wako Pure Chemical Industries, Ltd. (Japan).

3.2.2 Preparation of triblock copolymer gels (B gels)

A solution of triblock copolymer/N,N-dimethylformamide was poured onto the glass surface confined by a spacer with dimensions of 60 mm × 60 mm × 1.5 mm. The solution was fixed through surface gelation induced by spraying water vapor on the solution surface for several minutes. Then, the surface solidified solution was immersed in water for 3 days for solvent exchange.

3.2.3 Characterization

3.2.3.1 Rheology

An ARES-2 rheometer (TA Instruments) was used with a concentric cylinder geometry of 27.66mm bob diameter, 30 mm cup diameter and 41.5 mm bob length. Steady shear tests were performed in the shear rate range from 10^{-3} to 10^{3} s^{-1} with 5 min as the maximum point time to ensure equilibrium is attained at every test point. All the steady shear tests were performed at at 25 ºC for triblock concentration ranges from 7.92 mmol L^{-1} to 0.792 mol L^{-1}. Dynamic measurements were performed in the linear viscoelastic regime. The dynamic frequency sweep experiment was performed from 0.01 to 100 rad s^{-1} with a strain of 0.5% over a temperature range of -20 ºC to 35 ºC with a temperature interval of 5 ºC. The data was processed using the manual shifting mode to perform time-temperature superpositions (TTSP) and spectrum calculations.

3.2.3.2 Stress-relaxation test

A strain-controlled rheometer (ARES, TA Instruments) fitted with 25mm parallel plates was used for stress relaxation experiments. Humidity control is by means of a water bath. The gels were fixed on the parallel plate fixtures by glue. Due to the sensitivity to sample loading and shear history, protocols as following were adopted: (i) glue the sample to fixture, (ii) add water to the fixture container, (iii) heat the sample to 25 ºC (at the fluid state) and equilibrate for 10min, (iv) perform a pre-shear at strain 0.1% and frequency 1.0rad/s for 4000 s.

3.2.3.3 Uniaxial tensile test

The tensile stress-strain measurements were performed using a tensile-compressive tester (Tensilon RTC-1310A, Orientec Co.) at a deformation velocity of 100 mm/min at

25 °C with humidity control to prevent evaporation.

3.3 Results and discussion

3.3.1 Dependence of specific viscosity (η_{sp}) on concentration (C_P)

To Confirm the entanglement concentration in uncrosslinked triblock copolymer solutions, the specific viscosity η_{sp} of solution depending on triblock copolymer concentration is established (**Figure 1**). The specific viscosity is defined as follows:

$$\eta_{sp} = \frac{\eta_a - \eta_0}{\eta_0} \quad (2)$$

where η_a is the zero-shear viscosity of triblock copolymer solution and η_0 is the viscosity of the solvent. The η_a and η_0 can be obtained from the following relationships:

$$\eta_a = \lim_{\dot{\gamma}\to 0} \eta \text{ or } \eta_a = \lim_{\omega\to 0} \frac{G''}{\omega} \quad (3)$$

The η_{sp} increases as the concentration increases. It shows a power law relationship with the polymer concentration, and four transition concentration regions can be defined based on exponents:

$\eta_{sp} \sim C^{0.94}$ in dilute solution;

$\eta_{sp} \sim C^{1.45}$ in semidilute unentangled solution;

$\eta_{sp} \sim C^{3.24}$ in semidilute entangled solution;

$\eta_{sp} \sim C^{11.3}$ in concentrated entangled solution.

These values are similar to the theoretical exponents for polymers in good solvent in these three regions which are 1.0 in dilute solution, 1.3 in semidilute unentangled solution, and 3.9 in semidilute entangled solution[3]. As shown in **Figure 1c**, the critical

entanglement concentration is obtained as 0.08 g/mL.

3.3.2 Plateau modulus

Time-temperature superposition is an effective tool in rheology to probe entanglements in uncrosslinked polymer solutions[22,23]. **Figure 2** shown the master curves of triblock copolymer concentrations after TTSP referenced to 25 ºC, only with horizontal shift. As observed in figure, it is difficult to derive G_N since G′ in the plateau region cannot be strictly horizontal. Here the G_N was determined as following empirical equation based on crossover modulus-based method tailoring for polymers with low M_w and large molecular weight distribution[2]:

$$\log\frac{G_N}{G_x} = 0.38 + \frac{2.63log\frac{M_w}{M_n}}{1+2.45log\frac{M_w}{M_n}} \quad (4)$$

where the G_x is the crossover modulus.

The results are plotted versus triblock copolymer weight fraction on a log-log scale in **Figure 3**. A power law fit gives a slope of 2.89, which has a slight deviation from the theoretically predictions 2.3 for entangled solution of neutral polymer in good solvent.

3.3.3 Introduction of physical crosslinks

Solvent quality plays a key role in the self-assembly of block copolymer[24]. Here, we describe the use of solvent exchange for obtaining PBMA-PMAA-PBMA gel from DMF to water, where the DMF is good solvent for both blocks, and the water is a selective solvent for the polymer midblock PMAA. The volume swelling ratio from

uncrosslinked solution to B gel was defined as:

$$Q = \frac{V_{B\ gel}}{V_{solution}} \tag{5}$$

Where $V_{\text{B gel}}$ and V_{solution} is the volume of B gel and precursor solution, respectively. As shown in **Figure 4a**, the swelling ratio is almost independent of the concentration. What's more, the volume at B gel state is consistent with that at precursor solution state (Q~1). Here, we can assume that the entanglement contributions to the modulus in B gels is equal to the plateau modulus G_N of the uncrosslinked triblock copolymer solutions. This assumption was extensively used in previous research on the effect of entanglement on rubber elasticity[25–29]. For accuracy, the entanglement contribution G_e for elastic network of B gel is normalized by swelling ratio Q as follows:

$$G_e = \frac{G_N}{Q} \tag{6}$$

In addition, the polymer volume fraction ϕ_P of B gel was calculated as

$$\phi_P{}^{-1} = 1 + (\frac{c}{1-c})\frac{\rho_p}{\rho_w} \tag{7}$$

Here, ρ_p and ρ_w are densities of polymer and water, respectively. c is water content is defined as the ratio percentage between the weight of water in gel to the total weight of the gel. The corresponding ϕ_P of B gels prepared from different triblock copolymer precursor solutions are shown in **Figure 4b**. Based on above data, we can plot the G_e - ϕ_P curve in **Figure 5a**. Similar to **Figure 3**, the power law fit gives a slope of 2.5, which agrees well with the value ranges of 2-2.5 experimentally determined in other polymer solutions[30–32]. According to classical elastic theory, G_e can be expressed as[6] :

$$Ge = \frac{\rho RT}{M_e} \quad (8)$$

Where ρ is the network density (mass per volume), R is the gas constant, T is the Kelvin temperature and M_e is the number-average molar mass between neighboring entanglements. The M_e decrease as increasing the concentration, which is consistent with the theoretical prediction[3].

3.3.4 Elastic modulus of B gels

It is very known that network form by assembly of triblock copolymers existing defect (loop or dangling chain) at low concentration. The defect endows the ideal elastic triblock copolymer network with significantly viscoelasticity. Here, by tuning the midblock chain length and concentration, the triblock copolymer B gels with no defect were chosen for this research (data shown in Chapter 4). To further confirm that perfect network in B gels, the oscillatory frequency sweep was performed. As shown in **Figure 6**, storage modulus, G′ shows a nearly frequency-independent plateau in the observed region, while the loss modulus, G′′, is significantly smaller, which is similar with the systems with pure elasticity. Then the elastic modulus *G* can be derived from Young's modulus E by the relation[33]:

$$E = 2G(1 + \upsilon) \quad (9)$$

where υ is the Poisson's ratio. Because rubbery materials are virtually incompressible in bulk, the value of Poisson's ratio is close to 0.5. Then the G is therefore given by 1/3 E to good approximation.

Figure7a shows the uniaxial tensile curves in the tensile test of the B gels with different

polymer concentrations. The Young's modulus E was derived from their initial slopes (less than 10% strain) of the stress-strain curves. **Figure 7b** shows the dependence of the Young's modulus *E* on the polymer volume fraction ϕ_P in B gels. Based on equation 8, the total modulus *G* contributed by the simple sum of entanglements and physical crosslinks was calculated. As shown in **Figure 7c**, the plot log G -log ϕ_P is fitted well with the power law: G ~ $\phi_P^{1.3}$, while is larger than that from theoretical prediction: G ~ ϕ_P^1 for rubber elastic network without trapped entanglements. This result supports the assumption of the existence of a correlation between topology of the entangled solution prior to crosslinking and its contribution to the final network of B gel.

3.3.5 Assignment of modulus G in B gels from physical crosslinks and entanglements

In order to study the contribution of physical crosslinks to the elastic modulus, named as G_c, the modulus was evaluated by $G_c = G - G_e$. **Figure 8** also shows the double logarithmic plots of G_c vs ϕ_P. The least square method yields G ~ $\phi_P^{1.0}$. The experimental exponent is perfectly same with the predicted one, confirming that it is an effective way to separate the contribution of entanglements from crosslinks in physical B gel. It is worth to mention that the it will have large deviation in systems which has a short chain possibly caused by the defect (**Figure 9**). This issue will be discussed systematically in Chapter 4.

3.4 Conclusion

The individual contributions to the effective network from trapped chain entanglements and crosslinks in a physical triblock copolymer gels were successfully estimated by probing the modulus at uncrosslinked state (solution) and crosslinked state (B gel). The entanglements G_N in uncrosslinked solution were probed by TTSP. The trapped entanglements G_e was calculated by G_N normalized by swelling ratio from the solution to B gel. the contribution from crosslinks was calculated by subtracting the contribution of G_e from G, the total modulus of B gel. The ϕ_P dependence of G_e and G_c obeys power law with exponents of 2.5 and 1.0. The experimental exponent is perfectly conformed to the theoretical predictions, confirmed that our method is an effective method to separate the entanglements from crosslinks in physical hydrogels. It should be open the new door for designing new materials from theoretical viewpoint.

3.5 Reference

[1] O. Kramer, *Polymer (Guildf).* **1979**, *20*, 1336.

[2] C. Liu, J. He, E. Van Ruymbeke, R. Keunings, C. Bailly, *Polymer (Guildf).* **2006**, *47*, 4461.

[3] R. H. Colby, *Rheol. Acta* **2010**, *49*, 425.

[4] K. Urayama, T. Kawamura, S. Kohjiya, *J. Chem. Phys.* **2003**, *118*, 5658.

[5] J. D. Ferry, *Polymer (Guildf).* **1979**, *20*, 1343.

[6] M. Rubinstein, R. H. Colby, *Polymer physics*; Oxford university press New

York, 2003; Vol. 23.

[7] A. Kloczkowski, J. E. Mark, B. Erman, *Macromolecules* **1995**, *28*, 5089.

[8] S. F. Edwards, T. Vilgis, *Polymer (Guildf).* **1986**, *27*, 483.

[9] M. Rubinstein, S. Panyukov, *Macromolecules* **1997**, *30*, 8036.

[10] M. Kaliske, G. Heinrich, *Rubber Chem. Technol.* **1999**, *72*, 602.

[11] R. J. Gaylord, J. F. Douglas, *Polym. Bull.* **1987**, *18*, 347.

[12] S. F. Edwards, T. A. Vilgis, *Reports Prog. Phys.* **1988**, *51*, 243.

[13] M. Klüppel, In *Physics of Polymer Networks*; Springer, 1992; pp. 137–143.

[14] J. P. Gong, *Soft Matter* **2010**, *6*, 2583.

[15] J. P. Gong, Y. Katsuyama, T. Kurokawa, Y. Osada, *Adv. Mater.* **2003**, *15*, 1155.

[16] Y. Gong, M. Gao, D. Wang, H. Möhwald, *Chem. Mater.* **2005**, *17*, 2648.

[17] T. L. Sun, T. Kurokawa, S. Kuroda, A. Bin Ihsan, T. Akasaki, K. Sato, T. Nakajima, J. P. Gong, M. A. Haque, T. Nakajima, J. P. Gong, *Nat. Mater.* **2013**, *12*, 932.

[18] H. J. Zhang, T. L. Sun, A. K. Zhang, Y. Ikura, T. Nakajima, T. Nonoyama, T. Kurokawa, O. Ito, H. Ishitobi, J. P. Gong, *Adv. Mater.* **2016**, *28*, 4884.

[19] J.-Y. Sun, X. Zhao, W. R. K. Illeperuma, O. Chaudhuri, K. H. Oh, D. J. Mooney, J. J. Vlassak, Z. Suo, *Nature* **2012**, *489*, 133.

[20] Y. S. Zhang, A. Khademhosseini, *Science (80-.).* **2017**, *356*, 3627.

[21] T. Nakajima, *Polym. J.* **2017**, *49*, 477.

[22] K. S. Cho, In *Viscoelasticity of Polymers*; Springer, 2016; pp. 437–457.

[23] J. Liu, D. Cao, L. Zhang, W. Wang, *Macromolecules* **2009**, *42*, 2831.

[24] K. J. Henderson, K. R. Shull, *Macromolecules* **2012**, *45*, 1631.

[25] A. N. Gent, G. L. Liu, M. Mazurek, *J. Polym. Sci. Part B Polym. Phys.* **1994**, *32*, 271.

[26] M. Gottlieb, C. W. Macosko, T. C. Lepsch, *J. Polym. Sci. Part B Polym. Phys.* **1981**, *19*, 1603.

[27] S. Candau, A. Peters, J. Herz, *Polymer (Guildf).* **1981**, *22*, 1504.

[28] R. L. Carpenter, H. Kan, J. D. Ferry, *Polym. Eng. Sci.* **1979**, *19*, 267.

[29] H.-C. Kan, J. D. Ferry, *Macromolecules* **1979**, *12*, 494.

[30] H. Tao, C. Huang, T. P. Lodge, *Macromolecules* **1999**, *32*, 1212.

[31] S. Zhang, K. H. Lee, J. Sun, C. D. Frisbie, T. P. Lodge, *Macromolecules* **2011**, *44*, 8981.

[32] M. M. Mok, X. Liu, Z. Bai, Y. Lei, T. P. Lodge, *Macromolecules* **2011**, *44*, 1016.

[33] S. S. Vyalov, *Rheological fundamentals of soil mechanics*; Elsevier, 2013; Vol. 36.

Table 1. Description of triblock copolymers.

Polymer ABA	[a)]Mn [kg/mol]	[a)]M_w/M_n	[b)]f_B	[c)]L_A		[c)]L_B	
				L_{gauss}	L_{max}	L_{gauss}	L_{max}
$A_{75}B_{81}A_{75}$	28.6	1.38	0.35	1.89	18.75	3.84	13.07
$A_{93}B_{302}A_{93}$	52.5	1.31	0.62	2.1	23.25	7.42	48.75

a) The subscripts of m, n and p represent the degree of polymerization of the endblock, midblock and endblock respectively. A and B represent poly(butyl methacrylate) (PBMA) and poly(methacrylic acid) (PMAA), respectively. b) Molar fraction of midblock PMAA. c) Weight-average molecular weight and molecular weight distribution of the triblock copolymer, respectively.

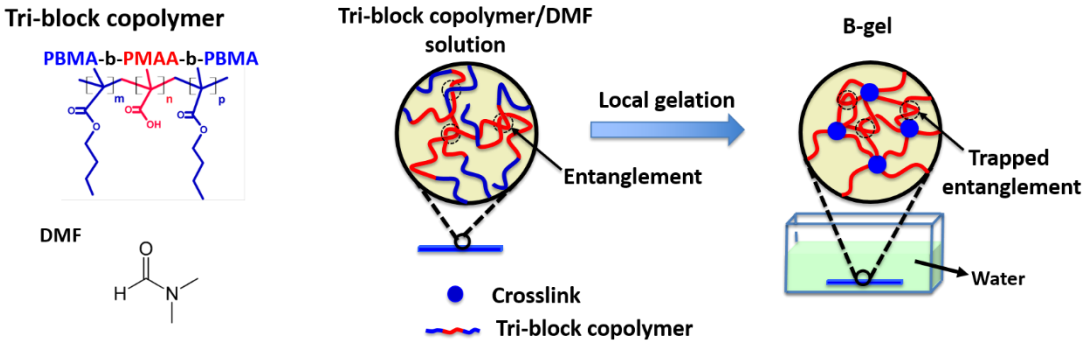

Scheme 1. Schematic diagram depicting the preparation of a B gel with trapped entanglements.

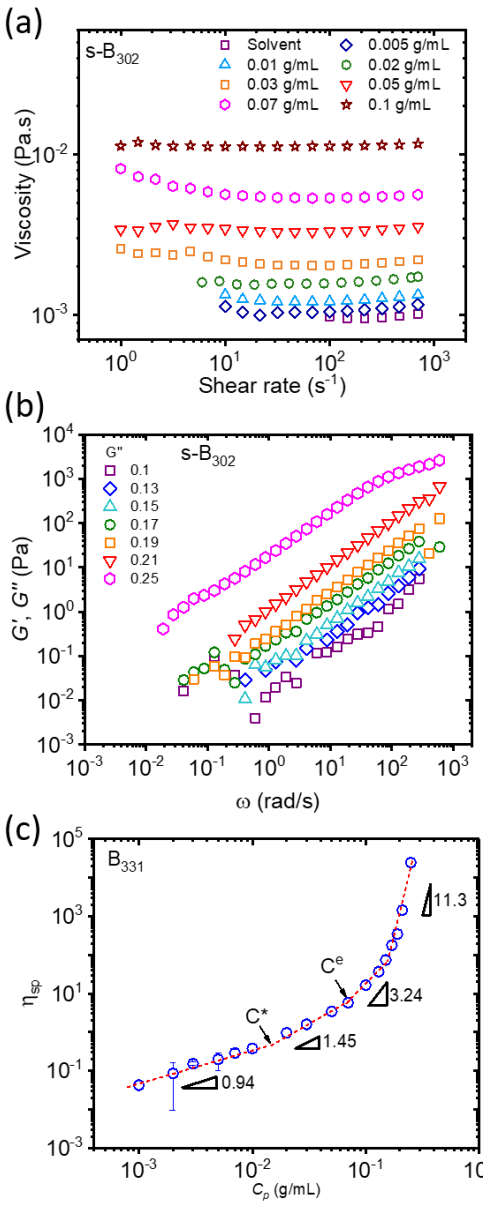

Figure 1. (a) Shear viscosity vs shear rate for triblock copolymer solutions at concentrations ranges from 0.001 to 0.1 g/mL. (b) Loss modulus vs frequency for triblock copolymer solutions at concentrations ranges from 0.1 to 0.3 g/mL. (c) Concentration dependence of the specific viscosity η_{sp}. The four domains are related to four different concentration regimes: dilute, semidilute non-entangled, semidilute entangled and concentrated entangled regions, respectively. Temperature: 25 °C.

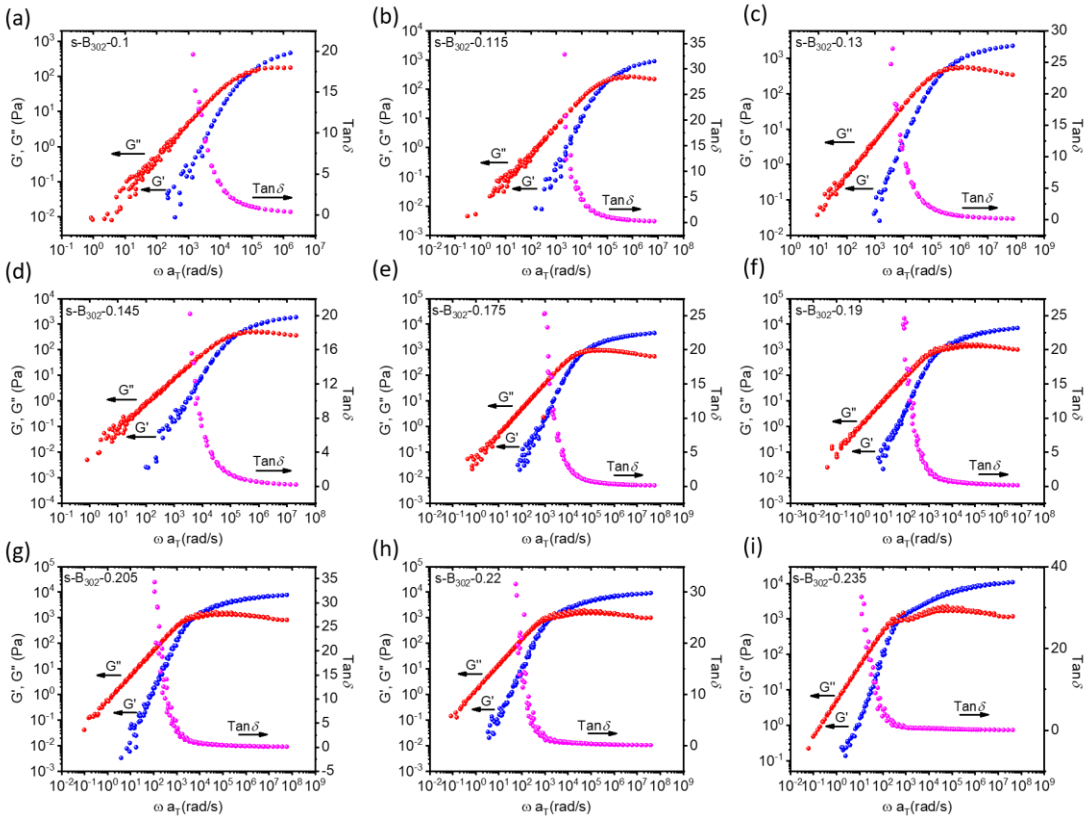

Figure 2. Representative Time-temperature superposition master curves of uncrosslinked triblock copolymer solution illustraing storage modulus *G′*, loss modulus *G″* for triblock copolymer solution with different concentrations. Reference temperature: 25 °C.

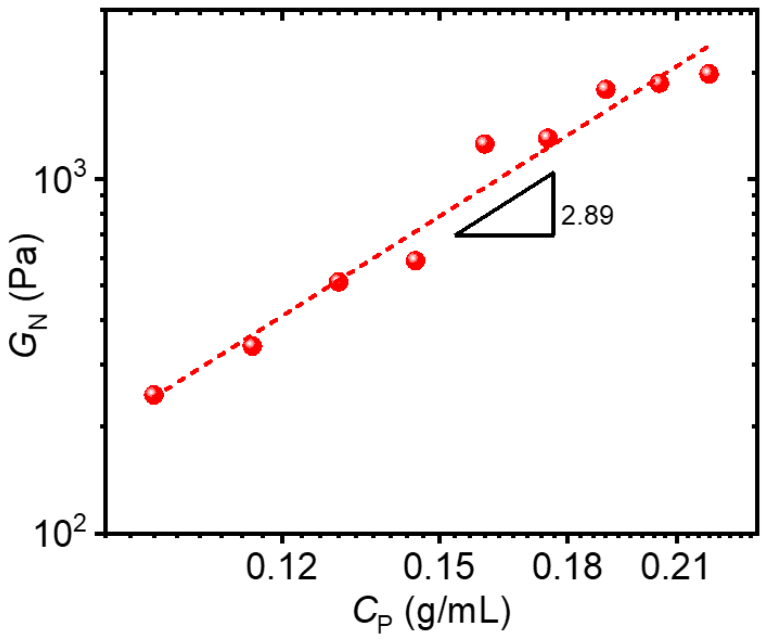

Figure 3. The plateau modulus GN of uncrosslinked triblock copolymer solution by time-temperature superposition as a function of polymer concentration C_P.

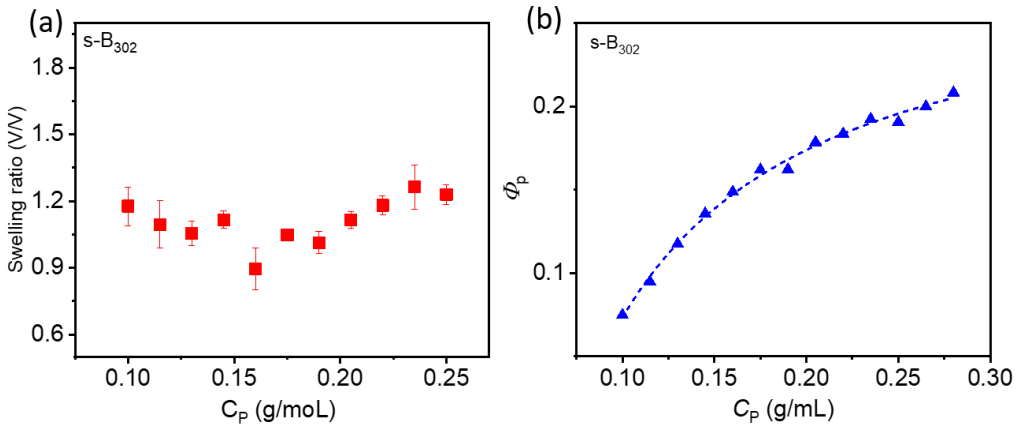

Figure 4. (a) Swelling ratio of B gels prepared at different precursor concentrations and (b) their corresponding volume fraction.

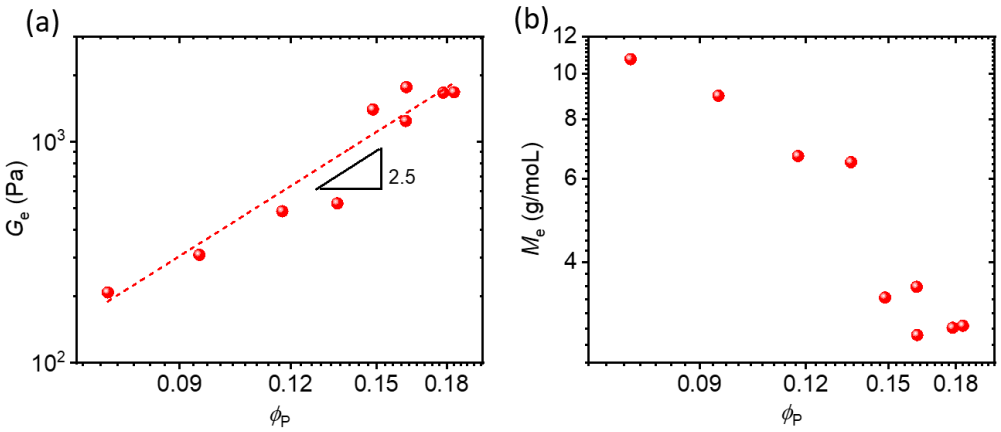

Figure 5. The entanglement contribution G_e (a) and the corresponding entanglement molecular weight M_e (b) as a function of volume fraction in B gels.

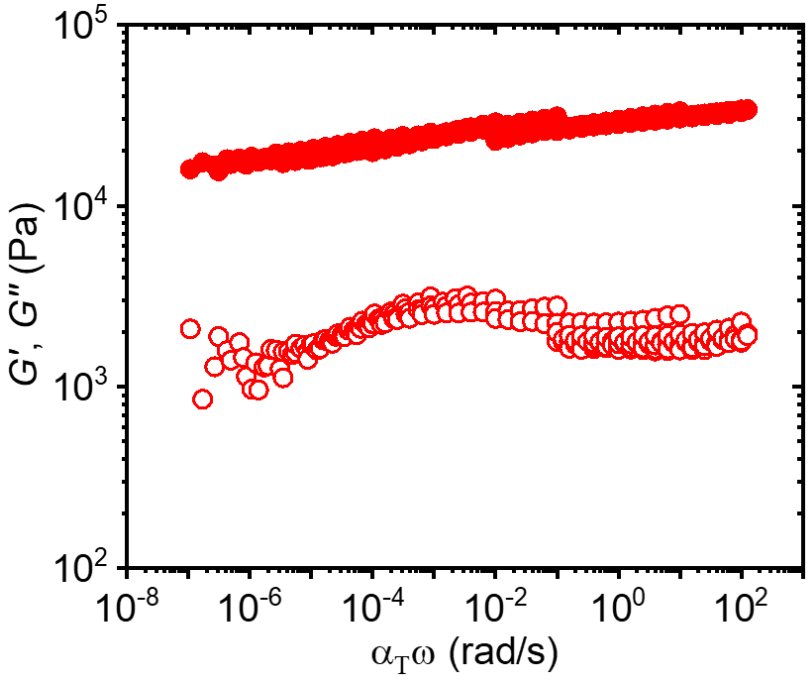

Figure 6. Representative Time-temperature superposition master curves of B gel illustraing storage modulus *G′*, loss modulus *G″* for triblock copolymer solution with different concentrations. Reference temperature: 25 °C.

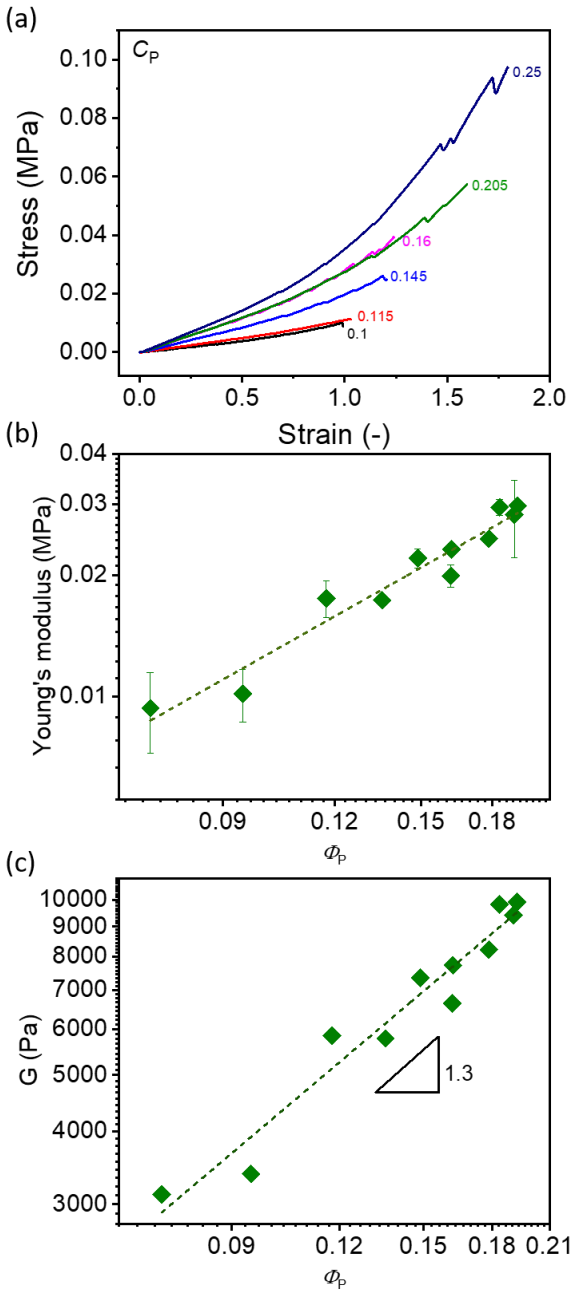

Figure 7. (a) Tensile behavior of the B gels prepared at different precursor triblock copolymer concentrations. (b) The trends of the Young's modulus E as a function of the polymer volume fraction ϕ_p. (c) The elastic modulus G derived from the E by $G = \frac{1}{3} E$.

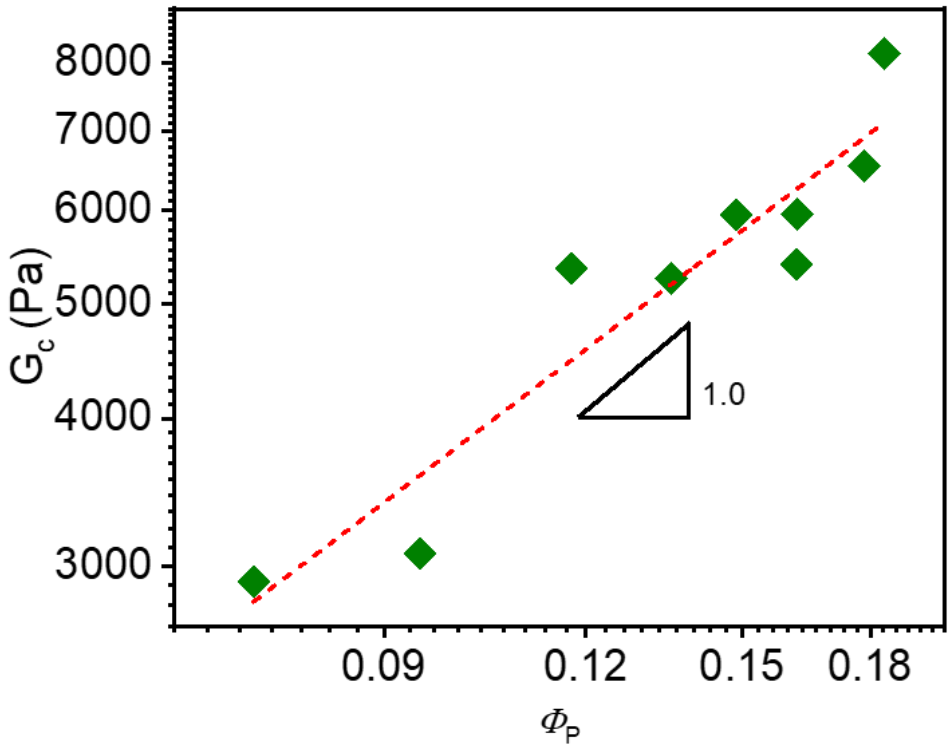

Figure 8. The concentration dependence of contribution of crosslinks G_c to the elastic modulus of B gel given by subtracting the G_e from G.

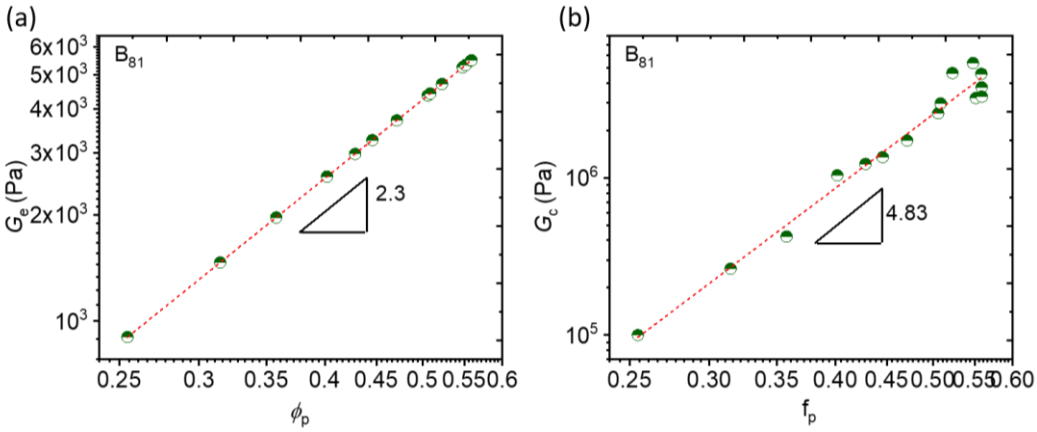

Figure 9. (a) The concentration dependence of contribution of entanglement G_e and (b) contribution of crosslinks G_c to the elastic modulus of B_{81} gel.

Chapter 4: Concentration Dependence of Bridged Chains in Triblock Copolymer Gels Visualized by Small-Angle X-ray Scattering

4.1 Introduction

When ABA triblock copolymers are dissolved in a midblock selective solvent, the endblocks aggregate to form micelles that act as high functionality cross-linking points[1]. At very low concentrations, the endblock forms a loop conformation whose two ends are anchored on the same domain. As the concentration increases, the endblock tends to form a bridge conformation whose two ends are pulled apart into the two micelles, resulting in the formation of a transient network[2,3]. Mattice et al. define the gelation point as the critical concentration where there are enough bridges to connect a sufficient number of micelles to span the entire system[4]. At critical concentration, the newly formed network coexists with defect such as loop, dangling micelles. Thus, the structure of the A-B-A triblock copolymer can be specified with the defect/bridge ratio or bridge fraction, ϕ_{bridge}. This fraction has significantly influence viscoelasticity, mechanical performance and other physical properties[5–7].

Theoretical efforts have been made to evaluate ϕ_{bridge}[8–10], however, there are a few experimental reports due to the difficulty to distinguish the bridge from defect accurately. Watanabe et al. performed a sequence experiments to evaluate ϕ_{bridge} for based on comparing slow dielectric relaxations of the dipole inverted polyisoprene

chains (I) in polystyrene-block-polyisoprene-block-polystyrene (SIS) with those of I chains in SI diblocks[11–13]. Takano et al. use rheological measurements to study the loop/bridge problem by blending cyclic-SI and SIS with different molar ratio, resulting in various loop/bridge conformation ratios, and the SIP sample was used as the 100% bridged reference sample[6].

Clearly, only in special systems by precise designs, it is possible to determine the loop/bridge ratio of an ABA triblock copolymer experimentally. It is often difficult to separate the effect of various contributions to macroscopic properties in universal systems, resulting in a quantitative understanding of triblock copolymer network, has been lacking. In this study, we firstly observed the separated signals of bridge and defect by SAXS measurements. In addition, the defect-to-bridge transition was visibly observed by changing triblock copolymer concentration, which is further confirmed by same trend of normalized Young's modulus vs concentration.

4.2 Experiments

4.2.1 Materials

The amphiphilic triblock copolymers, poly(butyl methacrylate)-b-poly(methacrylic acid)-b-poly(butyl methacrylate) (PBMA-b-PMAA-b-PBMA), and corresponding homo-PBMA and homo-PMAA were synthesized by the Otsuka Chemical Co., Ltd., Japan (**Table 1**). The solvent dimethylformamide (DMF) were purchased from Wako Pure Chemical Industries, Ltd. (Japan).

4.2.2 Preparation of triblock copolymer gels (B gels)

A solution of triblock copolymer/N,N-dimethylformamide was poured onto the glass surface confined by a spacer with dimensions of 60 mm × 60 mm × 1.5 mm. The solution was fixed through surface gelation induced by spraying water vapor on the solution surface for several minutes. Then, the surface solidified solution was immersed in water for 3 days for solvent exchange.

4.2.3 Characterization

4.2.3.1 Small angle X-ray scattering

The static SAXS measurements were performed at BL19U2 beamline at the National Center for Protein Sciences Shanghai. The wavelength of X-ray was 1.033 Å and the sample-to-detector distance was set to be 6225.6 mm. The *in-situ* SAXS measurements were performed at BL40B2 beamline at the Synchrotron X-ray Facility in SPring-8. The wave length of X-ray was 1.0 Å and the sample-to-detector distance was set to be 2310 mm. All scattering images were analyzed with Fit2D software from European Synchrotron Radiation Facility by taking off the detector spatial distortion, X-ray beam fluctuation and background scattering.

4.2.3.2 Uniaxial tensile test

The tensile stress-strain measurements were performed using a tensile-compressive tester (Tensilon RTC-1310A, Orientec Co.) at a deformation velocity of 100 mm/min at 25 ^{o}C with humidity control to prevent evaporation.

4.3 Results and discussion

4.3.1 Structure of triblock gels (B gel)

The B gel is transparent and smooth (insert in **Figure 1**). In order to determine the structure of B gel, small-angle X-ray scattering experiments were performed, and representative scattering patterns are shown in **Figure 1**. Scattering contrast in these types of micellar systems arise from electron density differences between the less solvated micelle core and the environment solvent. It is often modeled by treating the system as a randomly distributed hard sphere using an approach developed by Percus and Yevick[14]. In this model, the total scattering intensity is the product of the form factor which accounts for the geometry of the individual micelles and the structure factor which accounts for the distribution of micelles in the system. While in our curve, we found that the model becomes invalid due to the complex peak observed. As shown in Figure 1, there exists three peaks in the 1 D spectra derived from the 2D SAXS image (insert figure). To assign the peaks, the deformation experiments at small deformation were performed. **Figure 2a** shows the SAXS results of B gel at different strains. Here we can assume that at small strain, the micelles dose not deform, namely the peak representing the factor maxima remain unchanged. It needs to mention that the anisotropic structure observed when $\varepsilon = 0$ possibly caused by sample loading process. Same sample image was shown in insert image in **Figure 1**. With the increasing of strain, the anisotropic structure was observed when the gel is stretched. **Figure 2b-c** shows the one-dimensional scattering intensity distributions along with and

perpendicular to the stretching direction. The scattering intensity distribution of peak 1,2 shifts to the low q value toward smaller angles (for the parallel stretching) or larger angles (for the perpendicular direction), whereas there is no shift in the position of the maxima changes from peak 3. These results assign the peak 1 and peak 2 to the interdomain distance (structure factor), which was calculated as $d = \frac{2\pi}{q}$, and peak 3 is assigned to the domain size (form factor), which was calculated as $qD = 5.76$, where D is the diameter of the domain. The calculated results are shown in the **Figure 2d-e**, with increasing strain, the d_1 and d_2 increase at parallel direction and decrease at the perpendicular direction. While the D remains unchanged at both direction.

4.3.2 Concentration-induced structure transition

Figure 3a shows SAXS patterns for B gels prepared at different concentrations ranging from 0.1 to 0.25 g/mL. The corresponding one-dimensional scattering intensity distributions are shown in **Figure 3b**. At low concentration, only peak 1 was observed. While as concentration increases, the scattering intensity distribution changes from a one peak curve to two peaks at certain concentration (C_P^*: 0.17 g/mL) indicating the formation of new structures of different long period. Evidently, the scattering peak 1 denoting the original peak weakens accompanied by a gradual increase of the new peak showing the structure transition at high concentration. The position of the scattering peak from newly formed structure locates at larger q than the one from the original structure. With the increase of strain, the scattering peak position of the new lamellar stacks keeps almost constant. **Figure 4a** shows the domain distance d_1, d_2 of the two

scattering peaks as increase of concentration. At low concentration, original scattering peak 1 have a large interdomain distance, d_1. With the increase of concentration, d_1 become smaller firstly, finally showing the same value with that of new formed structure. As shown in **Figure 4b,** the domain sizes are independent of concentration, indicating that the increase in polymer concentration in the gel results in a larger number of domains. Simultaneously a decrease in domain distance of structure I illustrated the formation of new micelles. While for the structure II, the domain distance d_2 and domain size keep constant, implying the structure II have arrived the saturated and no space for the new formed micelles. Based on this result, we deduced that structure I is formed by micelles connecting to the network with defect, while the structure II origins from the near perfect network. As far as we know, it is first time to observed the separated structure by SAXS. Here, we named the micelles contributing to structure I and structure II as dangling micelles and bridged micelles, respectively.

4.3.3 Mechanical response of different micelle morphology

The mechanical response of bridged micelles and dangling micelles can be well described by different impact to the modulus. The dangling micelles, not be confined in the perfect network, cannot be bear the force to contribute the modulus during force loading. While the bridged micelles, are considered as the elastic contribution to the rubber elasticity[4,15]. To further confirm the origins of structure I and structure II, tensile tests of B gel prepared at different triblock copolymer solutions were performed (**Figure 5a**). The polymer volume fraction ϕ_P of B gel was calculated as

$$\phi_{\mathrm{P}}{}^{-1} = 1 + (\frac{c}{1-c})\frac{\rho_{\mathrm{p}}}{\rho_{\mathrm{w}}} \quad (1)$$

Here, ρ_p and ρ_w are densities of polymer and water, respectively. c is water content is defined as the ratio percentage between the weight of water in gel to the total weight of the gel. The corresponding ϕ_P of B gels prepared from different triblock copolymer precursor solutions are shown in **Figure 6**. Based on above data, we can plot the the ϕ_P dependence of Young's modulus, the fracture strain and fracture stress in **Figure 5b-c**. Young's modulus of a polymer gel is proportional to the number of effective chains that sustain the force. With the decrease in the water content of the gel, the number of elastic chains per unit volume of the gel increases. To remove the effect caused by the change in the polymer density, the Young's modulus, adding the fracture strain and fracture stress were normalized according to following equation[16]:

$$\text{Normalized modulus:} \quad E^{\mathrm{N}} = E/\phi_{\mathrm{P}} \quad (2)$$

$$\text{Normalized fracture strain:} \quad \varepsilon^N = \varepsilon/\phi_P^{1/3} \quad (3)$$

$$\text{Normalized fracture stress:} \quad \sigma^N = \sigma/\phi_P^{2/3} \quad (4)$$

The normalized mechanical data are equivalent to that of an elastic network in dry state. The calculated results are shown in Figure 7. After the normalization, all the data showed a first increase trends followed with a flat region that with similar critical concentration (0.17 g/mL). According to classical elastic theory, *G* can be expressed as[17] :

$$E^N = \frac{E}{\rho} = \phi_{bridge}RT \quad (5)$$

Where ρ is the network density (mass per volume), ϕ_{bridge} is the bridging fraction of B gels, R is the gas constant and T is the Kelvin temperature. From equation 5, the concentration dependence of E^N represents the change trends of bridge fraction. At the region I dominated by structure I, the E^N continues to increase, indicating that the dangling micelles gradually connects to the network and transfers to the bridged micelles. As the increase of concentration, the dangling micelles become minor and entering to the region II. In this region, all the dangling micelles convert into the bridged micelles to have a contribution to the elastic modulus. After the normalization, the E^N has no concentration dependent due to the saturation of bridged micelles. This is furthat confirmed by the gel swelling behavior. As shown in **Figure 8**, the swelling ratio has a weaker concentration dependence in region I because the new formed micelles occupy the defect region in structure I and no extra space needed, resulting in unchanged swelling ratio. While in region II, the defect region was occupied by the bridged micelles and no space for extra dangling micelles, the new added micelles expand new volume, resulting in increasing swelling ratio.

4.3.4 Dependence of the bridge fraction with polymer fraction

To quantify the bridged fraction ϕ_{bridge} for our system, the shear modulus, G, for an ideal Neohookean material that has been isotropically swollen by solvent is given by[18,19]

$$G = \upsilon \phi_{bridge} RT \frac{d^2}{{R_0}^2} \quad (6)$$

Where υ is the number density of total chains, d is the average distance between cross-links, R_0^2 is the mean-squared end-to-end distance for an equilibrium solution of

molecules with a molecular weight equal to the average molecular weight between cross-links. For triblock copolymer gels, *d* scales with the average distance between aggregates and reflects stretching of the midblocks due to geometric constraints. The υ can be calculated based on the polymer density in precursor solutions by:

$$\nu_{sol} = \frac{C_P N_A \rho}{M_n} \qquad \nu = \frac{\nu_{sol}}{Q} \tag{7}$$

Where υ_{sol} is the polymer density in precursor solution, C_P is weight fraction of triblock copolymer in precursor solution, ρ is density of precursor solution, N_A is Avogadro constant (6.02×10^{23}), M_n is number molecular weight and Q is swelling ratio (volume of B gel divided by volume of precursor solution). The calculated data are shown in **Figure 9**. As expected, the bridge fraction ϕ_{bridge} increased with increasing polymer concentration in region I, while at higher concentrations, the ϕ_{bridge} converges to ~0. 45. This value is smaller than that from theoretical prediction (~0. 75)[20], possibly caused by the excessive correction for chain conformation in equation 6. In addition, the plots of E^N against ϕ_{bridge} are shown in **Figure 9b**. In this equation, since ϕ_{bridge} is essentially proportional to E^N, an intercept b should be 0. In practice, surprisingly, b shows a negligible value, 0.03, which further confirm our calculation.

4.3.5 Effect of midblock size on structure transition

In the previous research, the middle block size always was considered to be have negligible effects on micellization and gelation of block copolymer[4,21]. However, we found the middle block size can significantly influence the structure I -to structure II transition by affecting the network integrity. In the triblock copolymer with longer

soluble midblocks, the endblock can start to form network while those with shorter soluble blocks remain as dangling micelles in solution because molecules with longer soluble blocks carry lower “free energy cost” for being bridged state than loop state. Here, we show that the soluble block plays a significant role in determining the network integrity by combing the SAXS and corresponding mechanical response. When the triblock copolymer has a short soluble chain B_{81}, as shown in **Figure 10a**, the peak 1 can be observed for the whole concentration region, indicating the coexistence of dangling micelles even at high concentration. This can be confirmed by the continuous bridge fraction as concentration increases (**Figure 10b**). It needed to notice that the calculated bridged fraction at high concentration is much larger than 1, which possible caused by the compact structure formed due to high concentration. While the triblock copolymers with a longer soluble chain B_{302}, B_{444}, as shown in **Figure 10c, e**, the peak 1 cannot be observed for the whole concentration regions, indicating that once the network formed, there is few defects in the network. This can be confirmed by the concentration independence of bridge fraction (**Figure 10d, f**).

4.3.6 Mechanism of structure transition

The effect of concentration and midblock chain length on structure transition was shown in **Figure 11**. Increase of the polymer concentration induces high possibility for bridged chain formation, resulting in more tendency for perfect network. Longer soluble midblocks tends to form bridge than loop due to the low energy cost.

4.4 Conclusion

This paper for the firstly time probe the the signals of defect and bridge by small angle X-ray scattering measurements. The concentration of triblock copolymer was used to tune the defect-to-bridge transition, which is further confirmed by same trend of normalized Young's modulus vs concentration.

4.5 Reference

[1] M. E. Seitz, W. R. Burghardt, K. R. Shull, *Macromolecules* **2009**, *42*, 9133.

[2] K. Inomata, D. Nakanishi, A. Banno, E. Nakanishi, Y. Abe, R. Kurihara, K. Fujimoto, T. Nose, *Polymer (Guildf).* **2003**, *44*, 5303.

[3] J. R. Quintana, M. D. Jáñez, I. Katime, *Polymer (Guildf).* **1998**, *39*, 2111.

[4] M. Nguyen-Misra, W. L. Mattice, *Macromolecules* **1995**, *28*, 1444.

[5] H. Watanabe, T. Sato, K. Osaki, *Macromolecules* **2000**, *33*, 2545.

[6] A. Takano, I. Kamaya, Y. Takahashi, Y. Matsushita, *Macromolecules* **2005**, *38*, 9718.

[7] M. Zhong, R. Wang, K. Kawamoto, B. D. Olsen, J. A. Johnson, *Science (80-.).* **2016**, *353*, 1264.

[8] M. W. Matsen, M. Schick, *Macromolecules* **1994**, *27*, 187.

[9] E. B. Zhulina, A. Halperin, *Macromolecules* **1992**, *25*, 5730.

[10] S. T. Milner, T. A. Witten, *Macromolecules* **1992**, *25*, 5495.

[11] H. Watanabe, T. Sato, K. Osaki, Y. Matsumiya, S. H. Anastasiadis, *Nihon*

Reoroji Gakkaishi **1999**, *27*, 173.

[12] H. Watanabe, T. Sato, K. Osaki, M.-L. Yao, A. Yamagishi, *Macromolecules* **1997**, *30*, 5877.

[13] H. Watanabe, *Macromolecules* **1995**, *28*, 5006.

[14] F. S. Bates, C. V Berney, R. E. Cohen, *Macromolecules* **1983**, *16*, 1101.

[15] T. Saleesung, P. Saeoui, C. Sirisinha, *J. Appl. Polym. Sci.* **2017**, *134*.

[16] H. Itagaki, T. Kurokawa, H. Furukawa, T. Nakajima, Y. Katsumoto, J. P. Gong, *Macromolecules* **2010**, *43*, 9495.

[17] M. Rubinstein, R. H. Colby, *Polymer physics*; Oxford university press New York, 2003; Vol. 23.

[18] J. D. Ferry, J. D. Ferry, *Viscoelastic properties of polymers*; John Wiley & Sons, 1980.

[19] M. E. Seitz, W. R. Burghardt, K. T. Faber, K. R. Shull, *Macromolecules* **2007**, *40*, 1218.

[20] T. L. Chantawansri, T. W. Sirk, Y. R. Sliozberg, *J. Chem. Phys.* **2013**, *138*, 24908.

[21] I. LaRue, M. Adam, E. B. Zhulina, M. Rubinstein, M. Pitsikalis, N. Hadjichristidis, D. A. Ivanov, R. I. Gearba, D. V Anokhin, S. S. Sheiko, *Macromolecules* **2008**, *41*, 6555.

Table 1. Description of triblock copolymers.

Polymer ABA	[a)]Mn [kg/mol]	[a)]M_w/M_n	[b)]f_B	[c)]L_A		[c)]L_B	
				L_{gauss}	L_{max}	L_{gauss}	L_{max}
$A_{75}B_{81}A_{75}$	28.6	1.38	0.35	1.89	18.75	3.84	13.07
$A_{73}B_{142}A_{54}$	30.3	1.43	0.53	1.74	16	5.09	22.92
$A_{93}B_{302}A_{93}$	52.5	1.31	0.62	2.1	23.25	7.42	48.75
$A_{86}B_{444}A_{86}$	62.8	1.38	0.72	2.02	21.5	9.00	71.67

a) The subscripts of m, n and p represent the degree of polymerization of the endblock, midblock and endblock respectively. A and B represent poly(butyl methacrylate) (PBMA) and poly(methacrylic acid) (PMAA), respectively. b) Molar fraction of midblock PMAA. c) Weight-average molecular weight and molecular weight distribution of the triblock copolymer, respectively.

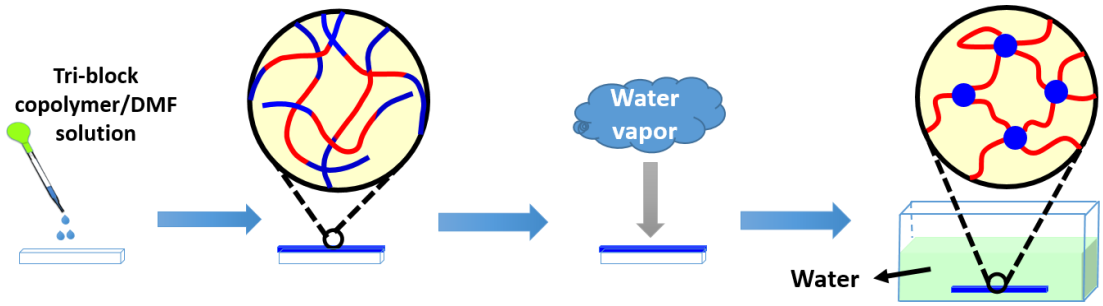

Scheme 1. Schematic diagram depicting the preparation of a B gel.

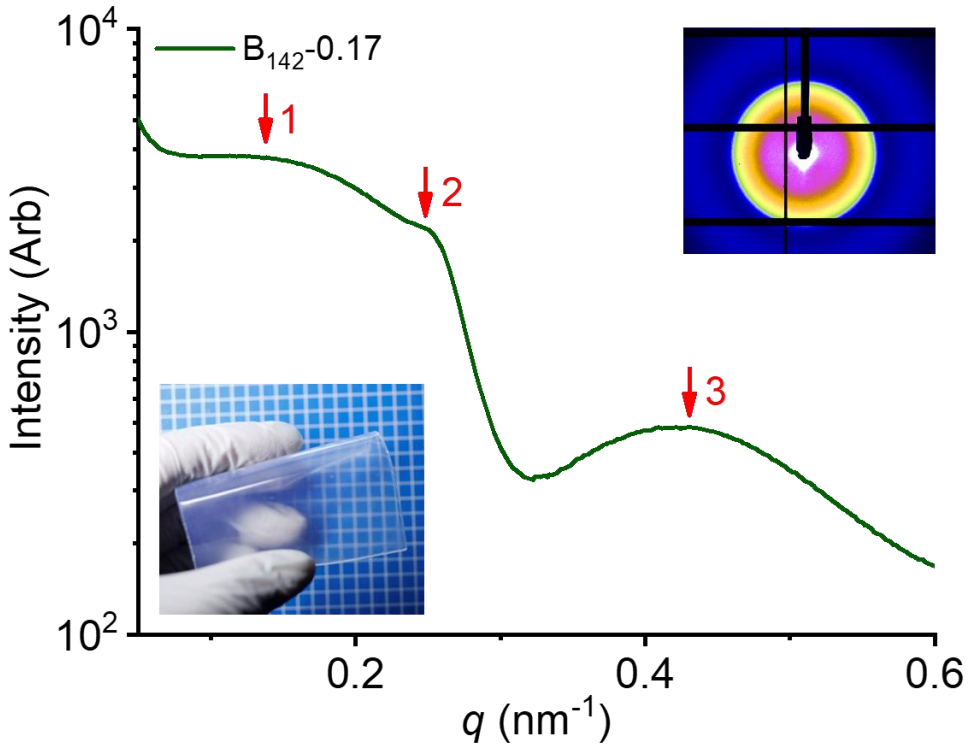

Figure 1. 1D scattering intensity profiles of B gel with a concentration of 0.17 g/mL.

The inserting figure is the corresponding 2D SAXS image and optical picture of B gels.

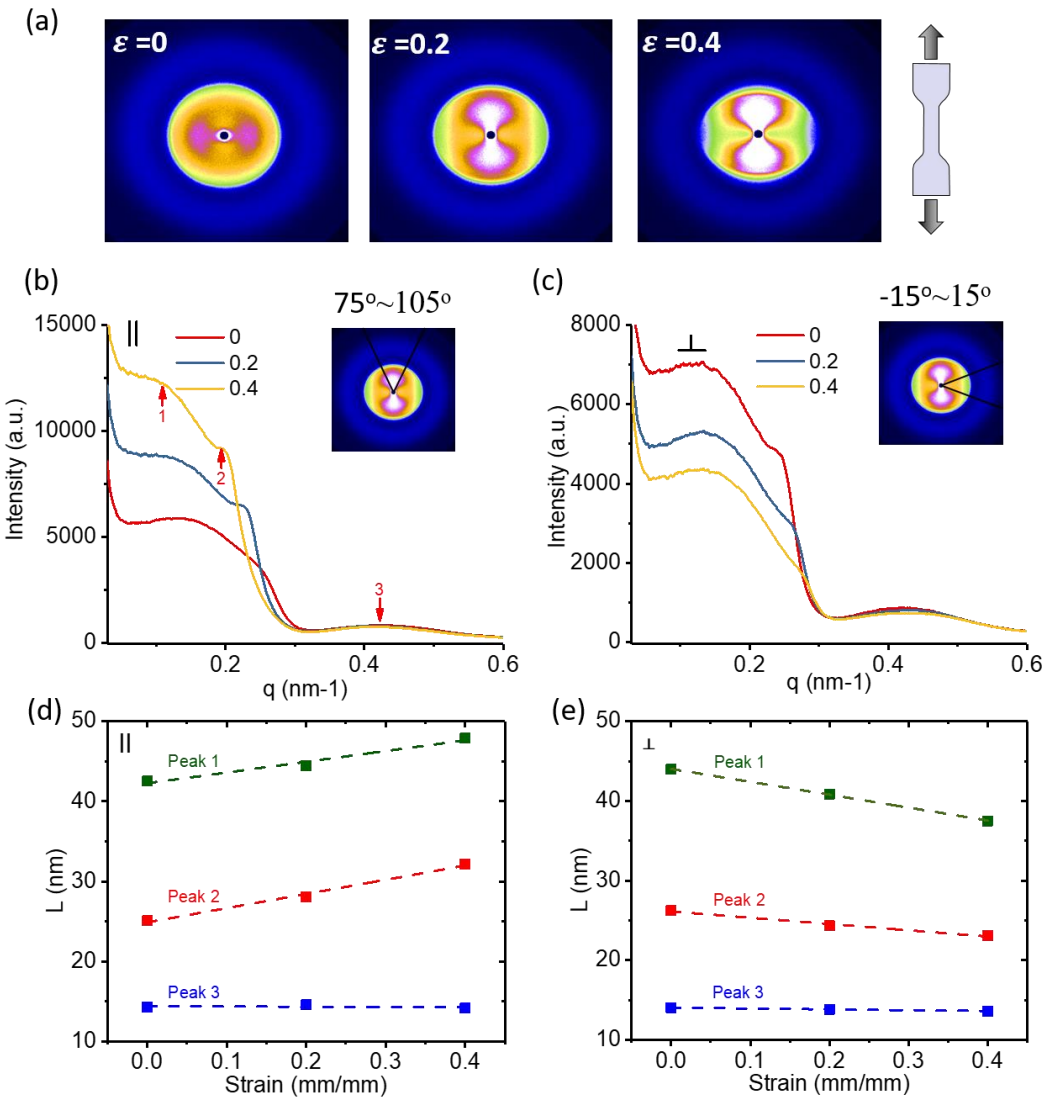

Figure 2. (a) 2D-SAXS images during the tensile process. The sample is stretched in the vertical direction. (b) Profiles of one-dimensional curves along the stretching direction (c) vertical to the stretching direction. (d) and (e) is the corresponding long spacing d_1, d_2 and micelles size for the (b) and (c), respectively.

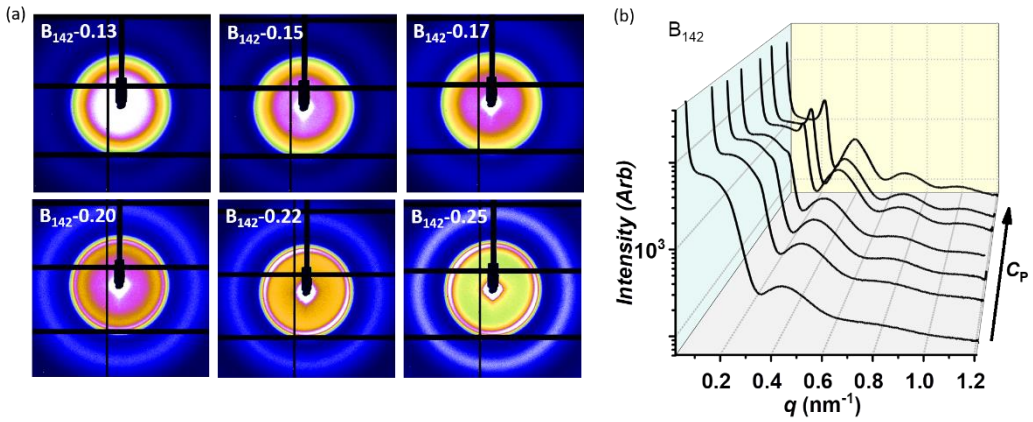

Figure 3. (a) 2D-SAXS images of the selected concentration of B_{142} gel. (b) Corresponding 1 D-SAXS curves.

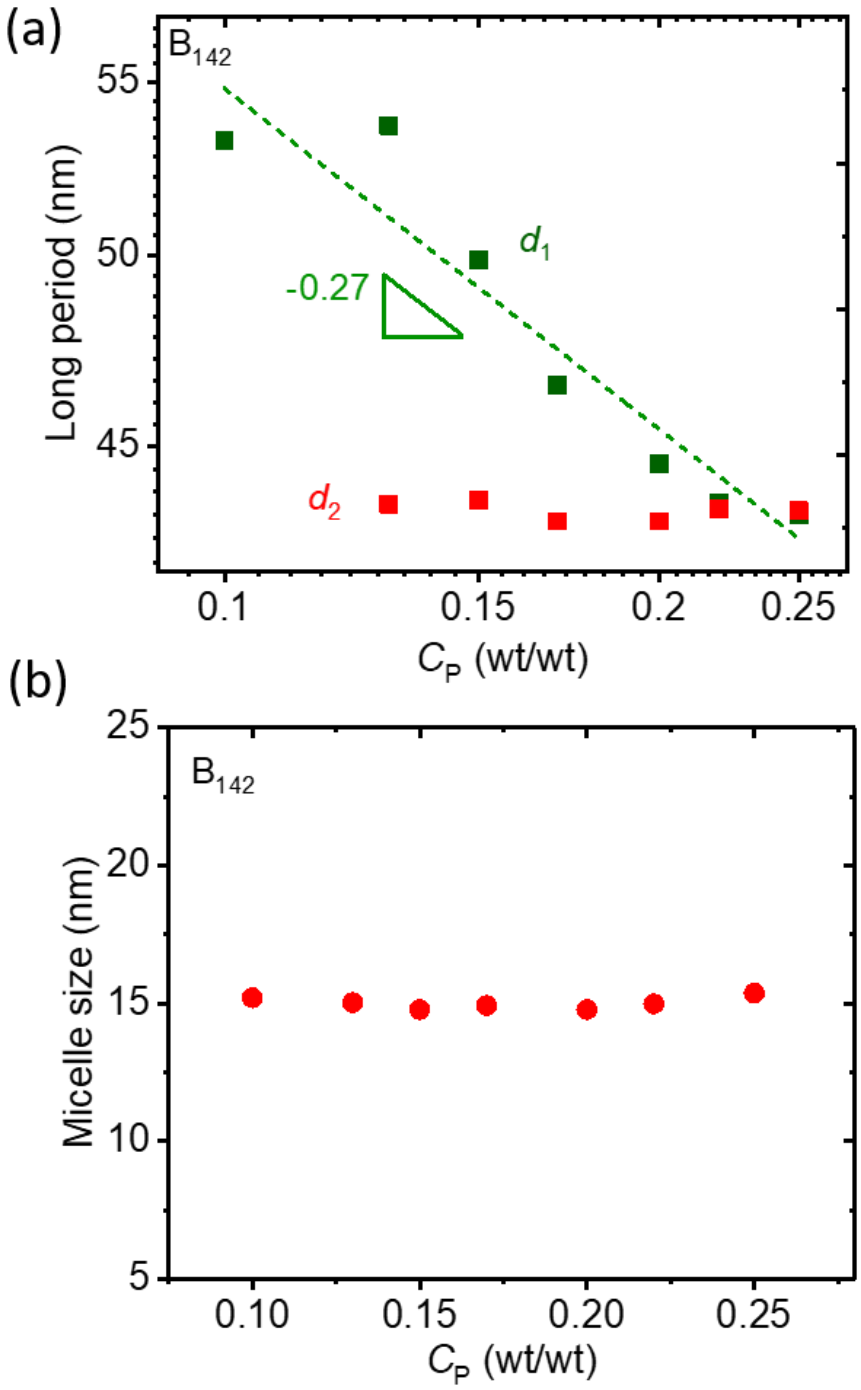

Figure 4. (a) Plot of the structure factors and (b) form factor vs concentration for B_{142} gel.

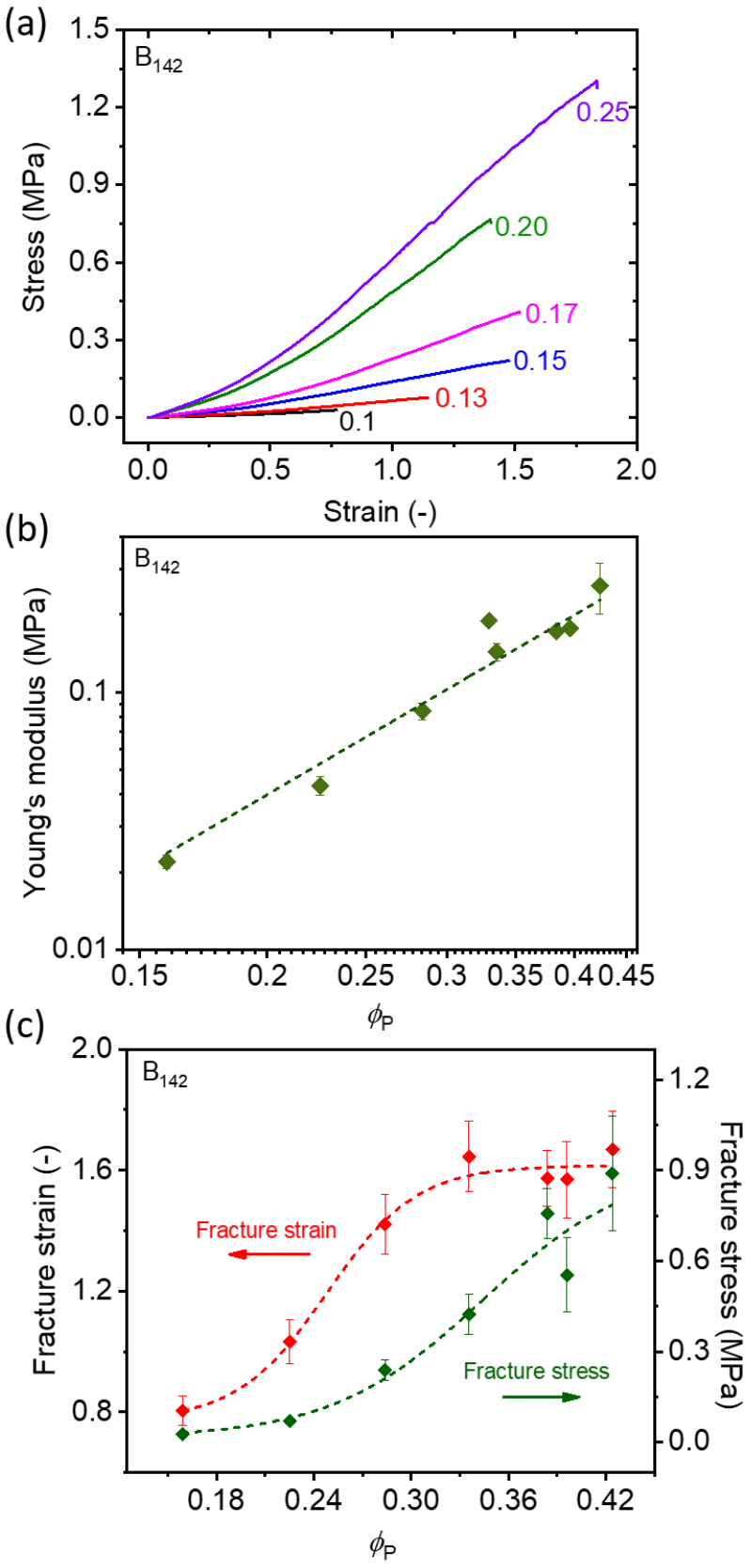

Figure 5. (a) Tensile stress-strain curves of the B_{142} gel on the concentration of triblock copolymer. Dependence of the Young's modulus (b), fracture strain and fracture stress

(c) on C_P.

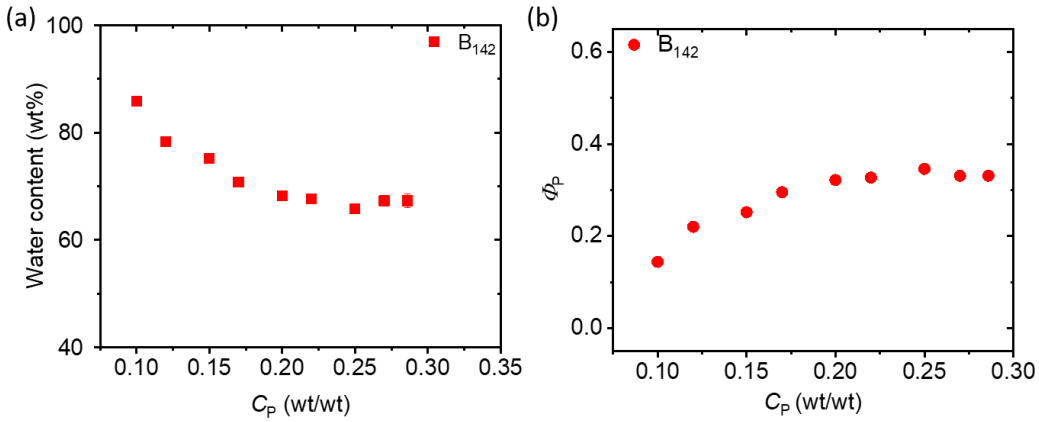

Figure 6. The triblock concentration dependence of water content (a) and polymer volume fraction (b) in B_{142} gel.

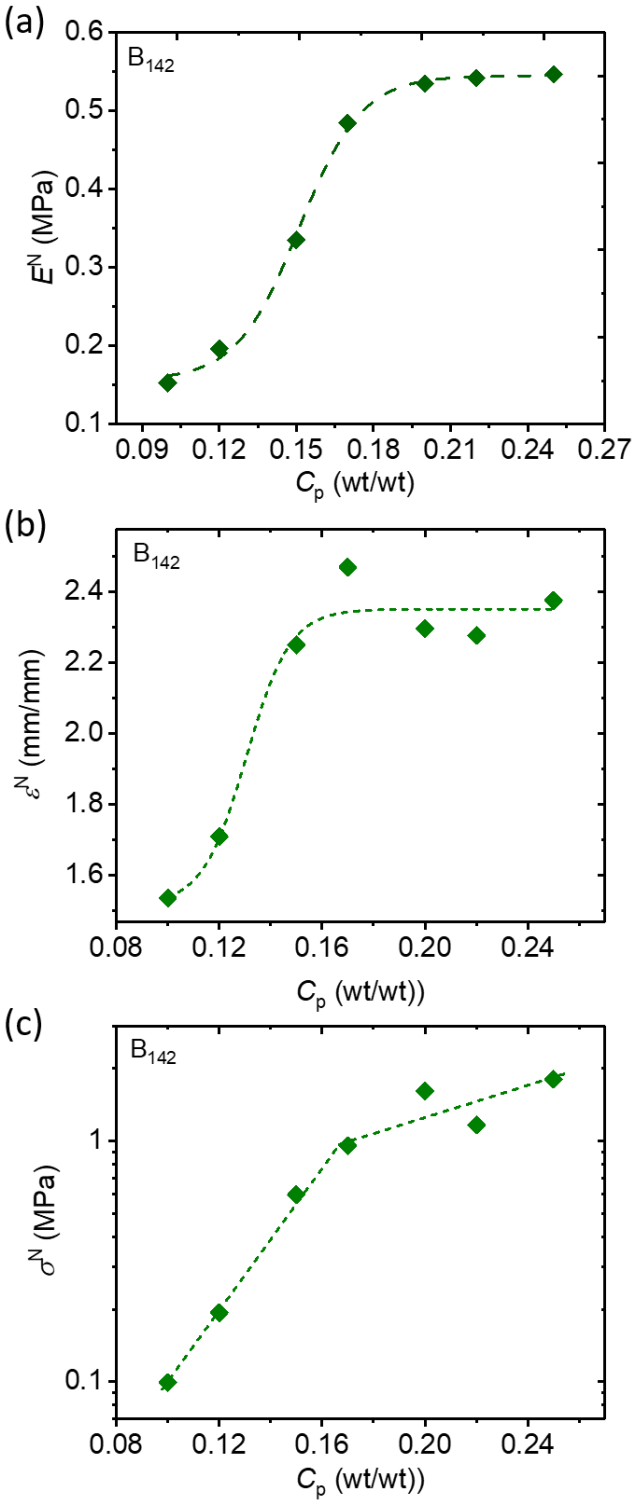

Figure 7. Triblock copolymer concentration dependencies of the nominal Young's modulus E^N (a), the nominal fracture strain ε^N (b), and the nominal fracture stress σ^N (c) for B_{142} gel.

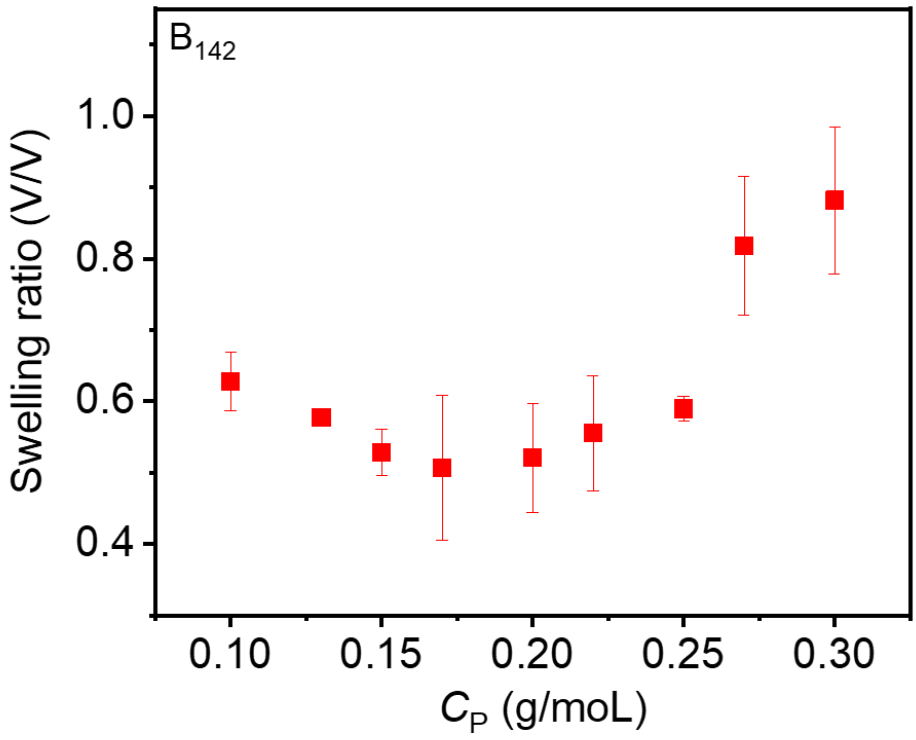

Figure 8. Triblock copolymer concentration dependence of swelling ratio.

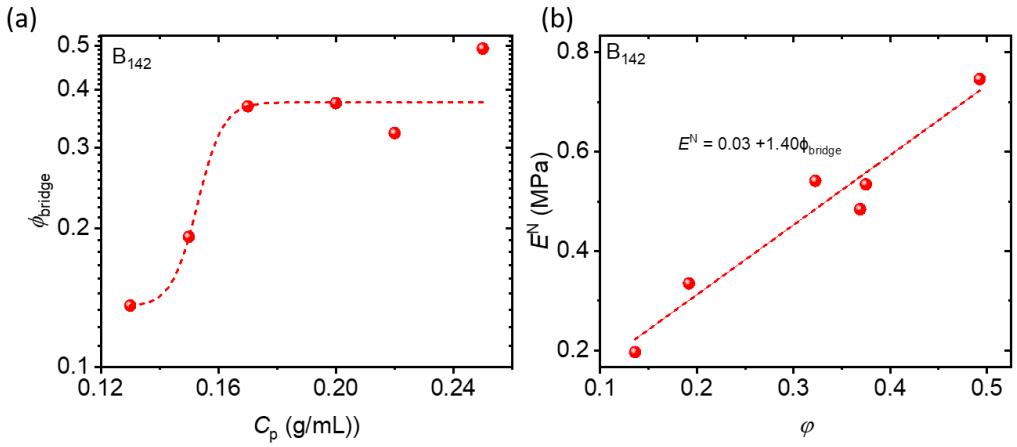

Figure 9. (a) (b) Plot of normalized E^{N} against bridge fraction ϕ_{bridge}. (b) Plot of normalized E^{N} against triblock copolymer concentration.

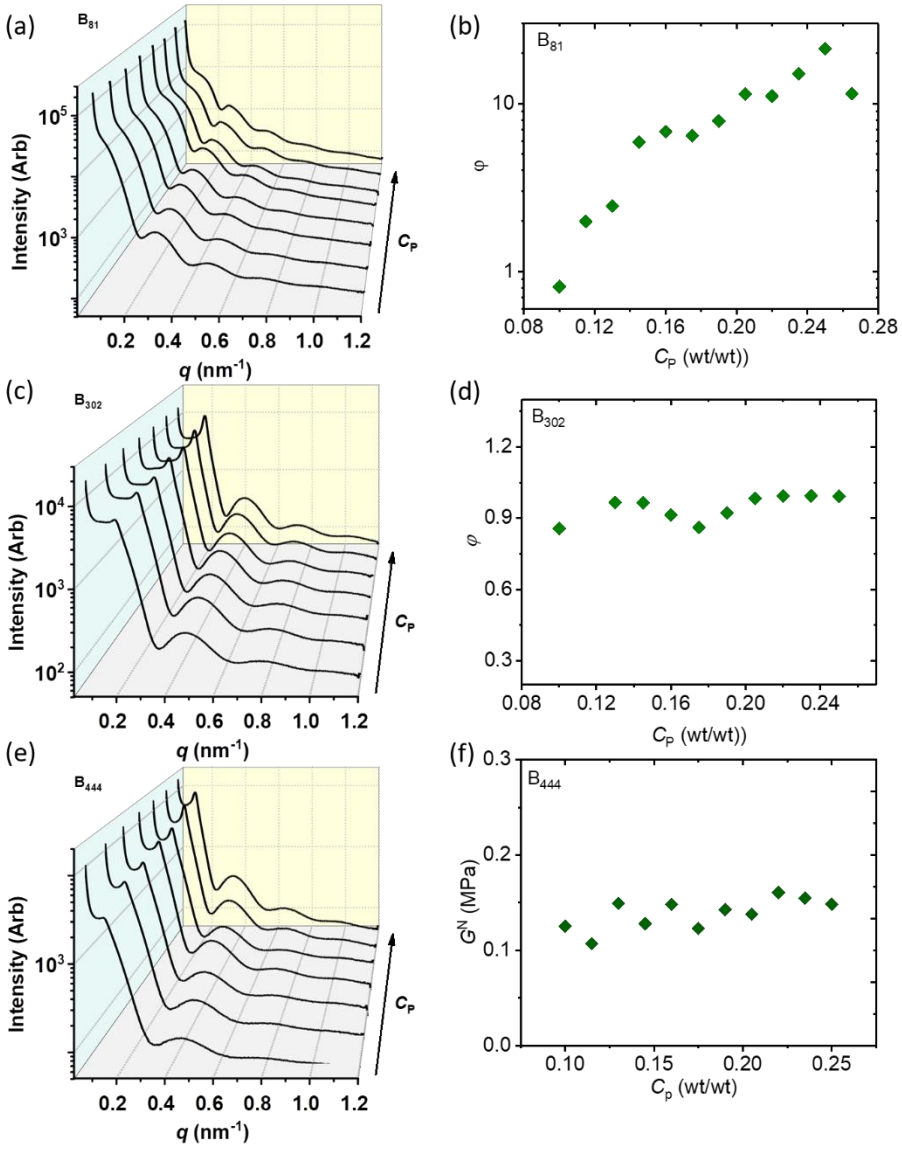

Figure 10. Scattering intensity vs q for B_{81} gel (a), B_{302} gel (c) and B_{444} gel (d) , respectively. Triblock copolymer concentration dependencies of the nominal modulus G^N for B_{81} gel (a), B_{302} gel (c) and B_{444} gel (d), respectively.

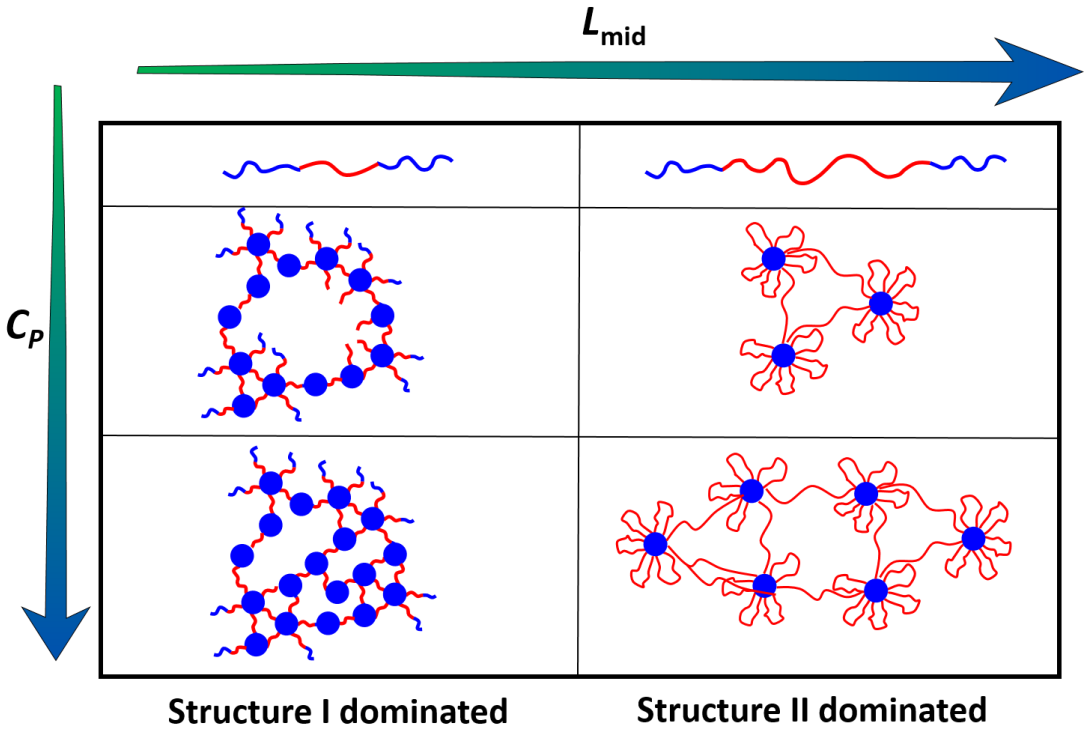

Figure 11. Scheme of the structure transition of B gels with different insoluble midblock chain.

Chapter 5: Toughening mechanism of B-DN gel by In-situ Small-Angle X-ray Scattering

5.1 Introduction

Hydrogels have drawn great attention as synthetic equivalents for a variety of applications in biological systems due to its resembled biological tissues[1–5]. Most hydrogels suffer from a poor mechanical strength, which limits their use. Using sacrificial bonds, the brittle hydrogel can be strongly reinforced in stiffness and toughness by introducing various kinds of pre-stretched chains or physical bonds that can break and dissipate energy before the material fails[6]. However, incorporating sacrificial bond introduces constraints in terms of processing and safety and requires careful dispersion. Alternatively, increasing the viscoelastic character of the hydrogel is used to increase fracture toughness through molecular friction[7,8].

Based on the sacrificial concept, three empirical strategies have been used to toughen hydrogels. The first strategy involves creating “weak or overstressed” bonds sacrificial bonds that break early due to either intrinsically weaker than the main bonds, or loaded more than the main bonds[9–11]. These hydrogels prepared by this method was called as double network gels. These gels are synthesized in two steps containing two networks: the 1st network closes to its maximum extensibility and the 2nd network containing large amount of entanglement upstretched chain. A second strategy is to introduce plasticity in the gel by incorporating stiffer domains that can only be deformed above a critical

force[12–21]. This creates a large damage zone in front of a crack but also permanent deformation. This method, which introduces an internal friction inside the material by creating strong but breakable interactions can be very effective in stopping crack propagation by blunting it. The last strategy is to introduce physical bonds in the gel that can break and reform at a different position[21–25]. This type of dual cross-link gel has a very strong strain rate dependence but can become very tough in a strain rate regime where the dynamic bonds do not much change the stress- strain curve but delay the propagation of cracks. This last strategy only works for a majority of dynamic bonds relative to the permanent bonds.

It is important to understanding the toughening mechanism of these new exciting materials in a more quantitative and predictive way. In our previous work, we prepared a supramolecular double-network hydrogel based on amphiphilic triblock copolymer that contains strong hydrophobic domains and sacrificial hydrogen bonds. This gel shows high toughness and partial self-recovery. While the toughening mechanism of this tough gel, however, still unclear. In this paper, by using *in-situ* small-angle X-ray scattering combing customized tensile device, the structure evolution during deformation was revealed. Based on structure evolution, the toughening mechanism was clarified with the aid of cycle test.

5.2 Experiments

5.2.1 Materials

The amphiphilic triblock copolymer poly(butylmethacrylate)-b-poly(methacrylic acid)-b-poly(butyl methacrylate) with the target degree of polymerization of 97-142-97 was synthesized by Otsuka Chemical Co., Ltd., Japan. The measured number-average molecular weight of the obtained block polymer is 30300 with a molecular weight distribution of 1.43.

5.2.2 Preparation of triblock copolymer gel (B gel)

A solution of 0.17 (g/mL) triblock copolymer/DMF was poured onto glass with a silicon spacer with a size of 60 mm × 60 mm × 1.5 mm, and the surface of solution was fixed by spraying water vapor on the surface of the solution for several minutes, during which a skin was formed by the endblock PBMA chains self-assembly. Then the solution with skin was immersed in water for final solvent exchange. The water was changed two times one day until arriving equilibrium.

5.2.3 Preparation of double network gel (B-DN gel)

The B gel was immersed in the second network precursor solution containing the 2 mol/L AAm monomer, and 0.05 mol% 2-oxoglutaric acid (relative to the monomer) as photo-initiator for 3 d. And then the sample was polymerized for 8 h. The as-prepared B-DN gel was immersed in purified water to reach equilibrium.

5.2.4 Characterization

5.2.4.1 *In-situ* small-angle X-ray scattering

The small-angle X-ray scattering (SAXS) measurement was carried out in BL19U2 beamline at the NCPSS, Shanghai, China. The distance from sample to detector is 6225.6 mm. A Pilatus 1M detector with resolution of 981×1043 pixels and pixel size of 172 μm was used to record 2D SAXS patterns. A homemade extensional rheometer with well controlled humidity (saturated water vapor) and temperature (25 ± 1 ^{o}C) was used to impose stretching on specimens. The specimens have rectangular shape 20 × 7 mm^2 with a thickness of ~1.5 mm.

5.2.4.2 Cyclic test

The cyclic tests were carried on Shimazu (Japan). The loading-unloading cyclic tests were performed from 0 to a certain stretching ratio λ at 100 mm/min, and then the sample was unloaded at the same speed until zero stress was achieved. After waiting for 15 min, the second cycle with same λ was repeated. The maximum λ used at each double cycle is from 1.5 to 6.0. The tensile speed is 100 mm/min with humidity control.

5.3 Result and discussion

5.3.1 Structure of B-DN gel

SAXS was performed to verify the structure of the B-DN gel. **Figure 1a-b** shows 2D SAXS patterns of B gel and corresponding B-DN gel, respectively. The structure of B gel has been clarified in **Chapter 4**. In the B_{142} gel, there exists structure evolution as

increasing the concentration. The B_{142} gel prepared at low concentration is occupied defect (dangling micelles), confirmed by the broaden peak at low q. At high concentration, the dangling micelles transfer to the bridged micelles by connecting to the bridged networks, demonstrated by original peak weakens accompanied by a gradual increase of the new peak showing the structure transition. After introducing the 2nd monomer AAm into the B gel, as shown in **Figure 1b**, the peak 1 from dangling micelles become much weaker, while peak 2 remain and slightly shifts to lower q value (0.25 to 0.22 nm^{-1}), indicating a decrease of the distance between domains. Due to the formation of hydrogen bonds between the first and the second network, the B-DN gel shrinks compared with the B gel. During the shrinkage process, the mobility of dangling micelles is much faster than that of bridged micelles, resulting the peak 1 shifts to the higher q value. Simultaneously, the dangling micelles only shifts slightly to the high q value to response for the shrinkage due to steric constraint. The synergetic movements result in the scattering intensity distribution changes from two peaks curve in B gel to one peak after introducing the second network. domains. For the much weaker peaks of form factor, it is possible caused by the weaker contrast between micelles and environments due to adsorption of PAAm chains on the surface of micelles[26].

5.3.2 Structure evolution of B-DN gel under deformation

SAXS is an effective tool to probe structures in a wide variety of soft materials, thereby extending our understanding of their macroscopic performance. It used to

analyze the structure of polymer under deformation as shear-induced crystallinity polymer chains[27–29], frozen inhomogeneities[30,31] or soft-hard composites[32,33] give rise to very informative anisotropic patterns. As shown in **Chapter 4**, the B gel is very weak and the isotropic SAXS pattern changed into arc-shape when the gel is stretched, indicating that the anisotropic structure was formed. While for the tough B-DN gel, the structure evolution is much more abundant, which possibly gives a rise to its toughening mechanism. **Figure 2a** shows the SAXS results of B-DN gel stretched at different elongation. With the increasing of strain, the SAXS pattern transforms from an isotropic ring to Arc-shape elliptical ring, then change into four-point scattering diagram at moderate strains and eventually to highly anisotropic scattering intensity distribution with two sharp scattering peaks vertical to the stretching direction.

The **Figure 3a** shows the one-dimensional scattering intensity distributions along the stretching direction. The scattering intensity distribution changes from a one-peak curve to a two-peaks one after stretching ratio 1.56, indicating the formation of new structure. Evidently, the scattering peak denoting the original peak weakens accompanied by a gradual increase of the new peak showing the gradual transition at larger strains. The two scattering peaks can be ascribed to the structure of dangling micelles and bridged micelles due to the equivalency of concentration and elongation. This is confirmed by each peaks intensity change along the elongation. Intensities change in **Figure 3b** shows that the peak 1 of dangling micelles in B-DN gel decrease and simultaneously peak 2 of bridged micelles increase as the moderate elongation. At

lager elongation, both intensities arrive a plateau, indicating that there are no bridged micelles change into dangling micelles, which can be confirmed from the disappearance of the peak 2 in **Figure 3a**. **Figure 3c** shows the evolution of the two scattering peaks during the elongation. The position of the scattering peak 1 from newly established dangling micelles locates at smaller q than the one from the bridged micelles. With the increase of strain, the long spacing distance d_1 of the dangling micelles continuous increasing. While the d_2 of the bridged micelles just shows a slight increase. This result is in agreement with previous findings that the longest distance between two bridged micelles obtained after tensile stretching is determined by midblock length of full-stretching, regardless of the macroscopic elongation[34]. In the triblock copolymer system, after enblock chain pulls out from the micelles at microscopic scale, the macroscopic crack propagation will render the materials fails. While in our B-DN gel, the chain pullouts cannot cause catastrophic crack propagation with the protection of 2nd stretchable network. As a result, we can be observed the total bridged chain changes into dangling micelles in the whole elongation regions.

The **Figure 4a** shows the one-dimensional scattering intensity distributions perpendicular to the stretching direction. Only one peak was observed in the whole elongation region. The peak monotonically shifts to the high q value, indicating a smaller long spacing distance. The long spacing distance and corresponding intensity was shown in **Figure 4b**. Interestingly, the intensity has a firstly short increase followed by a decrease after certain elongation ratio. Finally, the intensity continuous to increase

until fracture. In addition, the peak becomes broader as increase of elongation. Based on the intensity change, we can discuss the structure evolution in three regions: In region I ($\lambda < 1.56$), the midblock chain was stretched along the elongation direction, simultaneously, they get closer in the perpendicular direction due to the transverse compression, resulting in the intensity increase. As the elongation ratio increases, in region II, the chain begins to pullout to response to deformation. The micelles in detect region become ununiform and low periodicity, resulting in the wider peak at with low spacing distance at perpendicular direction. While for the region III, however, it is appeared along with the equatorial streak in the perpendicular direction, which is a clue for the formation of elongated microvoids or internal fibrillar structure[35]. To clarify the structure evolution in region III, the azimuthal profiles of PLLA, integrated from 2D SAXS patterns revealed in **Figure 2**, are listed in **Figure 5**. 90° and 180° represents direction perpendicular to elongation direction. As shown in **Figure 5a**, the scattering intensity along the vertical direction increases with elongation increasing in region I. This phenomenon indicates that structure of samples is not homogeneous after elongation and the micelles along the vertical direction is much more compact than that along the horizontal direction. While as increase of elongation entering region II, the intensity along the vertical direction separated to two parts in the 45° direction at beginning, where the shear force arrives maximum. The two spots shift to the vertical direction as the elongation increases. In the region III, the position of the two spots remain unchanged, while a equatorial streak become sharper and sharper as increase of

elongation (**Figure 5b**). To quantitatively investigate lamellar orientation of samples under different elongation ratio, full width at half maximum (represent the degree of orientation) was plotted as a function of elongation. From the azimuthal profile in **Figure 5c**, it is obvious to divide the profile into three regions, which corresponding to the region obtained in **Figure 4b**.

5.3.3 Self-recovery at different elongation

To demonstrated above statement, we performed loading-unloading test with elongation in those regions (**Figure 6a**). The hysteresis ratios are plotted as a function of elongation in **Figure 6b.** Here, the hysteresis energy was defined as the area enveloped by the loading-unloading curve. In region I, the first loading-unloading curve have the same hysteresis with that of second one and the mechanical performance of the gel can be fully recovery. It strongly demonstrated that there is no structure permanent destroy in region I, and the hysteresis originated from energy dissipation due to broken and reform of hydrogen bonding between first and second network in B-DN gel. In region II and III, chain pullout and microviods formation is permanent damage, resulting in the smaller hysteresis in 2^{nd} cycle than the 1^{st} cycle.

5.3.4 Strain-softening in three regions: Mooney-Revlin plot

To quantify the mechanical response to structure evolution, we analyze the tensile behavior shown in **Figure 7a** using the Mooney-Rivlin equation that describes the elasticity of rubbers[36] :

$$\sigma_{red} = \frac{\sigma}{\lambda - \lambda^{-2}} = 2C_1 + 2C_2 \frac{1}{\lambda} \quad (1)$$

Here σ and σ_{red} are the nominal and the reduced engineering stress, respectively, λ is the elongation ratio, C_1 and C_2 are materials constants. The $2C_1$ is related to the shear modulus G, while $2C_2$, the slope of σ_{red} as a function of $1/\lambda$, is related to the strain softening ($C_2 > 0$) or strain hardening ($C_2 < 0$). In the B-DN gel, the strain softening is usually due to breaking of hydrogen bonds or the structure destroy (chain pullout or microviods formation), while the strain hardening is traditionally attributed to the finite extensibility of network chains[36].

The Mooney-Rivlin plots of **Figure 7a** is shown in **Figure 7b**. The reduced stress exhibits a negative slope ($C_2 < 0$, larger $1/\lambda$) in region I indicating a strain hardening from the midblock chain stretching. In region II, the chain pullouts occur in the moderate elongation ratio, the corresponding reduced stress shows a positive slope indicating a strain softening. While in region III, the formation of macroviods intensifies the strain softening process, resulting in a lager slope than that in region II

5.3.5 Toughening mechanism

The complex structure evolution in deformed B-DN gels described above is a crucial issue for understanding the reinforcement mechanisms. As shown in **Figure 8**. in region I, midblock chain stretching to response to the elongation. Here, only the break and reform of hydrogen bonds to dissipate energy; In region II, the endblock chain continuously pullouts from the micelles with the protection of 2nd PAAm network. Besides the dynamic hydrogen bonds, the micelles destroy to dissipate energy; In

region III, all the bridged micelles break into dangling one, as continuously increase deformation, the microviods are formed to dissipate energy.

5.4 Conclusion

To conclude, our work study the structure evolution of tough self-recoverable B-DN gel during elongation. The structure evolution suggests that the high toughness of B-DN gels is a synergistic effect of multiscale energy dissipation. In initial small strain region, the breaking and reforming of hydrogen bonding in chain scale dissipates energy, resulting in 100% self-recovery; In the middle strain region, the chain pullout of endblock from the micelles and debris reorganization of 1st network for forming cluster dissipate energy; In the large strain region, microvoids form, which also dissipate energy. Our gels provide a possibility to design new tough and self-recoverable gels and other work materials.

5.5 Reference

[1] J. P. Gong, Y. Katsuyama, T. Kurokawa, Y. Osada, *Adv. Mater.* **2003**, *15*, 1155.

[2] X. Hu, M. Vatankhah-Varnoosfaderani, J. Zhou, Q. Li, S. S. Sheiko, *Adv. Mater.* **2015**, *27*, 6899.

[3] T. R. Hoare, D. S. Kohane, *Polymer (Guildf).* **2008**, *49*, 1993.

[4] C. W. Peak, J. J. Wilker, G. Schmidt, *Colloid Polym. Sci.* **2013**, *291*, 2031.

[5] C. Fan, L. Liao, C. Zhang, L. Liu, *J. Mater. Chem. B* **2013**, *1*, 4251.

[6] J. P. Gong, *Soft Matter* **2010**, *6*, 2583.

[7] M. Huang, H. Furukawa, Y. Tanaka, T. Nakajima, Y. Osada, J. P. Gong, *Macromolecules* **2007**, *40*, 6658.

[8] H. Tsukeshiba, M. Huang, Y.-H. Na, T. Kurokawa, R. Kuwabara, Y. Tanaka, H. Furukawa, Y. Osada, J. P. Gong, *J. Phys. Chem. B* **2005**, *109*, 16304.

[9] J. P. Gong, Y. Katsuyama, T. Kurokawa, Y. Osada, *Adv. Mater.* **2003**, *15*, 1155.

[10] T. Nakajima, T. Kurokawa, S. Ahmed, W. Wu, J. P. Gong, *Soft Matter* **2013**, *9*, 1955.

[11] R. E. Webber, C. Creton, H. R. Brown, J. P. Gong, *Macromolecules* **2007**, *40*, 2919.

[12] J.-Y. Sun, X. Zhao, W. R. K. Illeperuma, O. Chaudhuri, K. H. Oh, D. J. Mooney, J. J. Vlassak, Z. Suo, *Nature* **2012**, *489*, 133.

[13] C. Chen, Z. Wang, Z. Suo, *Extrem. Mech. Lett.* **2017**, *10*, 50.

[14] D. C. Tuncaboylu, M. Sari, W. Oppermann, O. Okay, *Macromolecules* **2011**, *44*, 4997.

[15] C. Bilici, S. Ide, O. Okay, *Macromolecules* **2017**, *50*, 3647.

[16] K. R. Shull, *J. Polym. Sci. Part B Polym. Phys.* **2006**, *44*, 3436.

[17] M. E. Seitz, D. Martina, T. Baumberger, V. R. Krishnan, C.-Y. Hui, K. R. Shull, *Soft Matter* **2009**, *5*, 447.

[18] K. J. Henderson, T. C. Zhou, K. J. Otim, K. R. Shull, *Macromolecules* **2010**, *43*, 6193.

[19] J. Li, Z. Suo, J. J. Vlassak, *J. Mater. Chem. B* **2014**, *2*, 6708.

[20] P. Y. W. Dankers, T. M. Hermans, T. W. Baughman, Y. Kamikawa, R. E. Kieltyka, M. Bastings, H. M. Janssen, N. A. J. M. Sommerdijk, A. Larsen, M. J. A. Van Luyn, *Adv. Mater.* **2012**, *24*, 2703.

[21] M. Guo, L. M. Pitet, H. M. Wyss, M. Vos, P. Y. W. Dankers, E. W. Meijer, *J. Am. Chem. Soc.* **2014**, *136*, 6969.

[22] X. Dai, Y. Zhang, L. Gao, T. Bai, W. Wang, Y. Cui, W. Liu, *Adv. Mater.* **2015**, *27*, 3566.

[23] K. Mayumi, A. Marcellan, G. Ducouret, C. Creton, T. Narita, *ACS Macro Lett.* **2013**, *2*, 1065.

[24] K. Mayumi, J. Guo, T. Narita, C. Y. Hui, C. Creton, *Extrem. Mech. Lett.* **2016**, *6*, 52.

[25] W.-C. Lin, W. Fan, A. Marcellan, D. Hourdet, C. Creton, *Macromolecules* **2010**, *43*, 2554.

[26] H. J. Zhang, T. L. Sun, A. K. Zhang, Y. Ikura, T. Nakajima, T. Nonoyama, T. Kurokawa, O. Ito, H. Ishitobi, J. P. Gong, *Adv. Mater.* **2016**, *28*, 4884.

[27] K. Cui, Z. Ma, N. Tian, F. Su, D. Liu, L. Li, *Chem. Rev.* **2018**.

[28] S. Dey, D. M. Agra-Kooijman, W. Ren, P. J. McMullan, A. C. Griffin, S. Kumar, *Crystals* **2013**, *3*, 363.

[29] K. Cui, L. Meng, N. Tian, W. Zhou, Y. Liu, Z. Wang, J. He, L. Li, *Macromolecules* **2012**, *45*, 5477.

[30] H. Guo, C. Mussault, A. Brûlet, A. Marcellan, D. Hourdet, N. Sanson,

Macromolecules **2016**, *49*, 4295.

[31] N. Mischenko, K. Reynders, M. H. J. Koch, K. Mortensen, J. S. Pedersen, F. Fontaine, R. Graulus, H. Reynaers, *Macromolecules* **1995**, *28*, 2054.

[32] K. Nishi, M. Shibayama, *Soft Matter* **2016**, *12*, 5334.

[33] S. Rose, A. Dizeux, T. Narita, D. Hourdet, A. Marcellan, *Macromolecules* **2013**, *46*, 4095.

[34] M. Nguyen-Misra, W. L. Mattice, *Macromolecules* **1995**, *28*, 1444.

[35] L. Xiao-Yun, L. Xiu-Hong, Y. Chun-Ming, H. Wen-Qiang, Z. Nie, M. Xia-Ran, T. Feng, W. Yu-Zhu, B. Feng-Gang, W. Jie, *Chinese Phys. B* **2013**, *22*, 46102.

[36] M. Rubinstein, R. H. Colby, *Polymer physics*; Oxford university press New York, 2003; Vol. 23.

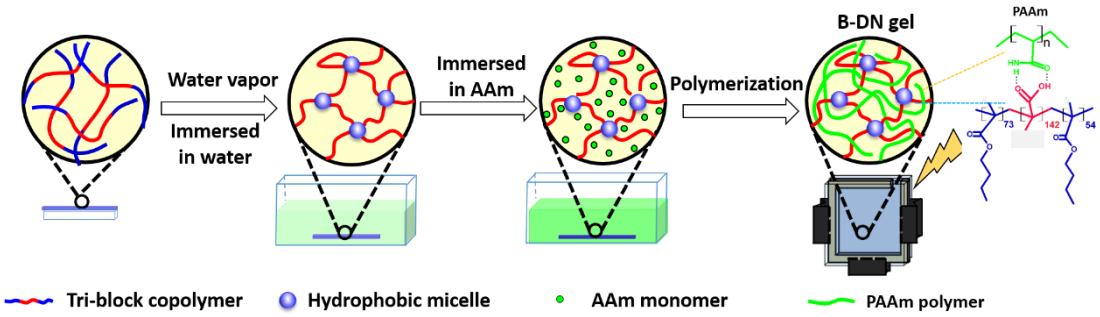

Scheme 1. Schematic diagram depicting the preparation of a B-DN gel.

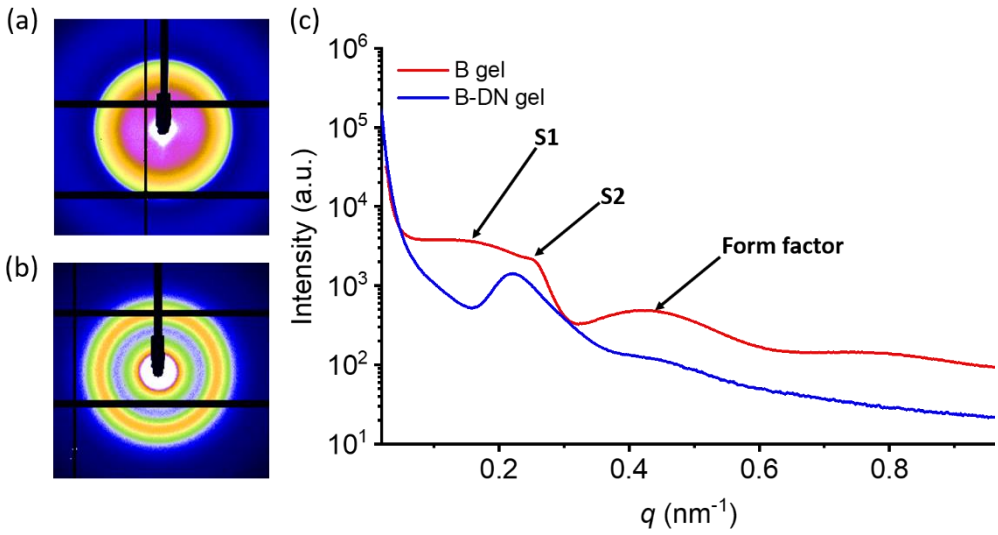

Figure 1. 2D small angle X-ray scattering images of B gel (a) and the corresponding B-DN gel (b). (c) integrated one-dimensional (1D) SAXS intensity profiles of B gel and B-DN gels.

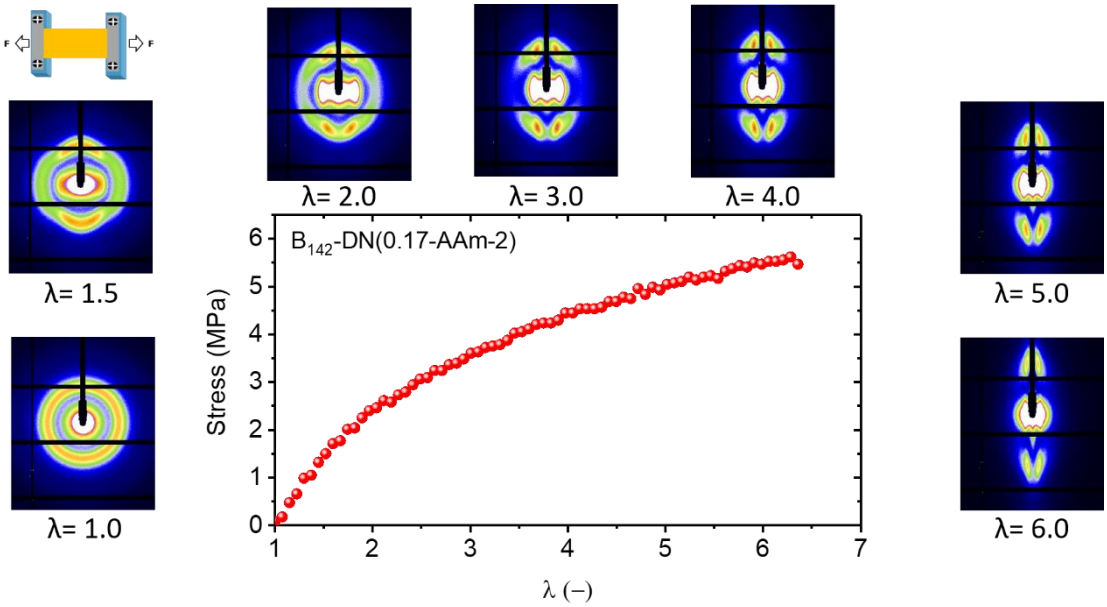

Figure 2. The tensile stress- strain curve and the selected 2D SAXS patterns of B-DN gels stretched at different strains as indicated on the graphs. Stretching direction horizontal.

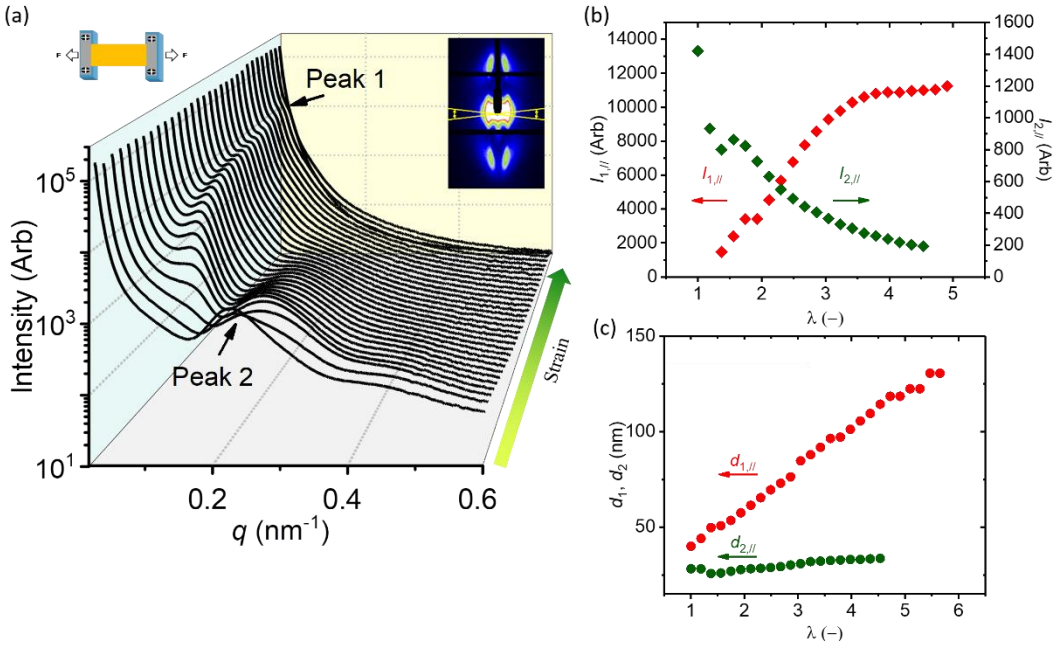

Figure 3. (a)The one-dimensional scattering intensity distribution profiles integrated along the stretching direction. (b) the long spacing d_1, d_2 and (c) corresponding peak maximum intensity as a function of elongation ratio.

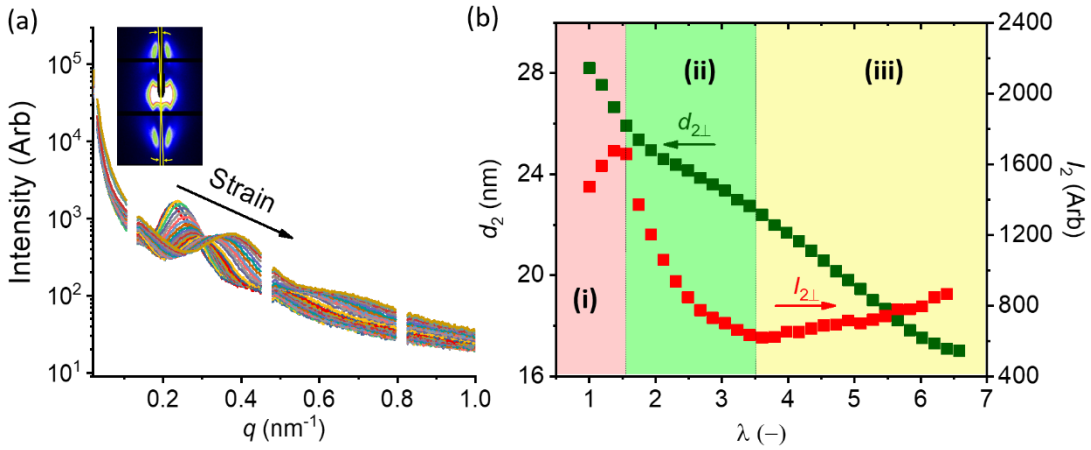

Figure 4. (a)The one-dimensional scattering intensity distribution profiles integrated perpendicular to the stretching direction. (b) the long spacing d_2 and peak maximum intensity as a function of elongation ratio.

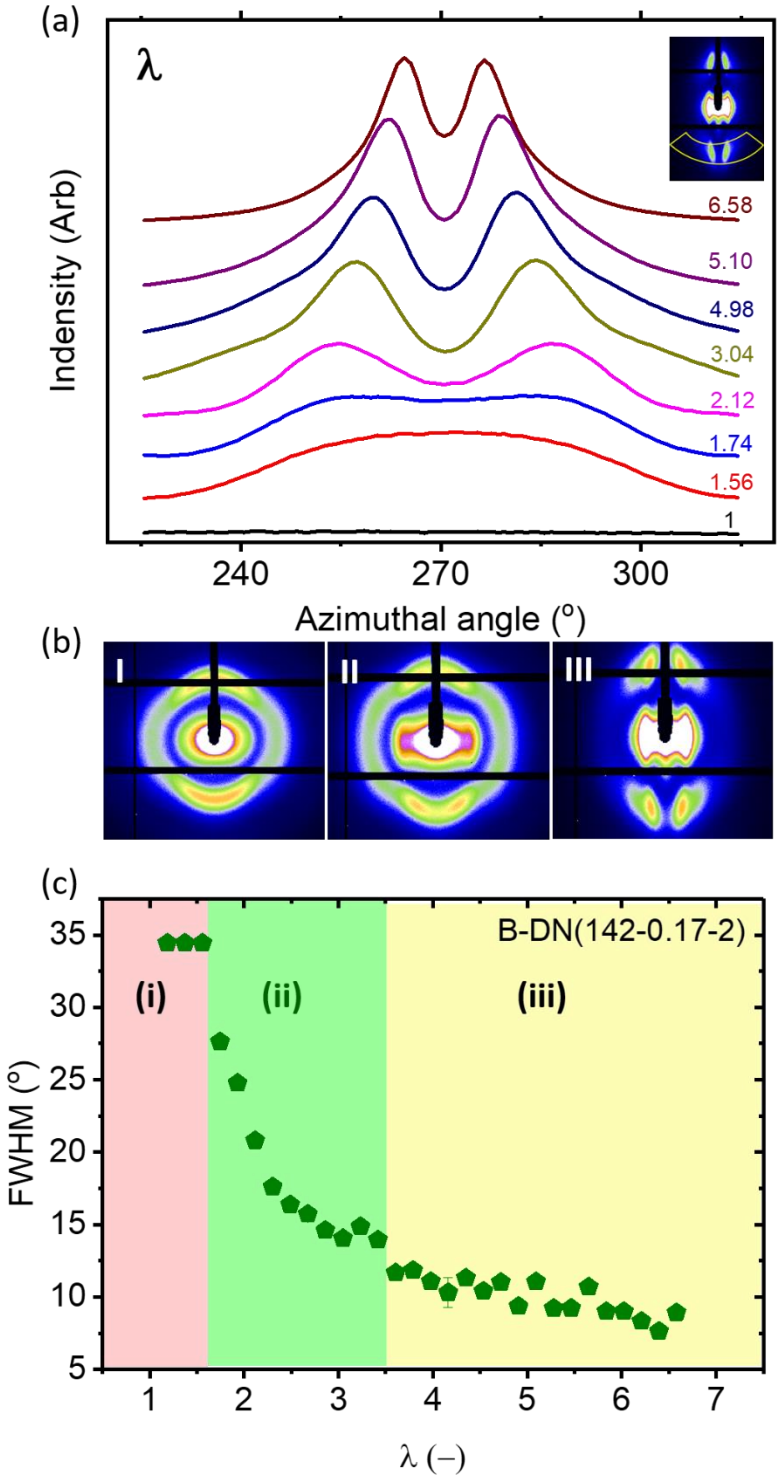

Figure 5. (a) Azimuthal profiles of 2D SAXS patterns of B-DN gel after elongation (b) the represent 2D SAXS images in (c) the three regions divided by degree of orientation of B-DN gel as a function of elongation.

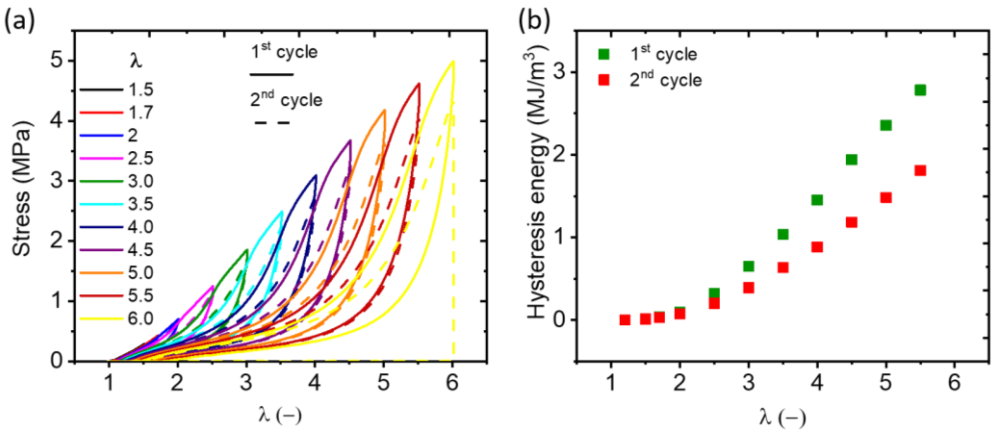

Figure 6. (a) Waiting time dependence of the cyclic tensile test at different strain in the three regions with a 15-min time interval and (b) Hysteresis (the area enveloped by the loading and unloading curve) as functions of elongation ratio.

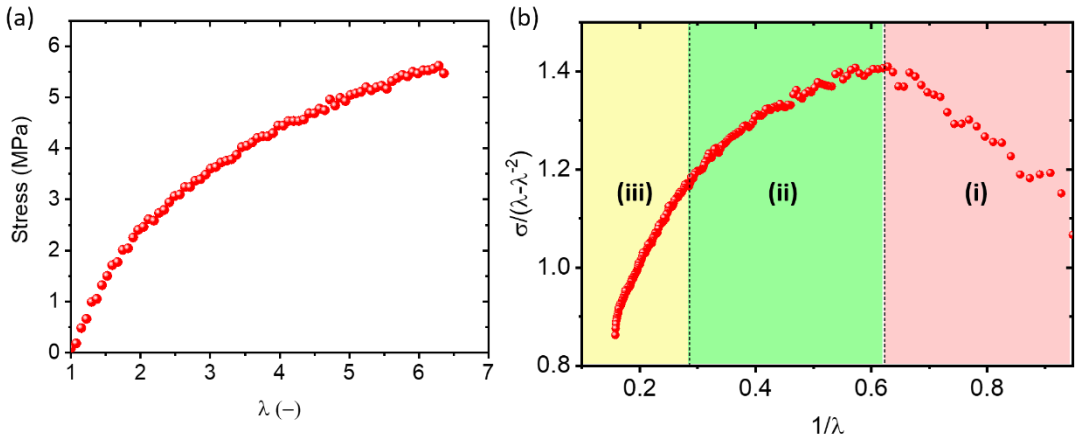

Figure 7. (a)Tensile stress-strain curves of B-DN gels and (b) corresponding Mooney-Rivlin curves $\sigma_{red} = \sigma/(\lambda - \lambda^{-2})$ as a function of $1/\lambda$ at various strain rates.

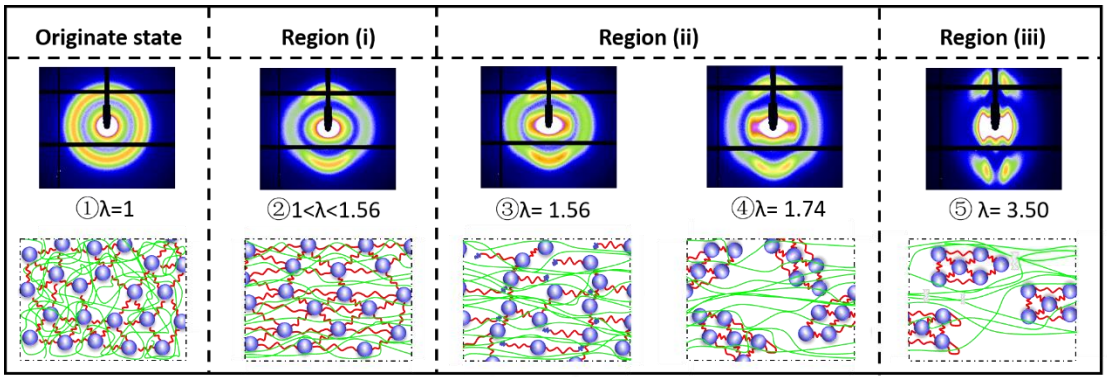

Figure 8. Illustration of structure evolution and energy dissipation mechanism of B-DN gels.

Chapter 6: Tough, Self-Recoverable B-DN Thin Gel Membranes for Various Applications

6.1 Introduction

Hydrogels are being paid more and more attentions owing to a promising wide range of applications as both industrial and medical materials[1], including actuators[2] [3], sensors[4] [5] [6], membrane separation[7], drug delivery[8], contact lenses[9] and artificial organs[10]. Considering the application as sensor and membrane separation, the ultrathin hydrogels are capable of fast responses and high separation efficiency compared with macro-scale hydrogel due to the characteristic time is directly proportional to the square of the thickness of the gel[11]. Hydrogel thin films have also attracted interest as an approach to responsive surfaces and interfaces[7,12,13]. Compared with polymer brushes, the hydrogel interfaces are much more stable, where the hydrogel network is linked to the surface via multiple anchoring points rather than only one functional group of a linear polymer chain. Furthermore, the storage function of the hydrogel thin films (their ability to accommodate various nanoparticles, chemicals, dyes, enzymes, etc.) can be explored for the substantial increase in the range of functional properties they will demonstrate and external signals they will respond to. However, most of ultra-thin hydrogel films, are brittle and weak, which seriously limits their extensive applications. To avoid fracture, the ultrathin hydrogel films are always linked to the supporting substrate by chemical or physical bonds[14]. However, these

methods are only feasible for the substrates which can be functionalized. Furthermore, the potential applications in areas desiring self-standing ultrathin film with high toughness such as aponeurosis[15], artificial skin[16] and septum, are limited. Therefore, it is imperative to create tough and self-standing ultrathin gel films. There are few reports about the preparation of self-standing ultrathin gel films. Tsou et.al[17] developed the thin and tough hydrogel composite films using pHEMA (poly 2-hydroxyethyl methacrylate) as matrix and various kinds of weaved and knitted fabrics and fibers as fillers. However, the swelling mismatch between pHEMA and fillers results folded and curled swollen gel films. It means the composite strategy is difficult to be applied to ultrathin hydrogel film preparation.

In the past several years, we have developed double-network (DN) hydrogel films with excellent mechanical properties, showing tensile fracture strain $\varepsilon_b \approx 1000\%$ and tensile strength $\sigma_b \approx 2$ MPa[18,19]. The DN hydrogel films consist of interpenetrating two chemically-cross-linked networks, which are the brittle first network served as sacrificial bond to dissipate energy after experiencing large deformation, and the ductile second network served as soft matrix[20,21]. The gel films are smooth at swollen state, overcoming the disadvantage of the composite hydrogel films (folding and curling). However, the fabrication process of the DN films is complex and time-consuming. Moreover, these DN gel films are permanently damaged after applying large deformation because the internal fracture of covalent bonds of the brittle first network is irreversible[22]. Therefore, it is imperative to find possible way to

remedy the limitation of chemical crosslinked tough DN thin films. There are few reports about tough reversible hydrogel thin films. While several recent works have replaced the covalent bonds with physical bonds such as hydrogen bond, ionic bond or hydrophobic association to allow the fractured bond to be re-formed[23][24][25].

Here we present a new class of ultrathin, tough, and self-recoverable hydrogel films, called B-DN films, based on the DN concept. Various parameters can be tuned to change the thickness and multiple mechanical properties of B-DN films over wide ranges. Those ultrathin B-DN hydrogel are semi-interpenetrating network gel consisting of the 1st network poly(butyl methacrylate) (PBMA)-*b*-poly(methacrylic acid) (PMAc)-*b*-PBMA triblock copolymer physical gel and the 2nd linear polymer with amino derivative groups. The hydrophobic association of the PBMA block of the 1st network serves as permanent crosslinking points for endowing elasticity, and hydrogen bonds between carboxyl of PMAc and amino of 2nd polymer serves as reversible sacrificial bonds to dissipate energy[25]. The thickness of the B-DN films were easily controllable from 3 μm to several hundred μm via changing spin velocity and triblock copolymer or 2nd monomer condition. The obtained B-DN films exhibit outstanding ultra-stretchability (≈1000 %), high toughness (fracture stress 8 MPa), self-recovery and fast response against external stimuli, which is a breakthrough in the current concept of responsive and tough ultrathin hydrogel films. Moreover, its thinness and the carboxyl group in the triblock copolymer realize fast responsiveness to pH.

6.2 Experiments

6.2.1 Materials

The amphiphilic triblock copolymer poly(butylmethacrylate)-b-poly(methacrylic acid)-b-poly(butyl methacrylate) with various degree of polymerization was synthesized by Otsuka Chemical Co., Ltd., Japan (**Table 1**). The dimethylformamide (DMF) (solvent for the triblock copolymer, Wako Chemicals USA, Inc.) was used as received. The acrylamide (monomer, TCI America) was recrystallized from chloroform, while the 2-oxoglutaricacid (initiator, Polysciences, Inc.) were used as received.

6.2.2 Synthesis of B-DN gel films

A spin-casted film was fabricated by 5 mL aliquot of triblock copolymer/dimethylformamide (DMF) solution (0.1-0.25 wt/wt) on the spin dish. Then thin film was immersed into water for the formation of first network B film via hydrophobic chain self-assembly. After arriving equilibrium, B film was immersed in the second precursor solution containing the prescribed concentrations of second monomer and 2-oxoglutaric acid (0.02 mol% relative to the monomer) as photo-initiator for several minutes. After that, the sample was irradiated with 365 nm UV for 7 h to synthesize second monomer. After polymerization, the as-prepared B-DN film was immersed in purified water for 10 min to reach equilibrium.

6.2.3 Characterization

6.2.3.1 Water content measurement

The water contents of B-DN gel membranes were measured using a moisture balance MOC-120H (Shimadzu Co.). During test, water was gradually evaporated from the hydrogel at an elevated temperature from 25 °C to 120 °C until the weight of samples did not change. The weight change of samples were obtained by heating the hydrogel membrane to 120 °C. The water content was defined as $c_{\mathrm{w}} = 1 - \frac{m_1}{m_0} \times 100\%$, where the m_0 and m_1 was the weight of gel in wet and dry state, respectively.

6.2.3.2 Thickness measurement

The membrane thicknesses were obtained via a 3D violet laser scanning microscope (VK-8700, KEYENCE Co., Ltd.) by step height measurement. The thicknesses of thin hydrogel membranes were defined by the orthogonal distance between two parallel planes representing the upper surface (red profile) of the membrane and a layer of the base material (substrate) contacting the lower surface (light gold profile), respectively. The measurements were carried out three times for precision.

6.2.3.3 Swelling ratio

The thickness swelling ratio Q was defined as the ratio of the sample thickness, t of B-DN gel membranes to that of B gel membranes t_0 at swelling equilibrium, $Q = t/t_0$.

6.2.3.4 Tensile and cyclic test

The tensile stress-strain measurements were performed using a tensile-compressive tester (Tensilon RTC-1310A, Orientec Co.) at a deformation rate of 10 mm/min in a

water bath to prevent water evaporation. The test was carried out on dumbbell-shaped samples with the standard JIS-K6251-7 size (12 mm (gauge length) × 2 mm (width) × 5~100 μm (thickness)). The work of extension at fracture W_b (MJ/m^3), a parameter that characterizes the work required to fracture the sample per unit volume, was calculated from the area below the tensile stress-strain curve until fracture. The fracture stress σ_b and the fracture strain ε_b were defined as stress and strain at fracture point, respectively. The Young's modulus E was defined as value of initial slope of the stress-strain curve. With humidity control, the cyclic tensile test were carried out on the samples of B_{273} (0.23-500/AAm-2) at the rate of 10 mm/min with maximum strain of 1.0.

6.2.3.5 Small angel X-ray scattering (SAXS)

SAXS measurements were performed at BL40B2 beamline at the SPring-8. The wave length of X-ray was 1.0 Å. For static measurements, the sample-to-detector distances was set to be 4301 mm. For *in-situ* SAXS measurements, samples were placed on a uniaxial stretching machine, where the sample strain were measured and the sample-to-detector distances was set to be 2310 mm. The data acquisition time was 20 s per frame for the SAXS two dimensional scattering spectra. All scattering images were analyzed with Fit2D software from European Synchrotron Radiation Facility taking off the detector spatial distortion, X-ray beam fluctuation and background scattering.

6.3 Result and discussion

6.3.1 Formulation for B-DN films

The self-assembly of triblock copolymer allowed a simple two-step preparation of robust hydrogel ultrathin films[26][27][28]. The thin 1st network films, called B films, are fabricated by spin-casting with the triblock copolymer/solvent solution and following self-assembly of PBMA into micelles acting as cross-linking points. Subsequently the linear polymer with amino derivative groups is imported to act as the second component to form B-DN films. Owing to its thinness, the B-DN films swelled rapidly and reached equilibrium within 10 min (**Scheme 1a**). The structure of triblock copolymer and second monomers are shown in **scheme 1b** and **Table 2**.

6.3.2 Structure uniformity of B-DN films

Although spin coating is a simple method for fabricating thin membrane, it is still challenging to fabricate homogenous thin membrane due to solvent evaporation. If the evaporation rate of solvent exceeds diffusion rate within the membrane, a substantial solvent concentration gradient will be generated. This solvent gradient will make the interface physically unstable[29]. In addition, spread-over of polymer solution on the substrate by centrifugal force has an tendency to form laterally phase-separated structure with radial striations from the center to the edge due to the Marangoni-like instability[30,31], which appears when the solvent evaporated quickly during spin casting process. To address this problem, the evaporation rate of solvent during spin coating

process should be controlled in order to get homogenous membrane. In this work, we selected DMF, whose evaporation rate is very slow due to high vapor pressure, as the solvent. In addition, the DMF vapor was introduced by blowing nitrogen inside a DMF bubbler. In order to evaluate solvent evaporation during spin coating process, the copolymer concentration after spin coating was measured. As shown in **Figure 1a**, the triblock copolymer concentration slightly increases as the spin speed increases, indicating that the solvent evaporates slightly during spin coating process. As shown in **Figure 1b**, the thickness uniformity of the B-DN gel membrane from the center to edge was also achieved by the well-controlled solvent evaporation. To further confirm the structure homogeneity of the B-DN gel membranes, small-angle X-ray scattering (SAXS) experiments at different distance from center were performed (**Figure 1c~e**). As shown in **Figure 1f**, the maximum scattering peak positions ($q1$) of the membrane is independent of the distance from the center of the sample. Moreover, the azimuthal angle independence of the scattering profile (insert of **Figure 1f**) indicates no orientation structure in the gels. The isotropic, homogeneous structure of the sample was also confirmed by the tensile stress-strain curves in the directions parallel with and vertical to the direction from center to the edge. As shown in **Figure 1g**, the tensile curves at the opposite directions almost overlap with each other, indicating the isotropic structure of the hydrogel membranes.

6.3.3 Mechanical property and self-recovery

The B-DN films are enough tough and self-standing. Despite its thinness (36.2 μm),

the B-DN film can sustain the impact from a metal ball (120 g) falling from height of 70 mm (insert of **Figure 2a**). By comparing the typical stress-strain curve of B-DN film and its counterparts (PAAm gel and B film) in **Figure 2d**, it is obvious that the thin B-DN film, with ≈75 wt% water content, had a large enhancement on mechanical properties than the PAAm gel and B film. The values of fracture stress σ_b and fracture strain ε_b of the thin and tough B-DN film reached 8.01 MPa and 9.39 mm/mm, respectively. These excellent mechanical performances demonstrate that the DN principle for creation of tough bulk gels is also effective at micro-scale. As mentioned in previous macro-scale hydrogel work, the huge enhancement originated from abundant of sacrificial hydrogen bonds formed between carboxyl groups of the midblock PMAc and amino groups of the second network poly(acrylamide)[25][32].

The B-DN films also show 100% self-recovery. As shown by the cyclic test in **Figure 1e**, the B-DN film exhibited large hysteresis for the first loading-unloading cycle, which dissipates significant energy. After that, the loading-unloading curve gradually recovered back to the first loading-unloading curve with increasing the waiting time to 60 h (**Figure 2f**). To clarify the structure evolution of long period, *in situ* SAXS was also performed during the cycle test. The 2D SAXS spectra of the B-DN film during cycle and after relaxation for 60 h were compared in **Figure 3**. The B-DN film at undeformed state and waiting for 60 h after deformation, the SAXS patterns are isotropic. This result highlights that the structure deformation due to the extension can be erased after waiting enough time. The recovery process is probably related to the

competition of the elasticity of the primary chain at undeformed state and the strength of the temporarily re-formed bonds. The elasticity of the primary chain raptured the re-formed hydrogen bonds and recovered to its equilibrium state. This result confirms that the residual area in the cyclic tensile test is not due to the rupture of covalent bonds but due to the rupture of the physical bonds which can fully recover after waiting enough time. To the best of our knowledge, it is the first report so far that the ultrathin hydrogel film with such high toughness and 100% self-recovery. The high toughness and 100% self-recovery endow the hydrogel films with great potential for the application as artificial skin, muscle sheaths or organ septum.

6.3.4 Thickness tunability

Besides its excellent mechanical properties and 100% self-recovery, the thickness and the mechanical properties can be tuned in wide range by altering experimental parameters. By altering the triblock copolymer concentration and the spin velocity, resulting thickness of the B-DN film could be precisely controlled. As showed in Figure 4a, uniform B-DN films with tunable thickness were successfully prepared at intermediate triblock weight concentration (c_p) ranges from 0.1 to 0.25 (wt/wt). When the c_p lower than 0.1, B films could not be formed because the triblock copolymers formed a looped conformation (where both endblock are located at the same micelle) instead of the bridge between two micelles, which acts as gelation points[33]. While as concentrations increase above 0.25, high viscosity of the solution resulted in an inhomogeneous film. The mechanical performance of B-DN films increases as the

increasing of c_p (**Figure 4c**). It is probably due to an increase of bridging fraction between neighboring micelles or more effective hydrogen bonds formed between bridging chain and second network. Besides that, spin velocity was taken into account to controlling thickness of thin films. As clearly displayed in Figure 4b, it is a simple and effective way to tuning the thickness from 103 μm to 15 μm by increasing the spin velocity from 500 rpm to 5000 rpm. The tensile performance is independent of thickness when spin velocity are slow; while it was noted that the tensile performance began to decrease when continue to increase spin velocity (**Figure 4d**).

6.3.5 Mechanical modulation

The hydrogen bonds formed between amino group from second monomer and carboxyl group from midblock are very essential for endowing B-DN films with excellent mechanical properties and self-recovery. Therefore, the molar ratio of hydrogen-bonding species was varied to tune mechanical properties. The tensile stress-strain curves of the B-DN film showed in **Figure 5b** demonstrate that mechanical performances were successfully tuned widely. There exists a critical concentration point (C_{AAm}: 2 mol/L), where the Young's modulus E and fracture stress σ_b is up to their maximum respectively, corresponding to molar ratio of 0.96 (**Figure 6** and **Table 3**). This ratio is close to the ideal stoichiometric ratio of 1:1. With continuous increase of C_{AAm}, excessive hydrophilic PAAm chain weaken the existing hydrogen bond due to restriction of polymer chain conformation, resulting in decrease of the E and fracture stress (**Figure 5c, d**).

Based on the enhancement of hydrogen bonds by hydrophobic interaction[34], the second monomer AAm was replaced by other amino derivative monomers having hydrophobic moieties N,N-dimethylacrylamide (DMA) and N,N-diethylacrylamide (DEA). As shown in **Figure 7a**, the mechanical properties of B-DN films strongly depended on the second monomer chemical structures. The B-DN film synthesized with AAm (C_{AAm}= 0.5 M) as the second monomer did not show any yielding point, whereas the hydrogel film synthesized with DMA and DEA as second monomers exhibited a distinct yielding points at low strain. Hydrogel film fabricated with DEA monomer shows a larger yielding stress (3.55 MPa) compared with that fabricated with DMA monomer (2.38 MPa). It is expected that the enhanced mechanical strength is due to the stronger hydrogen bonds formed in the hydrogel film based on DMA and DEA monomers. **Figure 7b-d** shows the effect of 2nd monomer concentration on the stress-strain curves of B-DN films synthesized with AAm, DMA and DEA, respectively, where the triblock copolymer concentration C_P is fixed at 0.17. The Young's modulus first increases then decreases as increasing of 2nd monomer concentration and all of them arrive the minimum at the critical concentrations. Before the critical point, the Young's modulus continue to increase due to more hydrogen bonding formation; After critical point, the hydrogen bond saturated and extra hydrophilic PAA make the gel swelling, resulting the decrease of the Young's modulus. It is worthy to mention is the critical point decrease in the B-DN gel based on AAm, DMA, DEA, respectively.

This facile method for the fabrication of B-DN gel membranes via the combination of spin-coating and the DN concept is general, and allows the mechanical performance of a wide range of triblock copolymers of different structure to be tuned. B-DN membranes from triblock copolymers with different midblock and total molecular-chain lengths were successfully fabricated (**Figure 8** and **Table 4**). The Young's modulus of these B-DN gel membranes was observed to increase with decreasing midblock-chain length, whereas fracture strain is proportional to the length of the midblock chain. For example, Young's modulus increased from 0.15 to 1.97 MPa as the degree of polymerization of the midblock, n, decreased from 390 to 220; Young's modulus also decreased from 1.97 to 0.36 MPa when the total molecular length of the triblock copolymer was increased by a factor of 1.3.

6.3.6 Ultrafast pH sensitivity

Owing to its chemical structure and thinness, the tough B-DN films showed ultrafast pH sensitivity. **Figure 10a** shows the image of gel films (thickness: 30.4 m) fully swollen in acidic and alkaline buffer solution. The gel film showed relatively shrunk state in the acidic condition at pH=2.2. However, when the gel was immersed in the alkaline solution at pH=13.0, the gel remarkably swelled and long axial length *L* of the gel increased 1.4 times from that in the acidic condition. This swelling is caused by increase of osmotic pressure of the gel induced by counterion dissociation of carboxyl group in PMAc block in the alkaline solution. The gel subsequently recovered to its original shrunk state when re-immersed in the acidic solution at pH=2.2.

Such repeated swelling and shrinking did not cause permanent damage to the sample. The **Figure 10b** shows the fast response-recovery properties by altering pH from 2.2 to 13. The calculated response time of B-DN film is within 4 s, which shows a much faster response-recovery when compared with the reported pH-responsive hydrogels[35–38]. The typical tensile curves of the B-DN films under the two different pH condition are shown in **Figure 10c** along with the film equilibrated at pH7. The sample in pH2.2 buffer solution show remarkably similar stress-strain curves, indicating structure of the hydrogel film does not change in acidic buffer solution. On the other hand, the Young's modulus, fracture strain and fracture stress of sample in pH13 buffer solution decrease because the hydrogen bonding between amino and carboxyl group was destroyed due to the dissociation of carboxyl groups (shown in **Figure 10d**). However, the gel in pH13 still keeps moderately-high mechanical performance such as 4.2 MPa of fracture stress and 10 of fracture strain. To the best of our knowledge, the B-DN film is only a stimuli-responsive gel that shows high mechanical performance both in swollen and shrunk state. Thus, those properties of mechanical robustness and ultrafast response give rise to the hydrogel films acting as a good candidate for soft actuators requiring high mechanical properties.

6.3.7 Application for postoperative adhesive membrane

6.3.7.1 Sterilization Stability

The biostability of the B-DN gel membranes permitted us to characterize their biocompatibility using the trypan blue live/dead exclusion method[39]. As biomaterials

used for implantation in body, proper sterilization is required[40,41]. However, in many cases, the sterilization process may destroy the physical bonds of the hydrogels and therefore bring negative effects on the mechanical and biological properties of the materials[42]. While for B-DN gel membranes, as shown in **Figure 11**, the use of autoclavation at 120 ºC, 7 minutes, and 101 kPa, for sterilization process does not result in statistical differences in tensile curves in comparison to the results obtained for non-sterilized B-DN gel membranes. The result permits us to use the B-DN gel membranes for biological tests.

6.3.7.2 In vitro biocompatibility

In order to evaluate the biocompatibility of B-DN gel membranes, cell viability was measured by directly seeding the cells on the surface of B-DN gel membranes. 293T cells (ATCC® CRL-3216™) were used to perform the cytotoxicity test. Tissue culture polystyrene (TCPS) was used as a negative and noncytotoxic control. Following ISO standard 10993-5, direct contact was implemented to evaluate whether there is a cytotoxic response to B-DN gel membranes. Then 5mL of the $2x10^4$ cells/mL cell suspension were seeded on sterilized B-DN gels and TCPS control and incubated for 72 and 120 h in a 5% CO_2 humidified atmosphere at 37ºC. Gel was covered by silicone rubber ring to prevent gel from floating. Cell counts were based on hemocytometric, tryphan blue exclusion detection (n>250 per dish). The morphology of cells on different substrates was observed under bright field microscope and fluorescence microscopy (Keyence BZ-9000), and the results are shown in **Figure 12**. We found that

cell viability on a B-DN gel membrane is as high as that of the negative control using tissue-culture polystyrene (TCPS), the common nontoxic cell cultivation material. Throughout 120 h of cell cultivation, cell viability was maintained above 95%, confirming that B-DN gel membranes are not cytotoxic. The mechanical robustness and the biocompatibility of this B-DN gel membrane provide opportunities for the construction of artificial tissue membranes using synthetic materials.

6.3.7.3 In vivo subcutaneous and liver implantation

Given that the DMA monomer itself is non-toxic and bio-inert, the B-DN(DMA) gel membrane was chosen for the *in vivo* biocompatibility test[27,28]. The B-DN(DMA) gel membranes were implanted underneath the rabbit skin and on surface of liver. The responses of the tissues were microscopically examined by pathologists at postoperative week 2. Representative histological images of the tissues for the subcutaneous experiment and liver experiment were shown in **Figure 13a, c**, respectively. Importantly, there was no inflammatory response and fibrosis found with the presence of gel membranes, as compared with the histological images of the control tissues without membrane implantation (**Figure 13b**, **d**), showing that the B-DN membranes did not induce any pathological reaction to the neighboring tissues. Furthermore, the B-DN membrane shows no microscopical adhesion to the surrounding organs, indicating the potential use of B-DN membranes as anti-adhesive sheets to reduce postoperative tissue adhesion formation which is one of the major problems after various surgical procedures. The mechanical robustness and

biocompatibility of these B-DN gel membranes provide the opportunities to construct artificial tissue membranes and surgical anti-adhesive membranes using synthetic materials.

6.3.8 Potential application for tissue membrane

We fabricated 5–100-μm-thick B-DN gel membranes with water contents of 60–95%. The Young's modulus of these membranes is tunable over the 0.1–100 MPa range, while maintaining very high fracture stress (0.9–8.0 MPa), fracture strain (2–13), and toughness (work of extension: 0.4–40 MPa/m^3) (**Table 4 and Figure 9**). These B-DN gel membranes are promising as replacement biological membranes, such as in Glisson's capsules, pericardia, and gastrointestinal walls, and so on. To study these possibilities, the structures and mechanical properties of a variety of tissue membranes, data that are not available in literature, were measured in this work (**Table 5**). These tissue membranes, containing 50–90% water, were 10–1000 μm thick. We found that the mechanical properties of our B-DN gel membranes overlap with, or are superior to, those of the biological-tissue membranes studied (**Figure 14**). Specifically, the Young's modulus and fracture stress of B-DN gel membranes are comparable with these tissue membranes, while their fracture strain and toughness are much higher than those of the tissue membranes. These results indicate that the B-DN gel membranes are suitable for use in replacement of tissue membranes. These properties enable the B-DN gel membranes to potentially replace injured tissue membranes. For such biomaterial purposes, stability in saline solution, tolerance to

extreme pH, stability against sterilization, and biocompatibility, are critically required for B-DN gel membranes. We found that the B-DN gel membranes are stable in saline solution, while their mechanical tolerances to extreme pH (2.2–10.0) are much higher than those of the various tissue membranes in this study, which are damaged when exposed to low or high pH solutions. Typical tensile curves of the B-DN gel membranes in saline solution and in buffer solution at different pH are shown in **Figure 15**. The samples in saline solution and in pH 2.2 buffer solutions show almost identical stress-strain curves to that obtained in pure water, indicating that the structure of the B-DN gel membrane does not change in saline solution and acidic buffer solution. On the other hand, the samples became soft and the fracture stress decreased in pH 13.0 buffer solution, suggesting that some of the hydrogen bonds between the amides and the carboxyl group are destroyed due to the dissociation of the carboxyl groups under alkaline conditions, however the membrane still exhibits moderately high mechanical performance, such as a fracture stress of 4.2 MPa and a fracture strain of 10. To the best of our knowledge, these B-DN gel membranes are the only existing hydrogel membranes that show high mechanical performance over such a wide pH range. The B-DN gel membranes also exhibit excellent mechanical performance in saline solution at human-body temperature (37 °C) (**Figure 15** and **Table 6**).

6.4 Conclusion

In summary, we have successfully synthesized tough, ultrathin and 100%

self-recovery B-DN hydrogel films with ultrafast pH response based on DN concept and spin casting method. Under micro-scale thickness, hydrogel films show super-high exhibited remarkable 100% self-recovery and ultrafast pH sensitivity (response time within 4s) while keeping tough mechanical properties due to the stability of hydrophobic micelles. The ultrafast pH-sensitive hydrogel films with toughness, 100% recoverability would extend soft materials as smart candidates in industrial and biomedical applications such as would dressing, artificial skin and actuators.

6.5 Reference

[1] A. L. Rutz, R. N. Shah, **2016**, 73.

[2] Y. Tsuda, A. Kikuchi, M. Yamato, G. Chen, T. Okano, *Biochem. Biophys. Res. Commun.* **2006**, *348*, 937.

[3] I. Tokarev, M. Orlov, S. Minko, *Adv. Mater.* **2006**, *18*, 2458.

[4] I. Tokarev, S. Minko, *Soft Matter* **2009**, *5*, 511.

[5] N. Meyerbröker, M. Zharnikov, *ACS Appl. Mater. Interfaces* **2014**, *6*, 14729.

[6] I. Tokarev, I. Tokareva, S. Minko, *Adv. Mater.* **2008**, *20*, 2730.

[7] I. Tokarev, S. Minko, *Adv. Mater.* **2010**, *22*, 3446.

[8] T. R. Hoare, D. S. Kohane, *Polymer (Guildf).* **2008**, *49*, 1993.

[9] L. Xinming, C. Yingde, A. W. Lloyd, S. V Mikhalovsky, S. R. Sandeman, C. A. Howel, L. Liewen, *Contact Lens Anterior Eye* **2008**, *31*, 57.

[10] M. I. Baker, S. P. Walsh, Z. Schwartz, B. D. Boyan, *J. Biomed. Mater. Res. Part B Appl. Biomater.* **2012**, *100*, 1451.

[11] T. Tanaka, D. J. Fillmore, *J. Chem. Phys.* **1979**, *70*, 1214.

[12] L. Chen, M. Liu, L. Lin, T. Zhang, J. Ma, Y. Song, L. Jiang, *Soft Matter* **2010**, *6*, 2708.

[13] P. W. Beines, I. Klosterkamp, B. Menges, U. Jonas, W. Knoll, *Langmuir* **2007**, *23*, 2231.

[14] I. Tokarev, S. Minko, *Soft Matter* **2009**, *5*, 511.

[15] C. N. Maganaris, M. V Narici, in *Tendon Inj.*, Springer, **2005**, pp. 14–21.

[16] P. P. Purslow, *J. Mater. Sci.* **1983**, *18*, 3591.

[17] C. D. Young, J. R. Wu, T. L. Tsou, *Biomaterials* **1998**, *19*, 1745.

[18] S. Liang, Q. M. Yu, H. Yin, Z. L. Wu, T. Kurokawa, J. P. Gong, *Chem. Commun.* **2009**, *48*, 7518.

[19] J. Hu, K. Hiwatashi, T. Kurokawa, S. M. Liang, Z. L. Wu, J. P. Gong, *Macromolecules* **2011**, *44*, 7775.

[20] J. P. Gong, Y. Katsuyama, T. Kurokawa, Y. Osada, *Adv. Mater.* **2003**, *15*, 1155.

[21] J. P. Gong, *Soft Matter* **2010**, *6*, 2583.

[22] S. Liang, Z. L. Wu, J. Hu, T. Kurokawa, Q. M. Yu, J. P. Gong, **2011**, *44*, 3016.

[23] Y. Gong, M. Gao, D. Wang, H. Möhwald, *Chem. Mater.* **2005**, *17*, 2648.

[24] T. L. Sun, T. Kurokawa, S. Kuroda, A. Bin Ihsan, T. Akasaki, K. Sato, T. Nakajima, J. P. Gong, M. A. Haque, T. Nakajima, J. P. Gong, M. A. Haque, *Nat. Mater.* **2013**, *12*, 932.

[25] H. J. Zhang, T. L. Sun, A. K. Zhang, Y. Ikura, T. Nakajima, T. Nonoyama, T. Kurokawa, O. Ito, H. Ishitobi, J. P. Gong, *Adv. Mater.* **2016**, *28*, 4884.

[26] K. J. Henderson, T. C. Zhou, K. J. Otim, K. R. Shull, *Macromolecules* **2010**, *43*, 6193.

[27] T. Vermonden, N. A. M. Besseling, M. J. van Steenbergen, W. E. Hennink, *Langmuir* **2006**, *22*, 10180.

[28] C. He, S. W. Kim, D. S. Lee, *J. Control. release* **2008**, *127*, 189.

[29] J. A. Moriarty, L. W. Schwartz, E. O. Tuck, *Phys. Fluids A Fluid Dyn.* **1991**, *3*,

733.

[30] M. Malmsten, B. Lindman, *Macromolecules* **1992**, *25*, 5440.

[31] P. Mokarian-Tabari, M. Geoghegan, J. R. Howse, S. Y. Heriot, R. L. Thompson, R. A. L. Jones, *Eur. Phys. J. E* **2010**, *33*, 283.

[32] Q. M. Yu, Y. Tanaka, H. Furukawa, T. Kurokawa, J. P. Gong, *Macromolecules* **2009**, *42*, 3852.

[33] T. L. Chantawansri, T. W. Sirk, Y. R. Sliozberg, *J. Chem. Phys.* **2013**, *138*, 24908.

[34] X. Hu, M. Vatankhah-Varnoosfaderani, J. Zhou, Q. Li, S. S. Sheiko, *Adv. Mater.* **2015**, *27*, 6899.

[35] M. Sadeghi, E. Mohammadinasab, F. Shafiei, *Curr. World Environ.* **2012**, *7*, 69.

[36] F. Soleimani, M. Sadeghi, *J. Biomater. Nanobiotechnol.* **2012**, *3*, 310.

[37] U. Schmidt, M. Guenther, G. Gerlach, *Curr. Dir. Biomed. Eng.* **2016**, *2*, 117.

[38] X. J. Liu, H. Q. Li, B. Y. Zhang, Y. J. Wang, X. Y. Ren, S. Guan, G. H. Gao, *Rsc Adv.* **2016**, *6*, 4850.

[39] W. Strober, *Curr. Protoc. Immunol.* **2015**, A3.B.1.

[40] E. Ohashi, I. Karube, *J. Biotechnol.* **1995**, *40*, 13.

[41] M. Furuta, M. Oka, T. Hayashi, *Radiat. Phys. Chem.* **2002**, *63*, 323.

[42] P. R. Marreco, P. da L. Moreira, S. C. Genari, Â. M. Moraes, *J. Biomed. Mater. Res. Part B Appl. Biomater.* **2004**, *71*, 268.

Table 1. Description of triblock copolymers studied in this work.

Code	Triblock copolymer [a)] $A_mB_nA_p$	[b)] f_B	[c)] Mw (kg/mol)	[c)] M_w/M_n
B_{390}	$A_{141}B_{390}A_{141}$	0.58	73.66	1.43
B_{297}	$A_{145}B_{297}A_{117}$	0.52	62.86	1.38
B_{220}	$A_{157}B_{220}A_{146}$	0.42	62.00	1.25
$1.3B_{220}$	$A_{247}B_{334}A_{215}$	0.42	74.22	1.46

[a)]Molar fraction of midblock PMAA. [b)]Weight-average molecular weight. [c)]Molecular weight distribution.

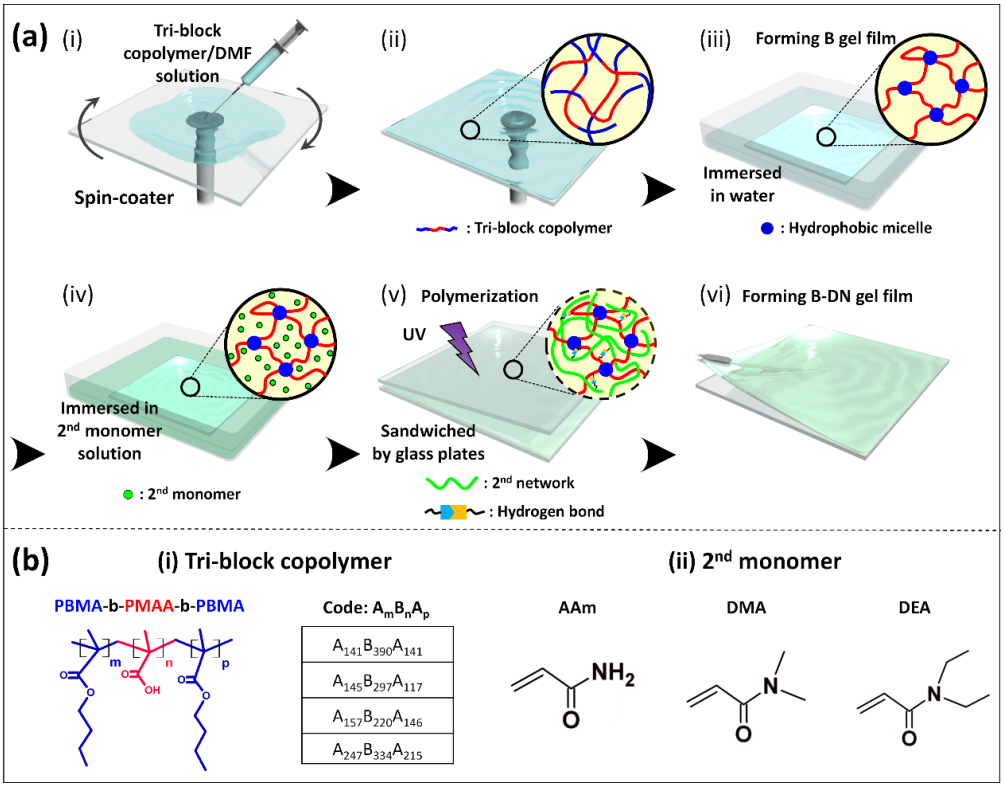

Scheme 1. Schematics of preparation of thin B-DN gel membranes. (a) Spin coated thin membrane of tri-block copolymer was fabricated by depositing certain amount of triblock copolymer solution onto a spin dish, followed by rapid acceleration of spin speed. After spin coating, the thin membrane was immersed in water for hydrophobic chain self-assembly to form weak B gel membrane as the first network. After reaching equilibrium, the B gel membrane was transferred to the second monomer/UV-initiator aqueous solution and soaked for several minutes. Finally, the second monomer was polymerized for 8 h to form the polymers that can form physical association with the first network. (b) The chemical structures of the triblock copolymer and second monomers.

Table 2. Sample codes and formulations of B-DN gel membranes studied in this work.

Sample code [a] B_n (C_P-s/m-C_2)	1st network		2nd network	
	Triblock polymer concentration, C_P (wt/wt)	Spin speed, s (rpm)	2nd monomer, m	Concentration, C_2 (mol/L)
B_{273} (C_P-3000/AAm-2)	0.1~0.25	300	AAm	2
B_{273} (0.23-s/AAm-2)	0.23	500~5000	AAm	2
B_{273} (0.23-3000/m-2)	0.23	3000	AAm, DMA, DEA	0.5
B_{273} (0.23-3000/AAm-C_2)	0.23	3000	AAm	0.2~7

a) N is the degree of polymerization of the midblock of the triblock copolymer, C_P is the weight fraction of triblock copolymer (wt/wt) in the precursor solution for preparing the spin coated membranes, s is the spin speed (rpm), m is the 2nd monomer types and C_2 is the 2nd monomer concentration (mol/L) in the precursor solution for the polymerization of the second polymers that form physical association with the first network. The 2nd monomer was polymerized at the initiator concentration of 0.05 mol% (in relative to 2nd monomer) in the absence of chemical crosslinker.

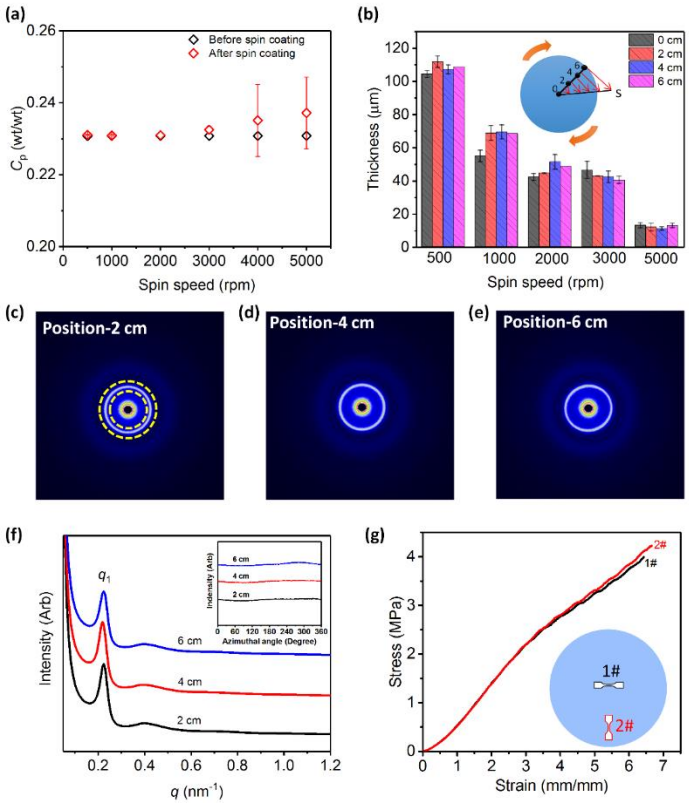

Figure 1. (a) Comparison of triblock copolymer concentration Cp before and after spin coating. (b) Thicknesses of B-DN gel membranes measured at different distances (indicated in the graph) from the center for different spin speed. Sample code: B273 (0.23-s/AAm-2). (c-e) 2D Small angle X-ray scattering spectra of B-DN gel membranes measured at different distances from the center and (f) the corresponding integrated one-dimensional SAXS intensity profiles. The inserting figure is the azimuthal angle distribution of the scattering intensity of the SAXS peaks along q value from 0.19 nm-1 to 0.26 nm-1 for (c) ~ (e). The region outlined between yellow short dash circles, corresponds to the region for azimuth integration. Spectra have been shifted vertically for clarity. Sample code: B273 (0.23-3000/AAm-2). (g) Stress-strain curves of B-DN gel membranes at radical and tangential direction. Sample code: B273 (0.23-3000/AAm-2).

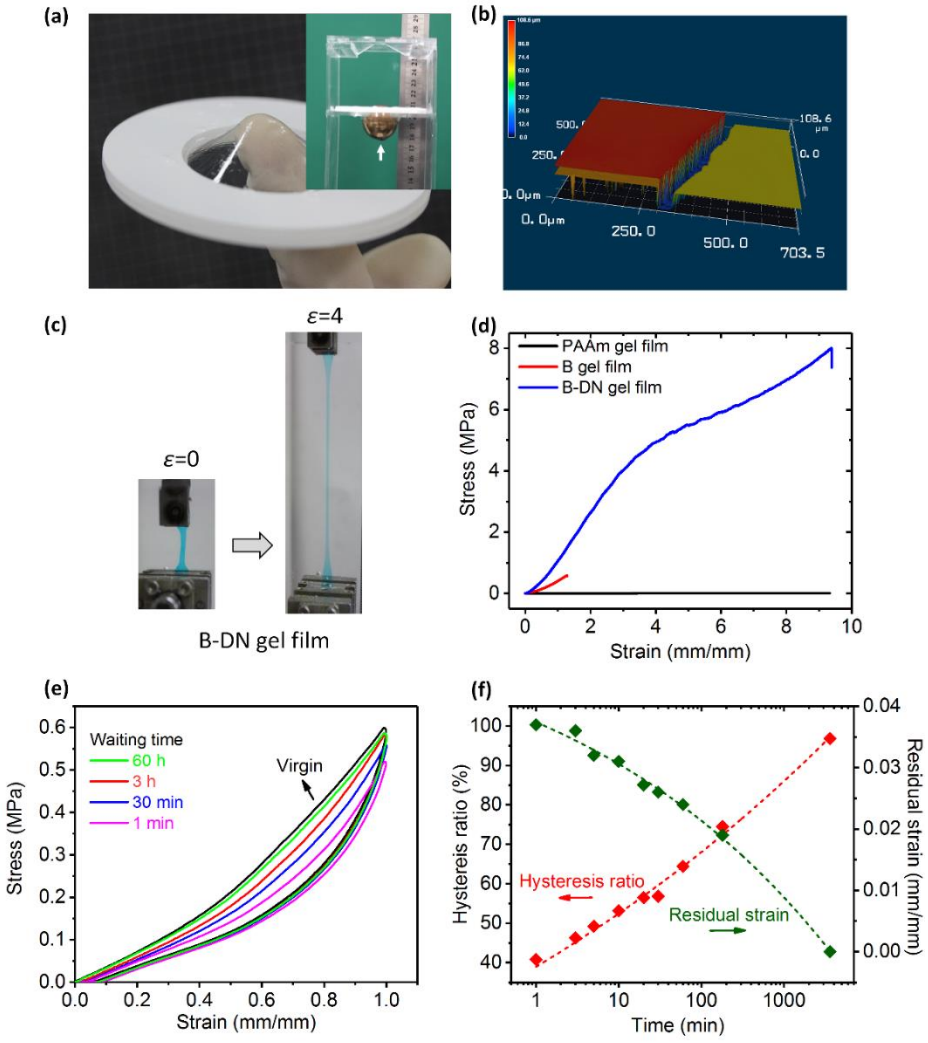

Figure 2. (a) Optical images of the B-DN gel membrane with a thickness of 36.2 μm which can sustain the impact of a 120 g ball (white arrow) falling from the height of 10 cm (inserted image). (b) Optical image showing aspiration process of the B-DN gel membrane, of 36.2-μm-thick and 16-cm^2-area, into a micropipette with a tip diameter of 800 μm. (c) 3D microscope image of the surfaces of B-DN membrane (red profile) and the glass substrate (light gold profile); the thickness of B-DN membrane was determined by the height difference of the two surfaces. Sample code: B_{273} (0.23-3000/AAm-2). (d) Comparison of tensile stress-strain curves between B-DN gel membrane and its

counterparts. The pure PAAm gel membrane, with a thickness of 523 μm, was prepared from a precursor solution of 2 mol/L AAm, 0.05mol% MBAA, and 0.05 mol% α-keto (relative to AAm concentration). B gel membrane: B_{273} (0.23-3000), thickness: 34.2 μm; B-DN gel membrane: B_{273} (0.23-3000/AAm-2), thickness: 36.2 μm. The insert figures show the B-DN gel membrane at its free-standing state and the stretching state at a strain of 4. The gel membrane was dyed for a clear visibility. (e) Waiting time dependence of the cyclic tensile test results, and (f) Waiting time dependence of the residual strain and hysteresis ratio (area ratio of the subsequent hysteresis loops to the virgin one). Sample code: B_{273} (0.23-500/AAm-2), thickness 113 μm.

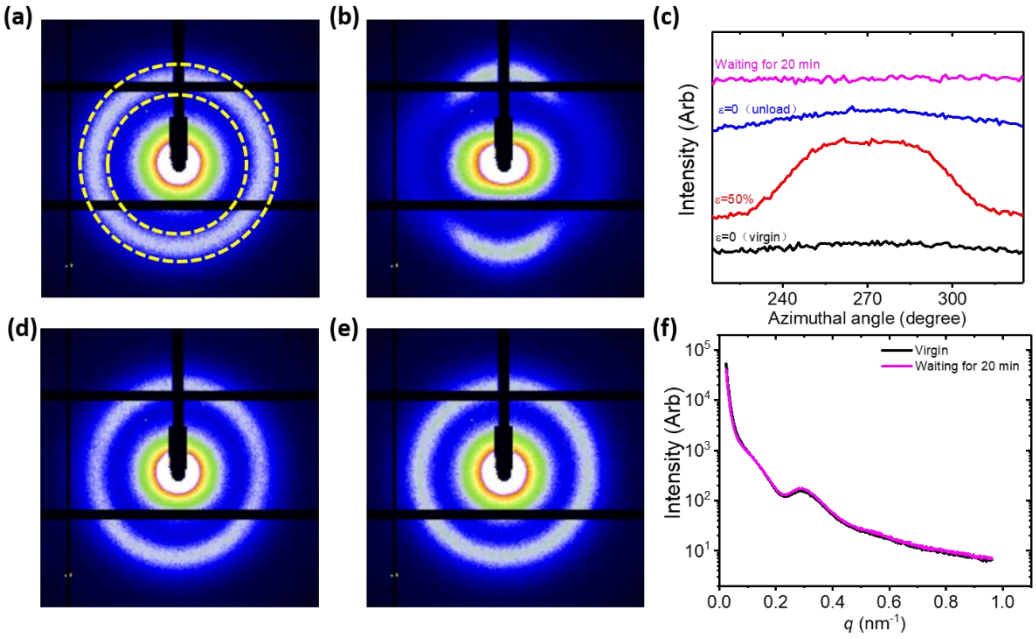

Figure 3. (a) Selected 2D SAXS spectra of B-DN gel membranes stretched at different strains (ε) during cyclic tensile test, and the 2D SAXS patterns of the loaded sample after waiting for 60 h at room temperature. Stretching direction is vertical. (b) Comparison of one-dimensional scattering intensity profiles of B-DN gel membrane integrated along the stretching direction between the virgin state and after-60 h recovery of the pre-stretched state (ε =1.0).

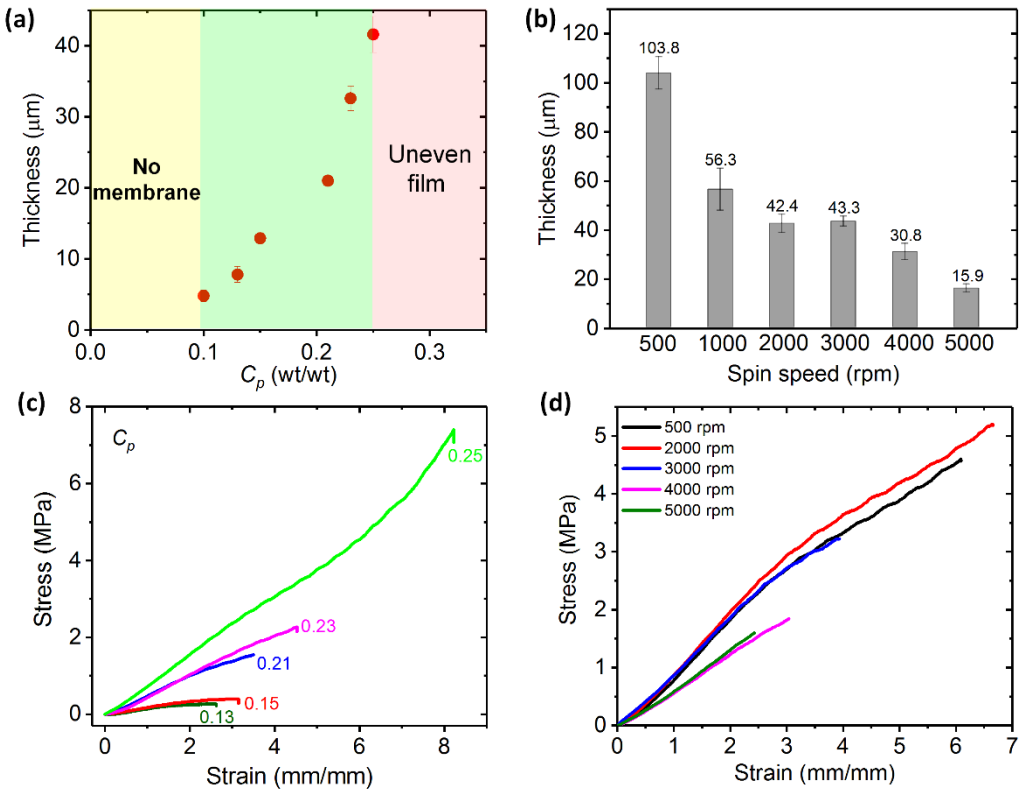

Figure 4 (a) Thickness of the B-DN gel membranes as a function of triblock copolymer concentration in precursor solution C_p and (c) corresponding stress-strain curves. Sample code: B_{273} (C_p-3000/AAm-2). (b)Thickness of the B-DN gel membranes as a function of spin speed, s. Sample code: B_{273} (0.23-s/AAm-2) and (d) corresponding stress-strain curves.

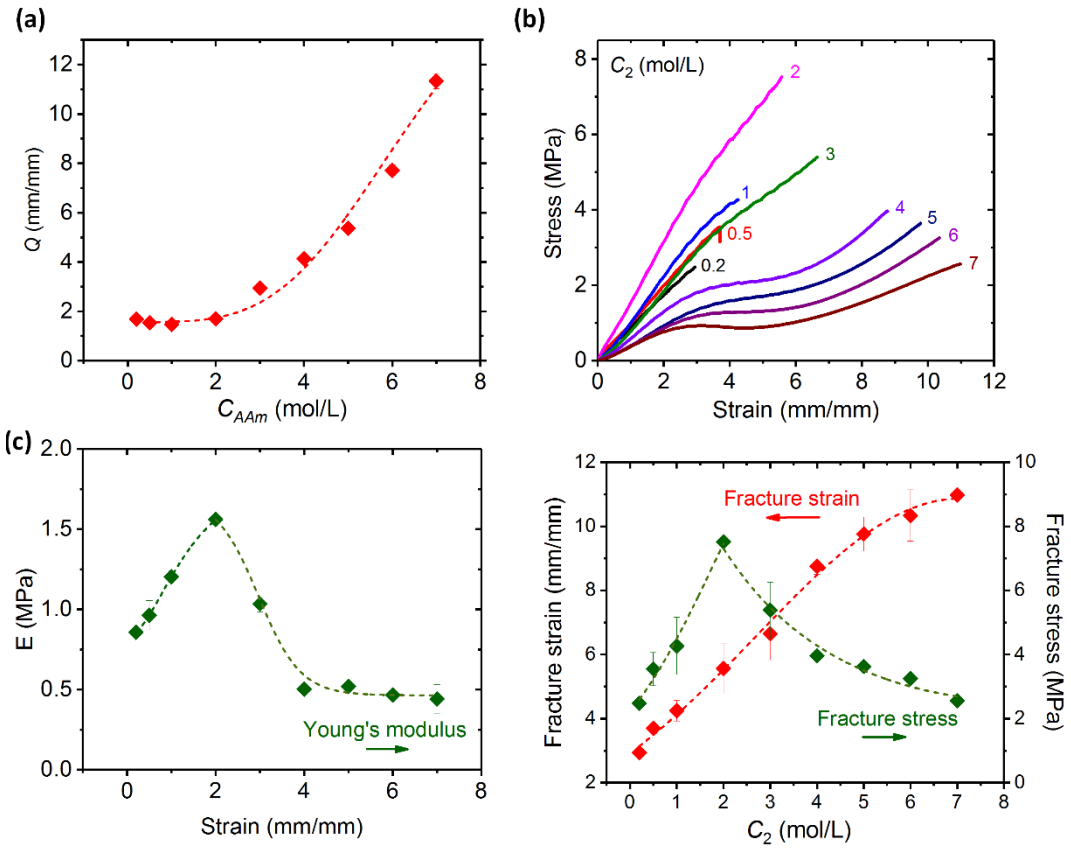

Figure 5 (a) The one-dimensional swelling ratio Q and (b) Tensile behaviors of the B-DN gel membranes prepared at different concentration of the second monomer AAm, C_2. Sample code: B_{273} (0.23-3000/AAm-C_2). (c) Dependence of the Young's modulus, (d) fracture strain and fracture stress on the C_2

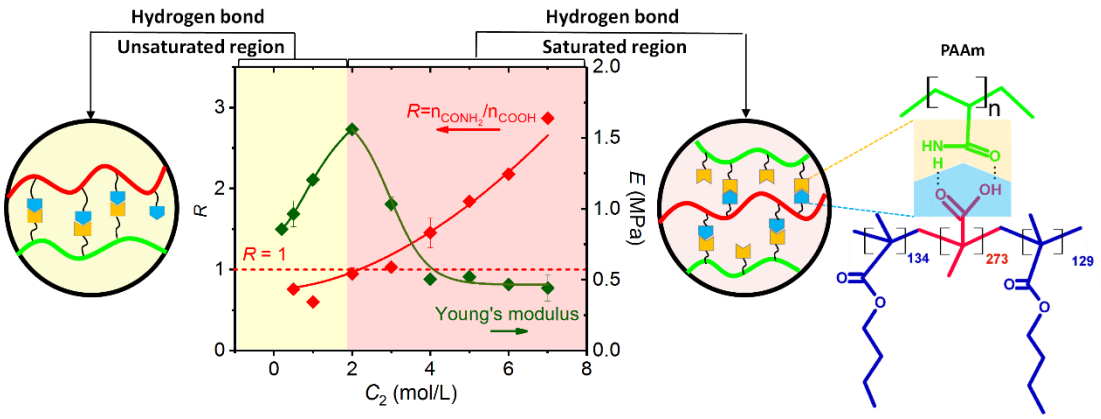

Figure 6 Molar ratio *R* of amino of 2nd polymer to the carboxyl of PMAA in B-DN gel membranes determined by the element analysis. The red horizontal dotted line denotes the 1:1 ratio of amino of 2nd polymer to the carboxyl of PMAA. Sample code: B_{273} (0.23-3000/AAm-C_2).

Table 3. Weight percentage of elements in various B-DN gel membranes of sample series (0.23-3000/AAm-C_2) obtained by element analysis.

C_2 in feed (mol/L)	C (wt%)	H (wt%)	N (wt%)	[a)] $R = n_{AAm}/n_{MAA}$ (mol/mol)
0.5	56.76	8.17	4.89	0.76
1	59.05	8.40	3.81	0.606
2	59.07	8.54	4.89	0.96
3	55.34	7.94	6.49	1.036
4	54.38	7.86	7.60	1.456
5	51.85	7.52	9.78	1.846
6	51.62	7.50	10.70	2.18
7	51.78	7.53	12.08	2.87

[a)]Molar ratio R of amino of 2nd polymer to the carboxyl of PMAA in B-DN gel membranes.

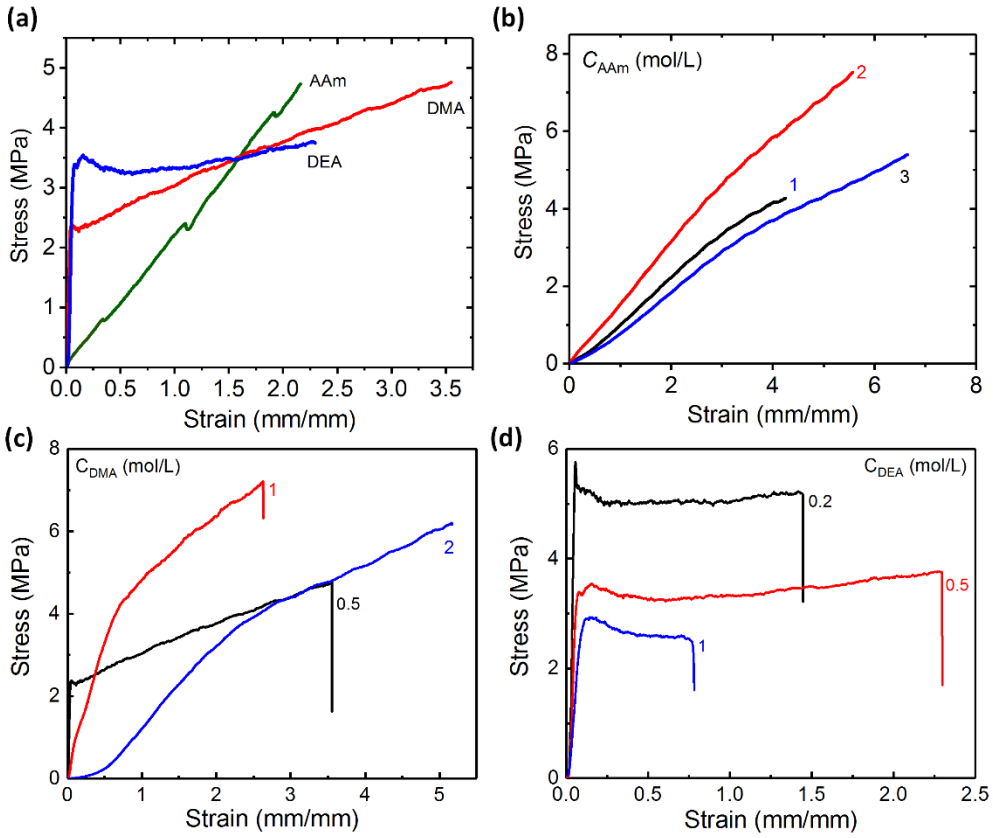

Figure 7 (a) Tensile behaviors of the B-DN gel membranes with different types of second network. Sample code: B_{273} (0.23-3000/m-0.5). Tensile behaviors of the B-DN gel membranes prepared at different concentration of the second monomer AAm (b), DMA (c) and DEA (d). Sample code: B_{273} (0.23-3000/AAm-C_2), B_{273} (0.23-3000/DMA-C_2) and B_{273} (0.23-3000/DEA-C_2).

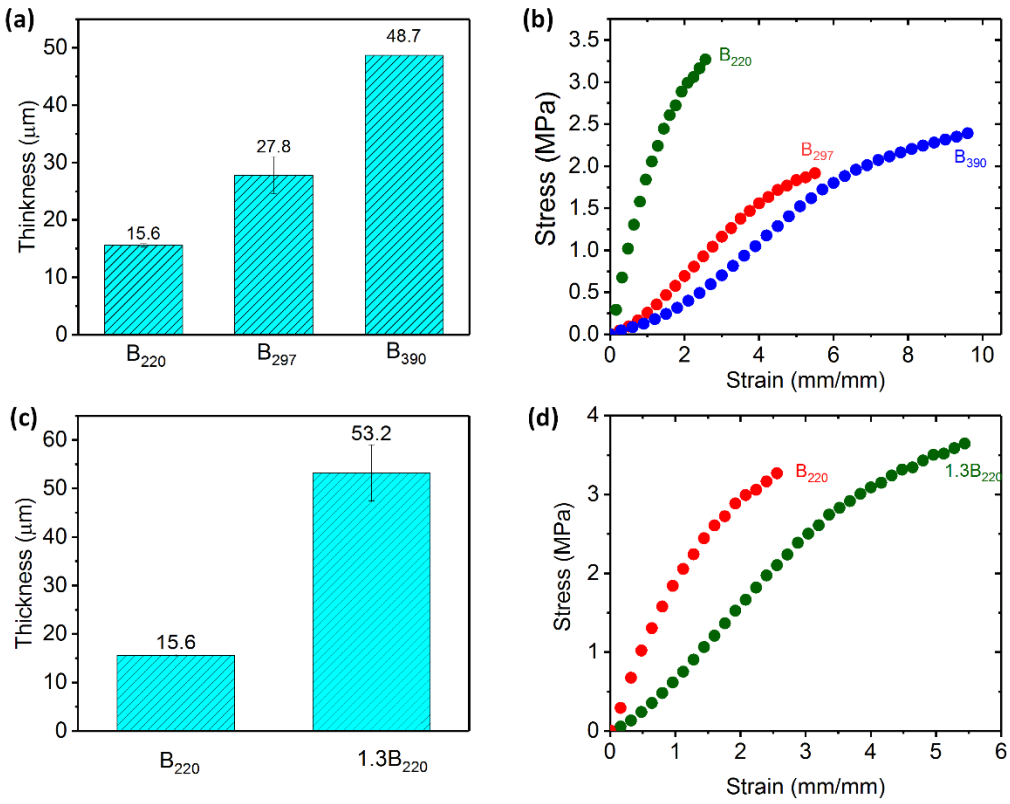

Figure 8. (a) Thickness of B-DN gel membranes prepared using triblock copolymers with different midblock length and (b) the corresponding tensile stress-strain curves. Sample code: B_N (0.23-3000/AAm-2); (c) Thickness of B-DN gel membranes prepared using triblock copolymers with different molecular weight and (d) corresponding tensile stress-strain curves. Sample code: B_{220} (0.23-3000/AAm-2), $1.3B_{220}$ (0.23-3000/AAm-2).

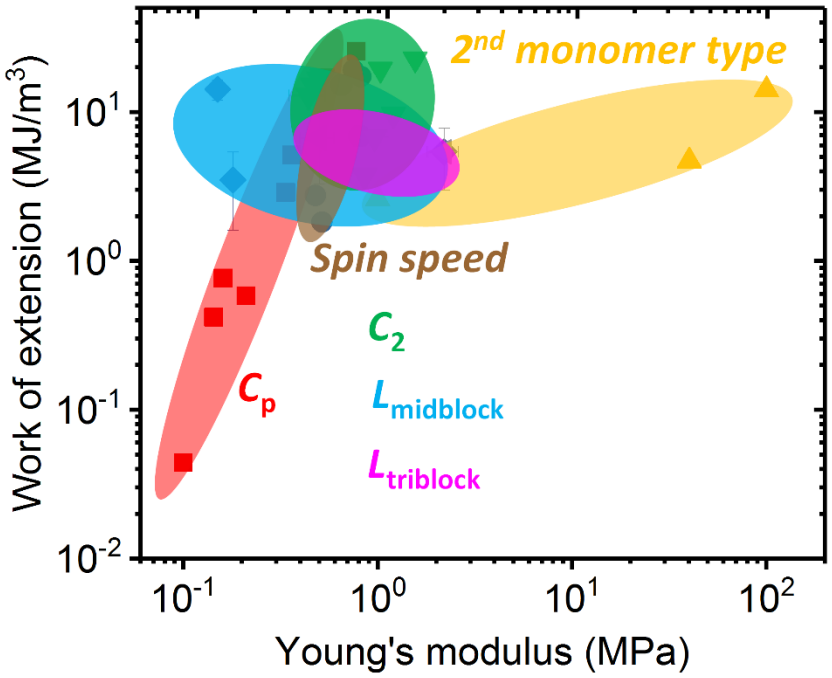

Figure 9. Work of extension and Young's modulus of B-DN gel membranes prepared at different formulations and spin conditions. Red, C_p, triblock concentration range from 0.1 to 0.25 (wt/wt); Gray, spin speed ranges from 500 to 5000 rpm; green, C_2, the 2nd monomer concentration ranges from 0.2 to 7 mol/L; orange, the 2nd monomer types (AAm, DMA and DEA) with same concentration 0.5 mol/L; cyan, $L_{midblock}$, the B-DN membranes prepared from different midblock length ranges from 220 to 390; pink, $L_{triblock}$, the B-DN membranes prepared from different total molecular weight.

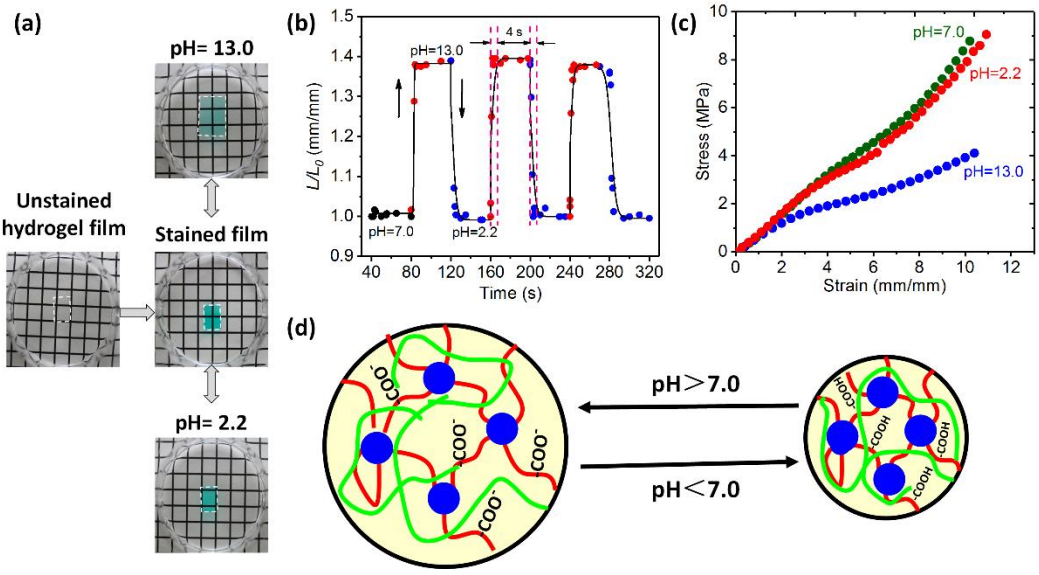

Figure 10. (a) Photographs of the B-DN gel membranes experiencing reversible swelling–shrinking upon changes in pH between pH13.0 and pH2.2. The B-DN gel membrane was dyed for a clear visibility. (b) Oscillatory swelling-shrinking (pH2.2 ↔ pH13.0) behavior of the B-DN gel membranes. (c) Tensile behaviors of the B-DN gel membranes tested in buffers with pH= 13.0, 7.0 and 2.2, respectively. (d) Schematic illustration of the mechanism of reversible swelling-shrinking for B-DN gel membranes in response to pH change. Sample code: B_{273} (0.23-3000/AAm-2), thickness: 30.4±0.6 μm.

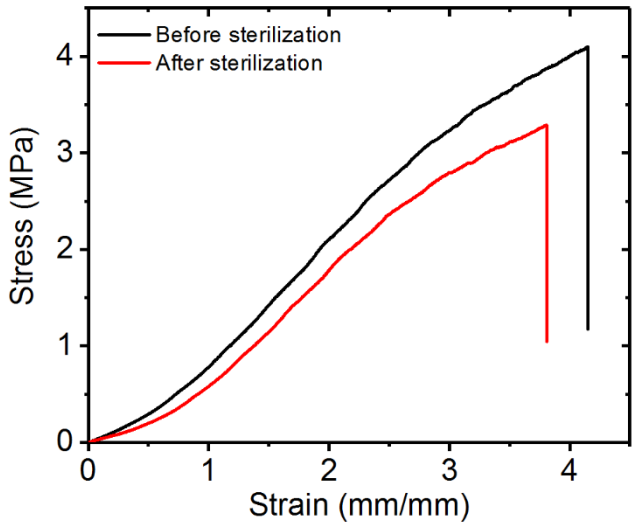

Figure 11. Tensile behaviors of the B-DN gel membranes tested before and after sterilization, respectively.

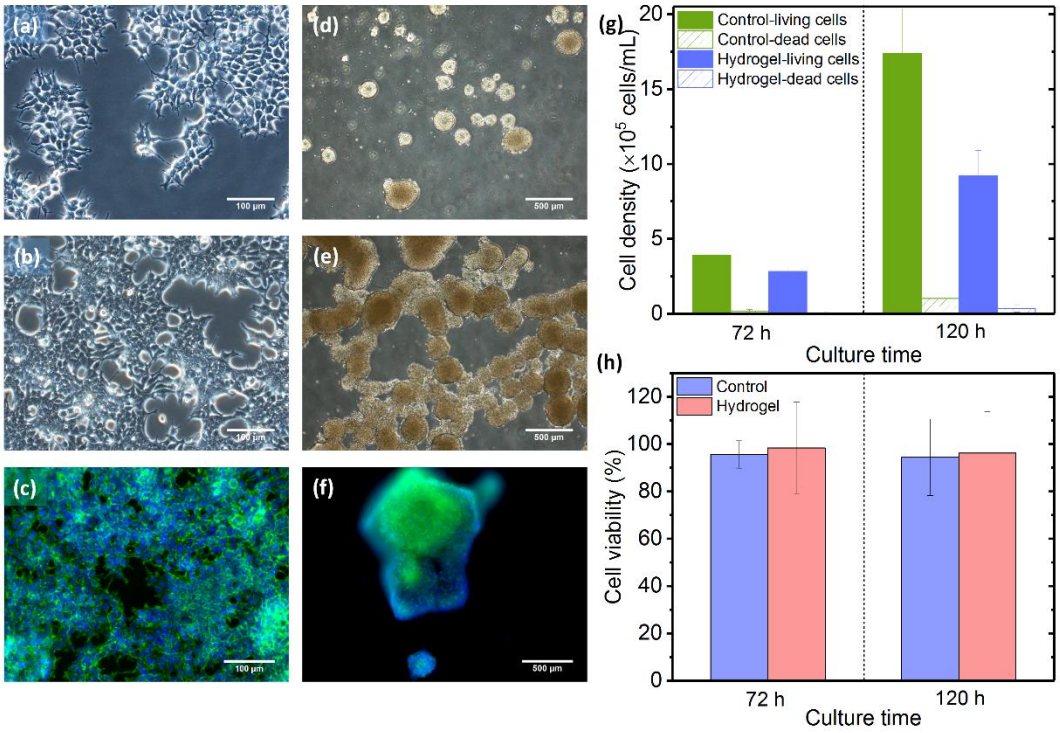

Figure 12. Photographs taken by bright field microscopy of 293T cell after the cells were cultured on the tissue culture polystyrene (TCPS) and B-DN gel film for 72h (a, d) and 120 h (b, e), respectively. Corresponding immunefluorescent images of (b) and (e) were shown in (c) and (f) at 4x magnification. (g) Cell density of live and dead of 293T cell after the cells were cultured on the tissue culture polystyrene (TCPS) and B-DN gel film for 72h and 120 h. (h) Cell viability of 293T cell after the cells were cultured on the tissue culture polystyrene (TCPS) and B-DN gel membranes for 72 h and 120 h. Sample code: B_{273} (0.23-2000/AAm-2), thickness: 44.1±8.1 μm.

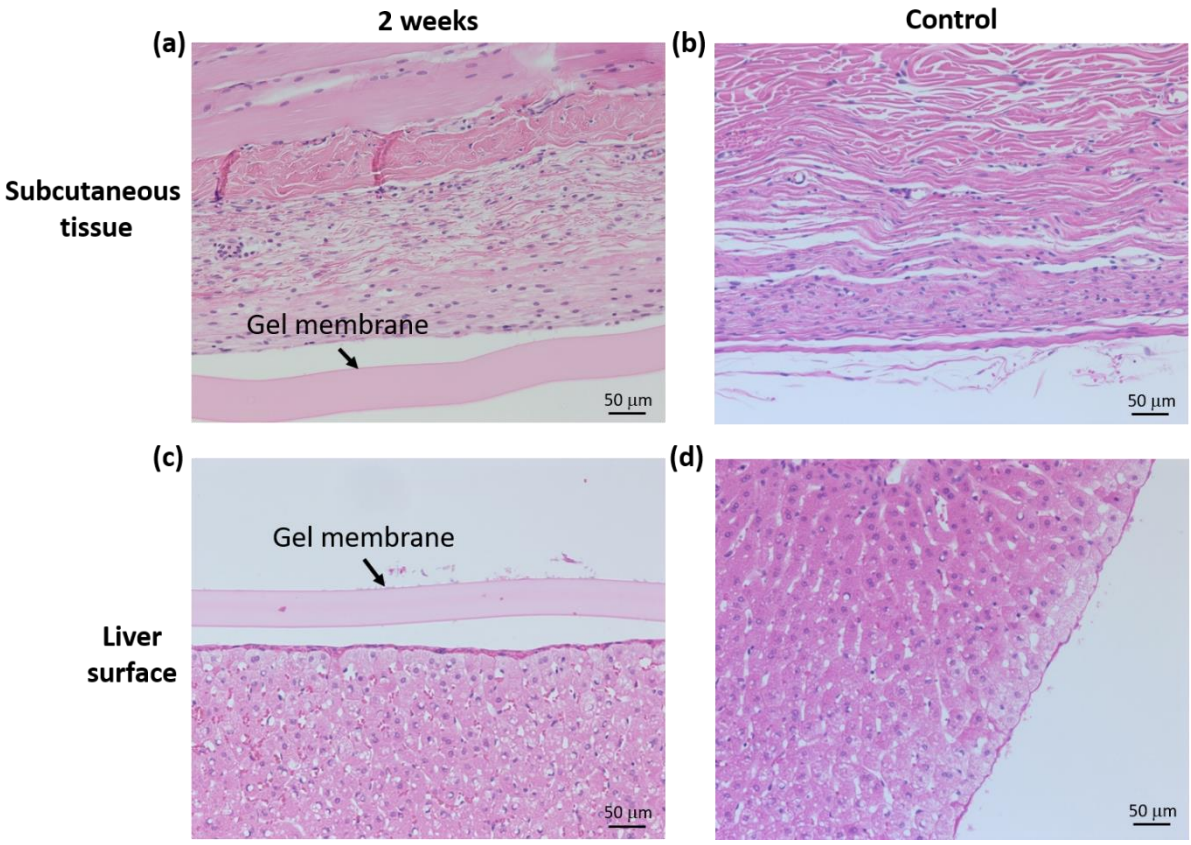

Figure 13. Microscopic observations of hematoxylin- and eosin-stained sections of subcutaneous tissue (a) and liver surface (c) implanted with B-DN gel membranes at postoperative weeks 2. (b) and (d) are the corresponding normal tissue as control without B-DN gel membranes implantation. Black arrows indicate the B-DN gel membranes. Sample code: B273(0.23-2000/DMA-2), thickness: 47.5 ± 5.1 µm.

Table 5. Summary of physical properties of various B-DN gel membranes.

	Sample code [a]B_N(C_p-s/m-C_2)	[b]t (μm)	E (MPa)	ε_b (mm/mm)	σ_b (MPa)	W_b (MJ/m^3)	c_w (%)
C_p	B_{273} (0.09-3000/AAm-2)	7.2±1.4	0.11±0.03	8.0±2.3	0.9±0.2	0.4±0.5	96.8±4.2
	B_{273} (0.17-3000/AAm-2)	14.8±0.2	0.30±0.10	4.1±1.3	2.4±0.6	6.3±2.5	90.3±8.1
	B_{273} (0.23-3000/AAm-2)	26.5±1.5	0.79±0.14	9.4±1.2	8.0±0.2	44.3±0.6	74.2±7.3
s	B_{273} (0.23-500/AAm-2)	113.1±12.3	0.65±0.03	6.1±0.2	4.6±0.3	15.3±0.2	73.9±7.5
	B_{273} (0.23-3000/AAm-2)	43.7±2.2	0.81±0.05	3.5±0.2	2.0±0.2	3.6±0.4	75.2±4.2
	B_{273} (0.23-5000/AAm-2)	11.8±0.9	0.52±0.05	2.3±0.1	1.9±0.1	2.1±0.3	84.6±3.5
m	B_{273} (0.23-3000/DEA-0.5)	39.0±5.6	40.20±13.40	1.6±0.7	3.5±0.3	4.7±2.7	75.9±12.3
	B_{273} (0.23-3000/DMA-0.5)	32.3±3.3	100.40±4.30	4.1±0.8	4.6±0.2	14.1±2.0	74.0±14.7
	B_{273} (0.23-3000/AAm-0.5)	37.9±1.3	2.24±0.10	4.4±0.5	3.6±0.4	2.6±0.5	62.0±2.9
C_2	B_{273} (0.23-3000/AAm-2)	36.9±3.3	1.56±0.02	7.0±0.9	8.0±0.9	29.1±5.8	72.2±4.8
	B_{273} (0.23-3000/AAm-4)	64.3±2.1	0.50±0.02	11.5±0.3	3.6±0.3	19.5±1.4	77.0±3.8
	B_{273} (0.23-3000/AAm-7)	123.8±3.0	0.44±0.10	13.0±0.9	2.5±0.6	15.4±3.1	78.8±2.1
L_B	B_{390} (0.23-3000/AAm-2)	48.7±1.7	0.15±0.01	9.9±0.6	2.7±0.2	14.2±2.2	92.0±2.4
	B_{297} (0.23-3000/AAm-2)	27.8±3.2	0.18±0.01	4.4±1.1	1.6±0.3	3.5±1.9	79.6±1.5
	B_{220} (0.23-3000/AAm-2)	15.6±0.5	1.97±0.40	2.5±0.6	3.3±0.5	5.4±2.4	65.8±2.2
M_n	1.3B_{220}(0.23-3000/AAm-2)	52.5±5.5	0.36±0.14	3.8±1.2	3.0±0.5	6.7±3.4	92.9±1.6

[a]N: degree of polymerization of the midblock of the triblock copolymer, C_p: the weight fraction of triblock copolymer in the precursor solution (wt/wt), s: the spin speed (rpm). m and C_2: the 2nd monomer type and corresponding monomer concentration (mol/L). L_B is the length of midblock in triblock copolymer. M_n is the number average molecular weight of triblock copolymer. [b]The parameters t, E, ε_b, σ_b, W_b, and c_w are thickness, Young's modulus, fracture strain, fracture stress, work of extension at fracture, and the water content of B-DN gel membranes, respectively.

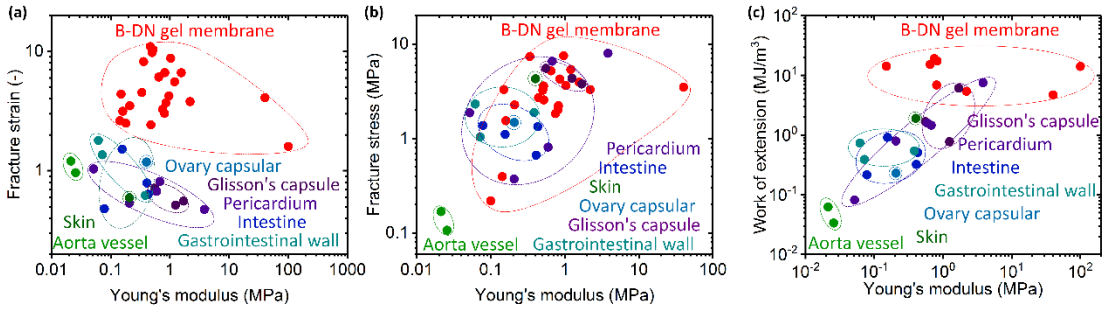

Figure 14. Depicting the mechanical properties of the B-DN gel membranes developed in this work and various biological-tissue membranes. (a) Fracture strain vs. Young's modulus; (b) fracture stress vs. Young's modulus; (c) Work of extension (energy density required to achieve tensile fracture) vs. Young's modulus. Numerical data are listed in Tables S3 and S4 for the B-DN gel membranes and the biological tissue membranes, respectively.

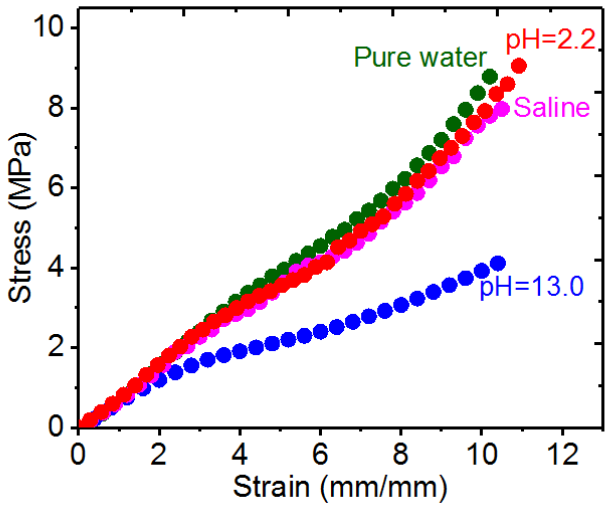

Figure 15. (a) Tensile behavior of the B-DN gel membrane at room temperature in saline solution, pure water, and in buffer solutions at pH 2.2 and 13.0. Sample code: B_{273} (0.23-3000/AAm-2), thickness: 30.4 ± 0.6 μm.

Table 6. Physical properties of selected B-DN gel membrane tested in saline solution at 37 °C

Test condition	Sample code $B_n(C_P$-s/m-$C_2)$	E (MPa)	ε_b (-)	σ_b (MPa)	W_b (MJ/m^3)
Saline solution at 25 °C	B_{273} (0.23-3000/AAm-2)	0.44±0.03	10.6±1.4	8.0±0.3	40.0±5.4
	B_{273} (0.25-3000/AAm-2)	0.53±0.01	6.3±1.7	5.5±0.3	22.6±0.2
	B_{273} (0.25-3000/DMA-2)	75.48±26.85	4.9±0.4	10.2±0.9	29.4±3.45
Saline solution at 37 °C	B_{273} (0.23-3000/AAm-2)	0.39±0.30	>9.4	>0.8	>6.7
	B_{273} (0.25-3000/AAm-2)	0.46±0.06	>9.9	>2.7	>14.9
	B_{273} (0.25-3000/DMA-2)	27.74±8.61	5.9±0.4	7.4±0.5	25.2±3.3

[a)] n is the degree of polymerization of the midblock of the triblock copolymer, C_P: the weight fraction of triblock copolymer in the precursor solution (wt/wt), s: the spin speed (rpm). m and C_2: the 2nd monomer type and corresponding monomer concentration (mol/L). [b)]The parameters E, ε_b, σ_b and W_b, are Young's modulus, fracture strain, fracture stress and work of extension at fracture of B-DN gel membranes, respectively.

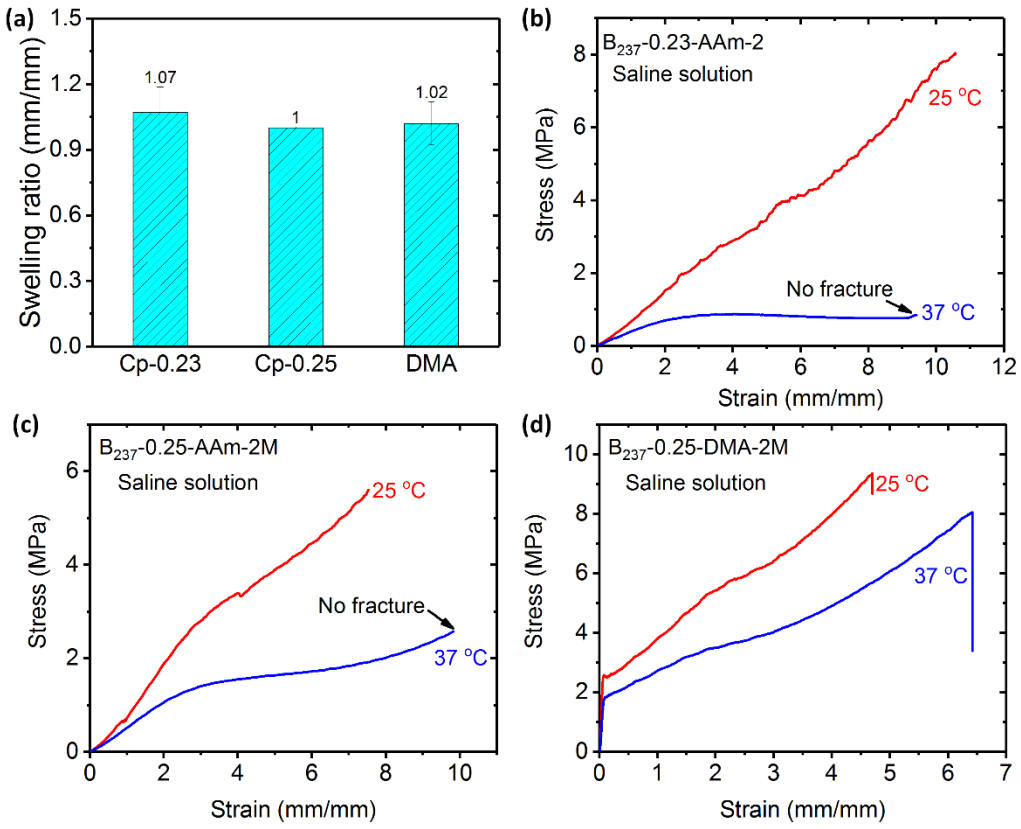

Figure 17. The swelling ratio (a) and tensile curves of selected B-DN gel membranes test at room temperature (25 ºC) and body temperature (37 ºC) in saline solution. Sample codes were shown in the figure.

Chapter 7: Summary

This work aims to get a better understanding of the structure and underlying toughening mechanism of tough and self-recoverable hydrogels. For this purpose, we chose the tough and self-coverable hydrogels based on self-assembly of ABA type triblock copolymer as a model system, and used NMR, rheology and time-resolved SAXS as detection technique. The effects of molecular parameters (including chain length of A or B block and triblock copolymer concentration) and external parameters (including temperature and) on preparation process, self-assembly structure, and structure-property relationship of gels were systemically studied. The main results and conclusions of this thesis are summarized as follows:

1). Relaxation dynamic of precursor solutions. The effects of temperature and polymer concentration on relaxation dynamics of precursor solution was studied by combing temperature-sweep rheological measurement and NMR. Our results suggest that this system obeys time-temperature superposition (TTSP) and time-concentration superposition (TCSP) quite well, and shows a sol-gel transition by decreasing temperature. This allow us to separate the activation energy of micelle relaxation from chain friction of entanglements. We found that the activation energy of micelle relaxation, originating from endblock chain pullout from micelle, is independent of the polymer concentration. While the sol-gel transition temperature increases with polymer concentration, which could be explained as a preferred intermolecular association

between endblock chains at high concentration.

2). Contribution of physical crosslinks and trapped entanglements in B gels. The individual contributions to the effective network from trapped chain entanglements and crosslinks in a physical triblock copolymer gels were successfully estimated by probing the modulus at uncrosslinked state (solution) and crosslinked state (B gel). The entanglements G_N in uncrosslinked solution were probed by TTSP. The trapped entanglements G_e was calculated by G_N normalized by swelling ratio from the solution to B gel. the contribution from crosslinks was calculated by subtracting the contribution of G_e from G, the total modulus of B gel. The ϕ_P dependence of G_e and G_c obeys power law with exponents of 2.5 and 1.0. The experimental exponent is perfectly conformed to the theoretical predictions, confirmed that our method is an effective method to separate the entanglements from crosslinks in physical hydrogels. It should be open the new door for designing new materials from theoretical viewpoint.

3). Structure evolution of B gels. In the gel (named as B gel), with increasing concentration, the elastic modulus originated from number of elastically active chains firstly increase followed by a plateau. In addition, structure evolution was also observed in small angle X scattering (SAXS). Based on micro SAXS and macro mechanical property, we concluded that the dangling chain which has no contribution, is dominant at low concentration; while at high concentration, the bridged micelles is dominant.

4). Toughening mechanism of B-DN gels. Based on results from a combination of

in-situ small-angle X-ray scattering and customized tensile device, the structure evolution during deformation was revealed, which suggests that the high toughness of self-recoverable B-DN gels is a synergistic effect of multiscale energy dissipation. In initial small strain region, the breaking and reforming of hydrogen bonding in chain scale dissipates energy, resulting in 100% self-recovery; In the middle strain region, the chain pullout of endblock from the micelles and debris reorganization of 1^{st} network for forming cluster dissipate energy; In the large strain region, microvoids form, which also dissipate energy.

5). Creation of tough and self-recoverable B-DN thin gel membrane. Benefiting from the thoroughly understanding of chain structure and self-assembly structure in gelation process and final gels, for the first time, we successfully prepared thin (10-100 um) but ultra-tough and 100% recoverable hydrogel membranes with high water content. Those membranes exhibit high pH sensitivity, excellent mechanical properties (even superior to those of various biological membranes), biocompatibility, and postoperative anti-adhesive property, foreshadowing their potential use as substitutes for biological membranes or postoperative anti-adhesive membrane.

Accomplishments

Original papers

(1) **Ya Nan Ye**, Martin Frauenlob, Lei Wang, Masumi Tsuda, Tao Lin Sun, Kunpeng Cui, Riku Takahashi, Hui Jie Zhang, Tasuku Nakajima*, Takayuki Nonoyama, Takayuki Kurokawa， Shinya Tanaka and Jian Ping Gong*, Tough and Self-Recoverable Thin Hydrogel Membranes for Biological Applications, Adv Funct Mater. Online (Journal Cover).

Presentations

(1) Yanan Ye, Huijie Zhang, Taolin Sun, Tasuku Nakajima and Jian Ping Gong, Tough and Self-Recoverable Thin Double Network Hydrogel Membranes, 4th International Life-Science Symposium, November 18, 2016, Sapporo, Japan.

(2) Yanan Ye, Huijie Zhang, Taolin Sun, Tasuku Nakajima and Jian Ping Gong, Ultrathin and tough physical hydrogels film with ultra-fast pH sensitivity, The 11th International Gel Symposium, March 7-9, 2017, Chiba, Japan.

(3) Yanan Ye, Kunpeng Cui, Taolin Sun, Huijie Zhang, Tasuku Nakajima and Jian Ping Gong, Ultra-thin and tough physical hydrogels with double network structure, SPSJ 65th Annual Meeting, May 25, 2016,Kobe, Japan (**Post Award**).

(4) Yanan Ye, Kunpeng Cui, Taolin Sun, Tasuku Nakajima and Jian Ping Gong, Structure Transition in Triblock Copolymer Gels: The Effect of Chain Architecture and Concentration on Mechanical Properties, 66th Symposium on Macromolecules, September 20, 2017, Ehime, Japan.

(5) Yanan Ye, Kunpeng Cui, Tasuku Nakajima and Jian Ping Gong, Toughening mechanism of B-DN gel by In-situ Small X-ray Scattering, ImPACT Joint Symposium, April 3, 2018, Tokyo, Japan.

Acknowledgements

For others, it is just a PhD dissertation, while for me, it witnesses my key transformation from naivety to maturity in my whole life. The dissertation is not an individual work, but a teamwork because I could never have the chance to reach such high-level understanding or explore such deep about my research without the help, support, guidance and efforts of a lot of people. Firstly, I would like to express my deepest and sincere appreciation to my advisor, Professor Jian Ping Gong, my role model. Her enormous enthusiasm and persevering pursue for science have a considerable impact on my career opportunities and choices. It is she who helps me to set up a correct attitude for research, to build confidence when I was frustrated. Her timely guidance, like a lamp, lights up my path in a sea of knowledge. I can say without doubt that without her encourage and guidance, I cannot meet the basic requirement for graduation. Here, I also would like to thank Assistant Professor Tasuku Nakajima for valuable discussions and suggestion during group meeting.

I would like to thank to Professor Takayuki Kurokawa, Tasuku Nonoyama, Daniel R. King and Dr. Tsutomu Indei for valuable discussions, suggestion and kind help for my research. I also want to express my thanks to the Master Martin Frauenlob, Assistant Professor Lei Wang, Associate Professor Masumi Tsuda and Professor Shinya Tanaka, who help me with the biomedical experiments. I would like to thank Professor Dominique Hourdet, Professor Liangbin Li, Professor Costantino Creton, Professor

Hiroshi Watababe and Thomas Salez for the fruitful discussion. I also want to thank Ms. Yukiko Hane and Dr. Yoshinori Katsuyama (my superman!) for their kind experiments support. Here, I thank Mr. Otsuka Chemical Company for their kind donation of the triblock copolymers.

I would like to take this opportunity to thank ex-assistant Professor Tao Lin Sun, Dr. Kunpeng Cui, who teach me step by step from experiment design to data analysis. I learn from them not only how to orderly, efficiently, and excellently finish my work, but also how to express your idea in a concise and logical way. Acquainted with you is the most valuable asset in my life. I also want thank Dr. Yiwan Huang, you are the window to extend my interpersonal relationship. It is no exaggeration to say that 80% person I met here was acquainted through you.

I would like to thank secretary Ms. Eiko Hasegawa, Ms. Yuki Ookubo for the lab daily life such as IGP scholarship application, conference scheduling, chemical purchase, dissertation defense, etc. With your kind help, I can survive here and never miss any important information even without linguistic ability. I also want to thank all my Chinese friends, Feng Luo, Huijie Zhang, Ran Shi, Aokai Zhang, Honglei Guo, Liang Chen, Ping Rao, Hui Guo, Yueyu Li, Hailong Fan, Junchao Huang, Wei Cui, Yunzhou Guo, Zhen Tao, Chengtao Yu, Yong Zheng, Tianlong Zhao. With your kind company, I never feel lonely abroad and always enjoy the happy time in the 4 years. I am also very thankful to all my Japanese friends, especially my supporter Taiki Fukuda, and Takuya Ikai, Yukei Ozaki, Riku Takahashi, Kei Mito, Koshiro Sato,

Kumi Ota, Satoshi Koike, Takahiro Matsuda, Ryuji Kiyama, Kazuki Fukao, Kohei Murakawa, and other international students such as Abu Bin Ihsan, Md. Anamul Haque, Muhammad Ilyas, Anouk L'Herm, Gabriel Gonzalez, Amber Hubbard, who always invite me for international extracurricular activities and help me to cross over the cultural differences and enjoy life in a fresh way.

Here I also want to thank my ex-boyfriend, the buddy onetime with me for 8 years. Thank you for bringing me enjoyment and happiness for my entire youth. Thanks for encouraging me to learn abroad even though there is enormous risk from the love spell for long distance relationship. What is so sad is that the spell is true for us. Maybe this is the so-called fate, maybe only when you leave me, I can grow up although growing is painful. We still have not said a proper goodbye to each other, right? Here, I want to take this opportunity to say a dignified goodbye to all the times we had. Thank you for telling me what the love is, and let's forgive the painful experience that brings to each other. And I hope you have a happy life with your right person.

I would like to dedicate this dissertation to my loved parents and other family members for their love, support and great sacrifice. Finally, I would like to thank my boyfriend, Shilei, the right person I met at the right time. Thank you for lighting the love lamp in the darkness, thank you for giving me the happiness what I desired. It is the best luck to have the honor to accompany you in your lifetime.

YANAN YE

July, 2018